RETRIEVAL OF VOLUME SCATTERER INFORMATION USING THREE-COMPONENT DECOMPOSTION MODEL, BASED ON COMPACT POLARIMETRY

VISHNU NANDAN N S
March, 2012

SUPERVISORS:
Mr. Shashi Kumar
Dr. V.A. Tolpekin

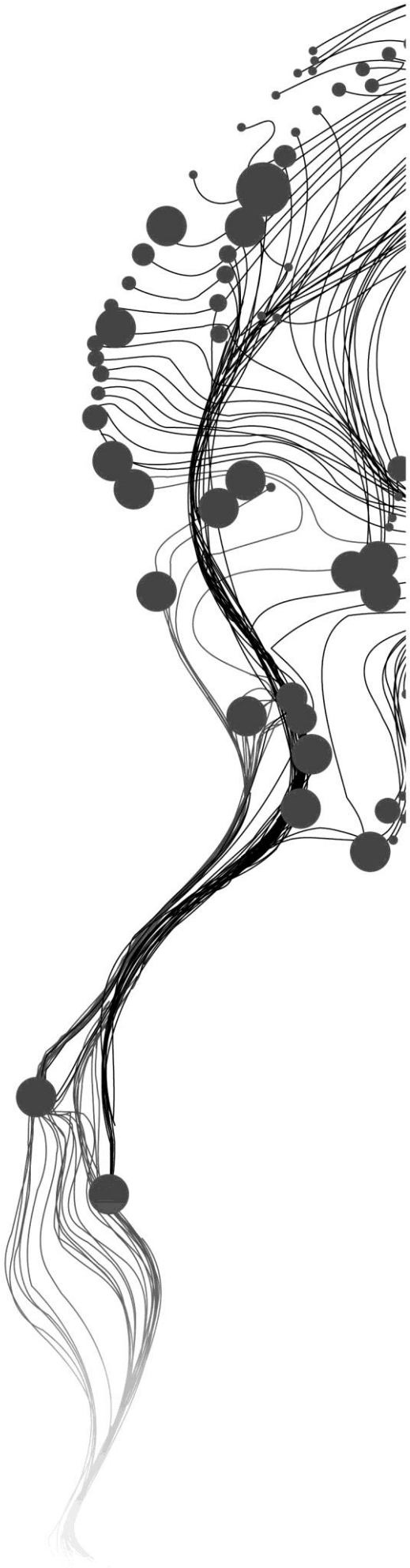

RETRIEVAL OF VOLUME SCATTERER INFORMATION USING THREE-COMPONENT DECOMPOSTION MODEL, BASED ON COMPACT POLARIMETRY

VISHNU NANDAN N S

Enschede, The Netherlands, March, 2012

Thesis submitted to the Faculty of Geo-Information Science and Earth Observation of the University of Twente in partial fulfilment of the requirements for the degree of Master of Science in Geo-information Science and Earth Observation.
Specialization: Geoinformatics

SUPERVISORS:
Mr. Shashi Kumar
Dr. V.A. Tolpekin

THESIS ASSESSMENT BOARD:
Prof. Dr. Ir. A. Stein (Chair)
Dr. Y. S. Rao (External Examiner, CSRE, IIT Bombay)

"Let my urge for triumph in life be dedicated to those who made me 'realize my existence' and gave me 'faith and constant support' to succeed in life"

03:17:11

ABSTRACT

Forest monitoring has become an important necessity nowadays for forest management authorities to prevent deforestation, human encroachment and even for researchers to understand forest dynamics and to develop advanced technology for monitoring forest ecology and resources with less effort. Radar remote sensing employing polarimetric techniques has proved its capability in monitoring these aspects. The high demand and stringent availability of the fully-polarimetric data from very few SAR sensors has made researchers think about using low cost, low power dual-polarimetric systems to reproduce the fully-polarimetric data through compact polarimetric techniques. The purpose of this research is to explore the prospective of the compact polarimetric technique in ($\pi/4$) mode to derive and reproduce the pseudo-quadrature polarized data from the dual-polarimetric scattering vectors, based on coherency matrix approach, thereby using to study and assess the effect of volume scattering contribution of tree leaves, trunk and ground from the Sal forests of Barkot, Dehradun and the ecologically important Mangrove forests of the Sundarbans. The three-component scattering model was used to decompose the reproduced coherency matrix to study the volume scattering information from the forest scatterers. The data used for this study was ALOS PALSAR fully-polarimetric L-band data. The methodology applied for this study used the polarization state extrapolation algorithm, developed for covariance matrix approach which was modified to transform the reconstructed covariance matrix to coherency matrix for compact polarimetric ($\pi/4$) mode. The reconstructed coherency matrix was then decomposed using the Freeman and Durden decomposition model, and compared against the original fully-polarimetric data. Different data analysis including entropy, total power, diagonal elements of the coherency matrices and polarization signature were carried out to investigate and study the variation between the original and the reconstructed data. The volume scatterer contribution from both the forested areas was validated against the fully-polarimetric data using the cross-polarized multi look image as the reference data. The results show the potential of the ($\pi/4$) mode to reconstruct the pseudo-quadrature polarized data using the coherency matrix approach. The results show uneven variation in the volume scattering power from both the forests, after reconstruction and decomposition procedure. The reasons behind this due to the assumptions in the algorithm, was reported and discussed based on physical interpretation. Further exploration of possibilities including modification of the algorithm for coherency matrix approach, validation employing field data in the form of biomass and comparison of different hybrid polarimetric modes based on coherency matrix approach has also been recommended.

Keywords: *$\pi/4$ mode, compact polarimetry, polarimetric decomposition, Polarimetric SAR, Volume scattering.*

ACKNOWLEDGEMENTS

At this moment of accomplishment, I owe my deepest gratitude to my IIRS supervisor Mr. Shashi Kumar Sir, for his continuous support, motivation and vast knowledge on the subject. Thank you Sir for your precious time, support throughout my academics at IIRS. You helped and supported me whenever I had approached you, even during my hard times. Thank you again Sir.

Dr. Valentyn Tolpekin Sir, my ITC supervisor, who has made me understand the value of becoming an independent researcher, through his noble advices. A really good teacher with immense knowledge, Gentle Human being from his heart to the core, critical in his comments, helped me in the best possible way, to make this work a real success. Thank you Sir. I have become your admirer, for your stylish English accent and your ever caring attitude towards students. It was a privilege to work under your guidance.

I would like to thank Dr. Nicholas Hamm Sir, for his encouragement and initiative to make this course easy and pleasant for me throughout the course period. Special thanks to him for making our course work and stay at ITC, The Netherlands, a really memorable one.

Mr. P.L.N Raju Sir, Group Head, RSGG Division. He gave us all the facilities, support, care and special attention for all of us to make this degree, a real cake walk. Thank you Raju Sir. You were one among the very few who gave me relief at hard times.

I would like to thank Dr. P. S. Roy Sir (Director, IIRS) and Dr S. K. Srivastav Sir (Head, Geoinformatics Department) for their support and excellent technical infrastructure to implement this research work. Thank you Srivastav Sir for your valuable advice throughout my research work. Special thanks to all the CMA members for providing the entire technical inventory for this work.

Special thanks to Dr. Sekhar Lukose Kuriakose Sir (Project Head, KSDMA), Dr. Shankar Sir (Scientist, CESS) and Dr. George Philip Sir (Scientist, WIHG), for their constant motivation to join this course and throughout my course period and even motivating me for pursuing my PhD dreams. Thank you! Special thanks to Dr. Didier Massonet (CNES, France), Dr. Alberto Moriera (Director, HR, DLR), Dr. Svein Solberg (UMB, Norway), Dr. Gianfranco Fornaro (IREA, Italy) and Dr. David Bruce (Associate Professor, University of South Australia) for their interest in my research work and extending their support for my future initiatives.

Special thanks to Mr. Rahul Raj Sir (PhD student, ITC) for extending his help for my research, especially giving the R-code, which he had developed.

Finally, deepest of gratitude to all my friends, Surya, Gourav, Teja, Ruchi, Priyanka, Chittaranjan, Ankit, Abhijeet, Suranjana, Rahul, Pratik and Jai for providing me all the support and help I got throughout my life at IIRS. Thank you all. Thanks to all my juniors Ajith, Akarsh, Anukesh, Shankar, Pavan, Bharadwaj and Bhavya for supporting me throughout my time at IIRS.

Special thanks to Ms. Preethi Malur Balaji for her constant motivation and support especially throughout my research phase.

My parents are everything for me. All through my life.

TABLE OF CONTENTS

List of Figures....viii
List of Tables....xi
List of Acronyms....xii
List of Symbols....xiii
1. INTRODUCTION....1
1.1. Background....1
1.2. Polarization....1
1.3. SAR Polarimetry....3
1.4. Covariance and Coherency Matrix....3
1.5. Coherent and Incoherent Decomposition....4
1.6. Problem Statement....5
1.7. Research identification....7
1.8. Thesis Structure....7
2. Literature Review....9
2.2. Literature Review Conclusion....19
3. Study Area....20
3.1. Barkot Forest Area....20
3.2. The Sundarbans....22
3.3. Why different Study Areas?....24
4. Materials and Methodology....25
4.1. Data....26
4.2. Method....26
4.3. Tools....32
5. Derivation of 3×3 coherency matrix (π/4 mode) and three-component decomposition modelling theory....33
5.1. Polarization State Extrapolation Algorithm....33
5.2. Three-component incoherent decomposition model....34
6. Analysis, Results and Validation....37
6.1. Derivation of pseudo-quadrature polarized data, using Polarization state extrapolation algorithm based on π/4 mode.....37
6.2. Analysis of backscattered power on diagonal elements of 3×3 coherency matrices....39
6.3. Estimation of volume scattering contribution from both modes, using three-component decomposition model....48
6.4. Validation....60
7. Discussions....64
7.1. Importance of coherency matrix approach- (π/4) mode.....64
7.2. Discussion on the analysis of the diagonal elements....64
7.3. Discussion on analysis of variation in volume scattering power....66
7.4. The "factor 2" factor....71
7.5. Relevance of Polarization Signature analysis....71
7.6. Entropy analysis....72
7.7. Selection of study areas....73
7.8. Validation....74
8. Conclusions and Recommendations....75

8.1. How, pseudo-quadrature polarimetric 3×3 coherency matrix can be derived and reproduced from dual polarimetric mode using compact polarimetric technique?....75
8.2. What is the relation between the entropy obtained from the fully polarimetric data and the entropy obtained from compact polarimetry mode? 75
8.3. How to validate the volume scattering contribution from the compact polarimetric data against the fully-polarimetric data?....76
8.4. What is the accuracy of the estimated volume scatterer contribution obtained from compact polarimetry mode against to that obtained from fully polarimetric data, using Freeman-III model?....76
8.5. Recommendations 77

List of References....78

Appendix-I....83
Appendix-II....84
Appendix-III....87

LIST OF FIGURES

Figure 1-1: Propagation of Electromagnetic plane wave. Source: [4] 2

Figure 1-2: Polarization Ellipse. Source: [6] 2

Figure 1-3: Scattering mechanisms (a)Single-bounce scattering (b) Double-bounce scattering and (c) Volume scattering. 5

Figure 1-4 Compact polarimetry (π/2 mode) 6

Figure 1-5: Compact polarimetry (π/4 mode). 6

Figure 2-1: Polarization Ellipse- Rotation Sense 10

Figure 2-2: (a) Linear Polarization (b) Elliptical polarization (c) Circular polarization 11

Figure 2-3: Polarization signature (a) Co-polarization channel (b) Cross-polarization channel 19

Figure 3-1: (a) India Map (b) Uttarakhand State map (c) Study area I - Geoeye-I Sensor, Source: Google Earth 21

Figure 3-2: (a) India Map (b) Part of Sundarbans (c) Study area I - Geoeye-I Sensor, Source: Google Earth 23

Figure 4-1 Methodology Flow Diagram 25

Figure 4-2: (a) SLC image-Study area I (b) Multi look image-Study area I (c) SLC image-Study area II and (d) Multi look image- Study area II. 27

Figure 6-1: (a) Coherency matrix element $T11$ (b) $T22$ (c) $T33$ - Study area I 37

Figure 6-2: (a) Area sensitive to Surface-bounce scattering (b) Double-bounce scattering (c) Volume scattering 38

Figure 6-3: (a) Coherency matrix element $T11$ (b) $T22$ (c) $T33$- Study area II 38

Figure 6-4: (a) Area sensitive to Surface-bounce scattering (b) Double-bounce scattering (c) Volume scattering 39

Figure 6-5: Variation of $T11$ elements for Study area I: 40

Figure 6-6: Dehradun airport runway (Road surface) 40

Figure 6-7: Regression analysis-Study area I - (a) Linear model (b) Residual plot 40

Figure 6-8: Variation of $T11$ elements - Study area II. The lines are added to assist interpretation 41

Figure 6-9: Portion of sea surface (Bay of Bengal) 41

Figure 6-10: Regression analysis-$T11$ element-Study area II-(a) linear model (b) Residual plot 42

Figure 6-11: Variation of $T22$ elements for Study area I. The lines are added to assist interpretation 42

Figure 6-12: Portion of Urban areas of Haridwar city 43

Figure 6-13: Regression analysis for $T22$ element-Study area I - (a) Linear model (b) Residual plot 43

Figure 6-14: Variation of $T22$ elements for Study area II. The lines are added to assist interpretation 44

Figure 6-15: Portion of Urban areas of Sundarbans 44

Figure 6-16: Regression analysis for $T22$ element- Study area II - Residual plot 44

Figure 6-17: Variation of $T33$ elements for Study area I. The lines are added to assist interpretation 45

Figure 6-18: Portion of Barkot forest area 45

Figure 6-19: Regression analysis for $T33$ element Study area I-(a) Linear model (b) Residual plot 46

Figure 6-20: Variation of $T33$ elements for Study area II. The lines are added to assist interpretation 46

Figure 6-21: Portion of Mangrove forests, Sundarbans 47

Figure 6-22: Regression analysis - $T33$ element Study area II - (a) Linear model (b) Residual plot....47

Figure 6-23: (a) - Volume scattering contribution Study area I - FP mode (b) CP mode (c) - Zoomed image - FP mode(d) CP mode 48

Figure 6-24: Volume scattering contribution Study area II – FP mode (b) CP mode (c) - Zoomed image - FP mode(d) CP mode....49

Figure 6-25: Boxplots (a) Study area I (b) Study area II....50

Figure 6-26: Variation of volume scattering power-FP and CP modes - Study area I....51

Figure 6-27: Portion of Barkot area – Volume scattering (a) FP mode (b) CP mode....52

Figure 6-28: Regression analysis- Study area I - (a) Linear model (b) Residual plot....52

Figure 6-29: Variation of volume scattering power-FP and CP modes - Study area II. 53

Figure 6-30: Portion of Mangrove forests, Sundarbans-Volume scattering 53

Figure 6-31: Regression analysis-Volume scattering- Study area II - (a) Linear model (b) Residual plot 53

Figure 6-32: Normalized signature (a) Co-pol channel -FP mode(b) Cross-pol channel -FP mode 54

Figure 6-33: Normalized signature (a) Co-pol channel -FP mode(b) Cross-pol channel -FP mode....55

Figure 6-34: Variation of total power FP and CP modes-Study area I. 56

Figure 6-35: Regression analysis-Total power- Study area I - (a) Linear model (b)Residual plot....56

Figure 6-36: Regression analysis-Total power-Study area II - (a) Linear model (b) Residual plot....57

Figure 6-37: Variation of entropy- FP and CP modes - Study area I. 57

Figure 6-38: Regression Analysis-Entropy - Study area I - (a) Linear model (b) Residual plot 58

Figure 6-39: Variation of entropy-FP and CP modes - Study area II. 58

Figure 6-40: Regression analysis-Entropy-Study area II - (a) Linear model (b) Residual plot 59

Figure 6-41: (a) Reference data $2S_{HV}$ - Barkot area (b) Forest area subset - reference data (c) - Forest area subset - volume scattering decomposed image-CP mode (d) Sample subset - reference data (e) Validation subset - volume scattering decomposed image-CP mode 60

Figure 6-42: Regression analysis – Validation - Study area I - (a) Linear model (b) Residual plot....60

Figure 6-43: (a) Reference data $2S_{HV}$ - Sundarbans area (b) Forest area subset - reference data (c) Forest area subset - volume scattering decomposed image-CP mode (d) Sample subset - reference data (e) Validation subset - volume scattering decomposed image-CP mode 62

Figure 6-44: Regression analysis-Validation- Study area II - (a) Linear model (b) Residual plot 62

Figure 7-1: a) Georeferenced $T22$ element-Sundarbans (b) zoomed image of the subset (c) Subset area from Geoeye-I sensor-Buildings (red), Agricultural areas (yellow), Trees (green) Source: Google Earth 65

Figure 7-2: (a) Georeferenced $T33$ element - Barkot forest (b) zoomed image-FP mode(c) CP mode (d) Freeman-volume-FP mode(e) CP mode (f) Image-Geoeye-I sensor. Source: Google Earth....66

Figure 7-3: (a) Georeferenced $T33$ element-Mangrove forest area, The Sundarbans (b) zoomed image-FP mode(c) CP mode (d) Freeman-volume-FP mode(e) CP mode (f) Image-Geoeye-I sensor. Source: Google Earth....69

Figure 7-4: (a) Marshy areas of the Sundarbans. Source: Google Earth (b) $T33$ element-CP mode (c) Freeman-volume-CP mode....70

LIST OF TABLES

Table 1: Compact SAR modes vs. Classical Modes 14

Table 2: Boxplot parameters - Study area I 50

Table 3: Boxplot parameters - Study area II 51

Table 5: Statistical summary for accuracy measures after validation-Study area I 61

Table 6: Statistical summary for accuracy measures after validation-Study area II 63

Table 7: Cross-polarized power variation before and after reconstruction 67

Table 8: Radar bands and designations 83

Table 9: Dataset description 83

Table 10: Dataset Characteristics 83

Table 11: Statistical summary (a) Regression analysis - Study area I (b) Study area II (c) Residual analysis - Study area I (d) Study area II 87

LIST OF ACRONYMS

RADAR	Radio Detection and Ranging
SAR	Synthetic Aperture Radar
RAR	Real Aperture Radar
PolSAR	Polarimetric Synthetic Aperture Radar
InSAR	Interferometric Synthetic Aperture Radar
PolInSAR	Polarimetric Interferometry Synthetic Aperture Radar
EM	Electromagnetic
CLTR	Circular Transmit Linear Receive
ALOS	Advanced Land Observation Satellite
PALSAR	Phased Array L-band Synthetic Aperture Radar
SLC	Single look Complex
MCSM	Multiple Component Scattering Model
dB	Decibel
RCS	Radar Cross Section
HH	Horizontal-Horizontal (Polarization)
HV	Horizontal-Vertical (Polarization)
VH	Vertical-Horizontal (Polarization)
VV	Vertical-Vertical (Polarization)
RMSE	Root Mean Square Error
ML	Multi Looked
FP	Fully-polarimetric
CP	Compact polarimetric

LIST OF SYMBOLS

ψ	Orientation angle
χ	Ellipticity
K_L	Scattering vector - Lexicographic format
K_P	Scattering vector - Pauli format
$K_{\pi/4}$	Scattering vector - Compact polarimetric (π/4) mode
S_{HH}, S_{HV}, S_{VH} and S_{VV}	Complex scattering amplitudes
$[S]$	Scattering matrix
$[C]$	Covariance matrix
$[C_{\pi/4}]$	Covariance matrix - Compact polarimetric (π/4) mode
$[T]$	Coherency matrix
T_{11}, T_{22} and T_{33}	Diagonal elements of the coherency matrix
H	Entropy
$[T_{FULL}]$	Coherency matrix - Fully-polarimetric mode
$[T_{MOD}]$	Coherency matrix - Compact polarimetric (π/4) mode
T_p	Total power
r	Correlation coefficient
R^2	Coefficient of determination
$[A]$	Unitary transformation matrix
R_{th} , R_{tv} R_{gh} and R_{gv}	Fresnel reflection coefficients
f_v	Volume scattering contribution
f_d	Double-bounce scattering contribution
f_s	Single-bounce scattering contribution

1. INTRODUCTION

1.1. Background

The need for understanding and monitoring forests has nowadays become an important research area in scientific community. Forests are one among the most important vegetation cover when it comes to area and volume. With the technological advancements in geosciences applications, remote sensing has become an effective method for detection and investigating various factors concerning forests, like estimating tree height, basal area, stem diameter, stem volume, aboveground biomass.

The science of remote sensing deals with the collection of images of features on the Earth surface without having any physical contact with the objects. Radar remote sensing utilizes microwave region of electromagnetic spectrum from 1 mm to 1.3 m [1] wavelengths. Radar is not only used for detection and ranging applications but can also be used for imaging the earth surface. Radar antenna is used to transmit the energy to the object on the ground and records the backscattered portion of the signal from the object. The penetration capability of an electromagnetic wave depends on its wavelength. The high penetration ability of radar waves enables the sensor to acquire information on sub-surface features beneath the ground. The radar waves can penetrate through clouds, light rain, smoke with limited attenuation and serves as an all-weather remote sensing system. Radar waves with longer wavelengths such as L-band enables higher penetration capability through forest canopy making it very useful to measure the bio-physical properties of forests.

Imaging of the earth surface using Real Aperture Radar (RAR) systems limits the resolution by the power and size of the footprint of the radar beam, which depends on the aperture size and therefore RAR systems are used only for few remote sensing applications [2]. In case of SAR system, a large antenna is synthesized using Doppler Effect in the acquired data employing offline processing techniques. SAR uses signal processing techniques and satellite orbital information which thereby provides a much higher resolution in range (across-track) and azimuth (along-track) directions when compared to RAR systems. Radar imaging through Synthetic Aperture Radar (SAR) systems has revolutionized and expanded the technology of Microwave remote sensing especially in geosciences applications using different techniques like SAR Polarimetry (PolSAR), SAR Interferometry (InSAR) and Polarimetric SAR Interferometry (PolInSAR). SAR systems in general helps in understanding glacier and ice movement to give better understanding on long term variation in climate, developing highly accurate and detailed elevation maps, flood and oil spill monitoring, land use and land cover change, soil moisture and biomass estimation, assessing the health of crops and forests and even in urban planning and development.

1.2. Polarization

An electromagnetic (EM) wave consists of two components-namely electric and magnetic field, which at any moment of time and in any position in space, is orthogonal to each other. Polarization is defined as the orientation of the electric field plane, whether it is horizontal or vertical or at some other angle, in a plane perpendicular to the direction of propagation. The behaviour of the electric field of an electromagnetic wave is described by polarization.

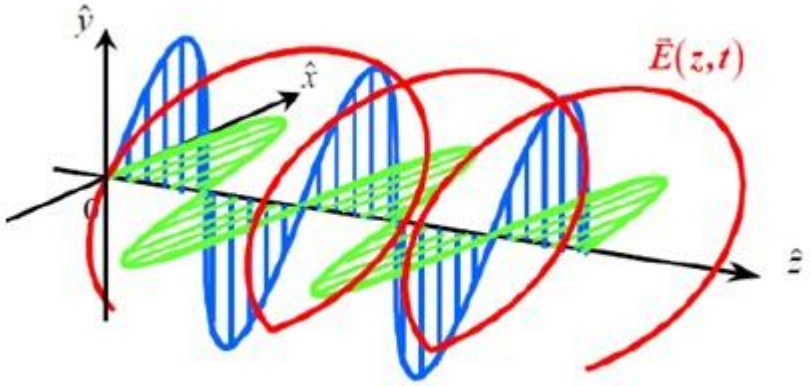

Figure 1-1: Propagation of Electromagnetic plane wave. Source: [4]

The electric field vector has both vertical (blue) and horizontal (green) components, which in turn combines to yield the net electric field vector (red). The vector sum of horizontal and vertical components, which are orthogonal to each other, describes the electric field of a plane wave [3]. These two components are characterized by their amplitudes and relative phase between them. When viewed along the propagation direction, the tip of the electric field vector of a fully polarized wave traces out in an elliptical pattern referred to as Polarization ellipse [4].

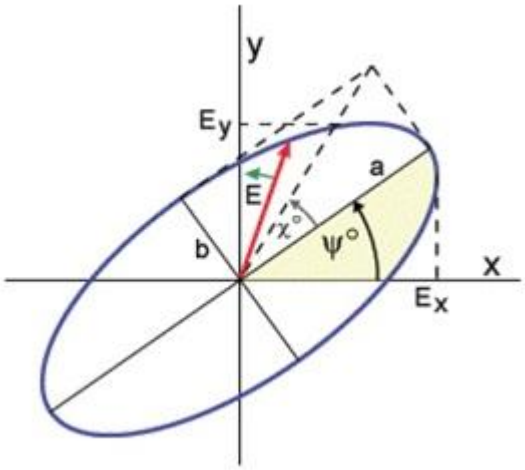

Figure 1-2: Polarization Ellipse. Source: [6]

The semi-major and semi-minor axis of the polarization ellipse (figure 1-2) are represented by 'a' and 'b' respectively. The orientation angle ψ of the EM wave is the angle between the semi-major axes from the positive horizontal axis measured in counter clockwise direction. The orientation angle ranges from 0° to 180°. Ellipticity or eccentricity χ represents the shape parameter, which describes the degree to which the shape of the polarization ellipse is oval and takes values between -45° to +45°. The magnitude and their relative phase of the horizontal and vertical components govern the shape of the polarization ellipse [3]. When components are in phase with zero ellipticity and 45° orientation, the polarization is linear. As the phase angle increases along with the orientation, the shape of the ellipse also changes. For example, when the phase angle between the horizontal and vertical components become 90° with same magnitudes, the ellipse becomes a circle. In this case, depending on the ellipticity value $\chi = \pm 45°$ the polarization can be left circular or right circular.

1.3. SAR Polarimetry

In SAR Polarimetry, the information about the target will be encoded or embedded in the polarization of the electromagnetic wave. SAR system creates polarized waves by using antennas designed to transmit and receive EM waves of specific polarization. Single-polarized SAR either transmits horizontal (H) or vertical polarization (V) and correspondingly horizontal or vertical polarization will be received. However in case of dual-polarized SAR, for H transmit, it can receive both H and V (HH, HV) and for V transmit, it can receive both V and H (VV, VH). Here HH and VV are called co-polarized terms and HV and VH are called the cross-polarized terms. Fully-polarimetric SAR data uses all four polarization channels which means more information about the features which is not possible from dual-polarized SAR data. Basic or operational SAR systems, for economy aspect tend to have one single polarization, while for research systems tend to have multiple polarizations. Multiple polarizations help in distinguishing the physical structure of the scattering structures.

Polarization has an important role in radar backscatter whose intensity depends on different factors like surface roughness, moisture content, and orientation along with signal characteristics such as wavelength, polarization and incidence angle. When radar signal interacts with different earth features, depending on the size, shape, orientation and dielectric property of the features, it changes its polarization direction which is referred to as scattering of the signal. This change affects the way in which the scene under study appears in a polarimetric SAR imagery and thereby the type of the surface can be deduced from the image at times [5]. When the entire signal incident is absorbed or transmitted, sensor receives no returns. If the sensor receives a portion of the incident energy back from earth features, it is referred as backscatter. The scattering data and information obtained from the earth features has to be preserved in a polarimetric form. The measured complex information has to be stored using polarization synthesis in the form of scattering matrix which can used to understand coherent or pure scatterers. Depending on the complexity of the scatterers, the scattering matrix can be used as second order derivatives in the form of covariance and coherency matrices. These matrices can de decomposed using different decomposition techniques to separate the polarimetric radar measurements to basic scattering mechanisms.

Polarimetry has proved to be an important tool to compute scattering matrix, polarization signature, Stokes matrix for each pixel for all polarization channels. This in turn has made polarimetry, a powerful classification tool for both visual as well as machine type classification. SAR polarimetry, using scattering matrix helps in synthesizing radar return for any transmit/receive polarization. It also helps in investigating the scattering properties of different earth surfaces [5].

1.4. Covariance and Coherency Matrix

When a horizontal or vertical polarized wave is incident on an earth feature, the backscattered portion of the radar signal can have contributions in both horizontal and vertical polarizations. As these components form a complete basis set to describe the electromagnetic, the backscattering properties of the earth feature under study can de described using scattering matrix given by

$$[\mathrm{S}] = \begin{bmatrix} S_{HH} & S_{HV} \\ S_{VH} & S_{VV} \end{bmatrix} \tag{1-1}$$

The scattering matrix $[\mathrm{S}]$ is a 2×2 matrix, which consists of four complex elements, in which the diagonal elements represent the co-polarized information while the off-diagonal elements represent the cross-polarized information. Polarimetry, using scattering matrix can compute the strength, polarization and polarization signature of a scattered wave for any polarization of an incident wave at every imaged

pixel [3]. The complex elements of the scattering matrix are obtained from the magnitude and phase of the four polarimetric channels HH, HV, VH and VV. The scattering matrix can be used to describe the backscattering properties in case of coherent or pure targets. In case of distributed scatterers, where partially polarized waves dominate, it is not possible to obtain information using just scattering matrix. The second order derivative of scattering matrix which are the covariance and coherency matrices has to used in case of distributed scatterers. In order to obtain the covariance and coherency matrices from the scattering matrix, the vectorized form of scattering matrix has to be used in the form of lexicographic basis and Pauli basis. The lexicographic format assuming reciprocity condition $S_{HV} = S_{VH}$ is given by

$$K_L = \begin{bmatrix} S_{HH} \\ \sqrt{2}\, S_{HV} \\ S_{VV} \end{bmatrix} \tag{1-2}$$

The covariance matrix is obtained by multiplying the above vector with its complex conjugate transpose represented by $\mathrm{C} = K_L . K_L{}^{\dagger}$. Therefore the covariance matrix C becomes

$$C = \begin{pmatrix} S_{HH}.\ S_{HH}^* & \sqrt{2}\, S_{HH}.S_{HV}^* & S_{HH}.\ S_{VV}^* \\ \sqrt{2}\, S_{HV}.S_{HH}^* & 2\, S_{HV}.S_{HV}^* & \sqrt{2}\, S_{HV}.S_{VV}^* \\ S_{VV}.\ S_{HH}^* & \sqrt{2}\, S_{VV}.S_{HV}^* & S_{VV}.\ S_{VV}^* \end{pmatrix} \tag{1-3}$$

The Pauli format assuming reciprocity condition is given by

$$K_P = \frac{1}{\sqrt{2}} \begin{bmatrix} S_{HH} + S_{VV} \\ S_{HH} - S_{VV} \\ 2\, S_{HV} \end{bmatrix} \tag{1-4}$$

The coherency matrix is obtained by multiplying the Pauli basis vector with its complex conjugate transpose represented by $\mathrm{T} = K_P . K_p{}^{\dagger}$. Therefore the coherency matrix T becomes

$$T = \frac{1}{2} \begin{pmatrix} \langle |S_{HH} + S_{VV}|^2 \rangle & \langle (S_{HH} + S_{VV})(S_{HH} - S_{VV})^* \rangle & 2\langle (S_{HH} + S_{VV}) \times S_{HV}^* \rangle \\ \langle (S_{HH} - S_{VV})(S_{HH} + S_{VV})^* \rangle & \langle |S_{HH} - S_{VV}|^2 \rangle & 2\langle (S_{HH} - S_{VV}) \times S_{HV}^* \rangle \\ 2\langle S_{HV} \times (S_{HH} + S_{VV})^* \rangle & 2\langle S_{HV} \times (S_{HH} - S_{VV})^* \rangle & 4\langle |S_{HV}|^2 \rangle \end{pmatrix} \tag{1-5}$$

1.5. Coherent and Incoherent Decomposition

The polarimetric information from an earth feature can give information on physical characteristics and geometrical structure of the feature under study. The polarimetric decomposition theorems express the total scattering mechanism from every imaged pixel as a sum of individual scattering mechanisms which may be present in the pixel. The objective of coherent decomposition is to express the measured scattering matrix synthesized by the radar as a combination of the scattering responses of simpler objects. The decomposition of scattering mechanisms using scattering matrix is only possible when the incident and the scattered waves are completely polarized and therefore coherent decomposition is only applicable to point or pure or coherent features. The different coherent decomposition techniques preserve the amplitude and phase, however gets exposed in the presence of speckle. Moreover, coherent decomposition techniques cannot be applied in case of natural dynamic and variable features like vegetation (e.g. forests).

The speckle noise must be reduced for decomposing individual scattering mechanisms present in every imaged pixel. Therefore only the second order derivatives of scattering matrix such as the coherency or

the covariance matrix can be used for analyzing distributed or incoherent targets. The main objective of incoherent decomposition is to separate these second order derivatives of scattering matrix as a combination of simpler scattering mechanisms for easier physical interpretation.

1.5.1. Freeman-III component scattering model (Incoherent Decomposition)

It is a physically based, three component scattering mechanism based model to fit the Polarimetric SAR observations, without utilizing ground truth. This model fit uses an equal number of parameters as input and scattering contribution as output. Freeman and Durden in [6] modelled the second order covariance matrix as a combination of three different scattering mechanisms. This model is used to describe the backscattering from naturally occurring scatterers [6].

- *Surface or single bounce scattering*- modelled by first-order Bragg surface scatterer
- *Double or even bounce scattering*- modelled from a pair or orthogonal surfaces with different dielectric constants.
- *Volume scattering*- where a canopy scatterer is modelled as a cloud of randomly oriented dipoles.

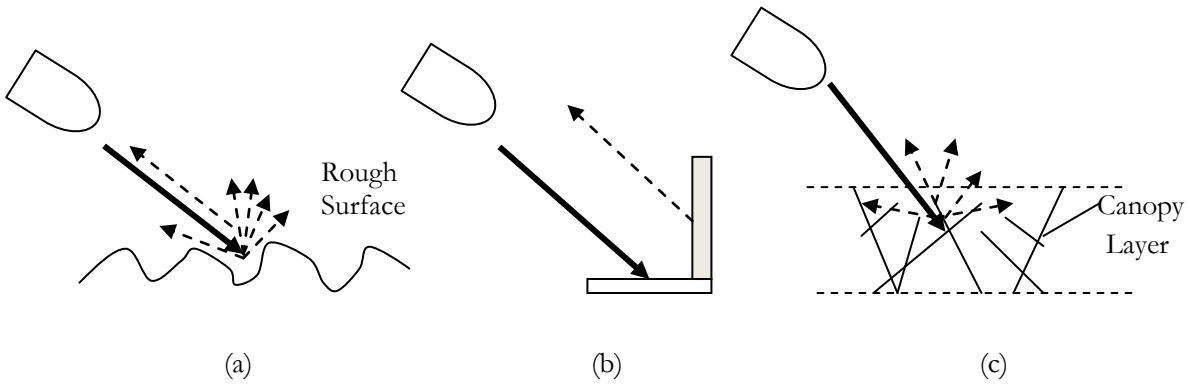

Figure 1-3: Scattering mechanisms (a) Single-bounce scattering (b) Double-bounce scattering and (c) Volume scattering.

1.6. Problem Statement

The 2 × 2 scattering matrix obtained after processing the fully-polarimetric SAR system contains values for all the four polarization channels and hence complete polarimetric scattering information at every imaged pixel [7]. This allows the polarimetric synthesis of any combination of H and V. Dual-pol polarization mode takes only half of the scattering matrix; thereby reducing the data processing requirements and the information content in the imagery [7]. Even though complete pixel information content is absent in dual-polarimetry, it collects a wider swath width (in case of ALOS PALSAR) when compared to quad-pol and therefore greater area coverage. The implementation of fully-polarimetric system requires the pulse repetition frequency ("transmission of interleaved polarizations") to be doubled which reduces the swath width [6], thereby reducing the area coverage. Another limitation of quadrature-polarimetric mode is the complexity in system design, antenna technology, data downloading and the high power consumption [8] which indeed has to be dealt critically when there is a high demand for fully-polarimetric data. Polarimetry has become an important utility in geosciences applications. Even though fully-polarimetric data is useful for characterizing point target, applications based on the analysis of

features containing multiple scattering mechanisms (for example, in case of forests and vegetation cover with their complex structure), yield redundant information from the scattering matrix [9]. The solution for these above mentioned limitations was suggested by Souyris et al. [10], where they introduced a compact dual-polarimetric mode named as Compact polarimetry, in which the transmitted polarization is either right circular or left circular (CLTR mode) with 90° phase angle between vertical and horizontal components and the ellipticity $\chi = \pm 45°$ or linearly polarized with an orientation angle of $\psi = 45°$ ($\pi/4$ mode) and both vertical and horizontal polarizations were received simultaneously [8].

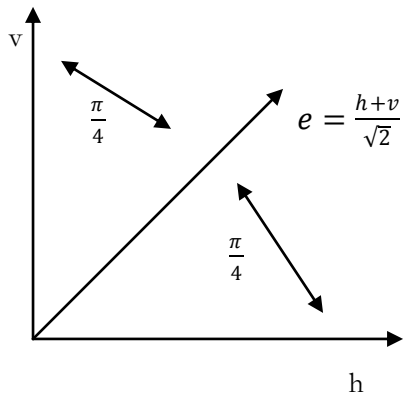

Figure 1-5: Compact polarimetry ($\pi/4$ mode).

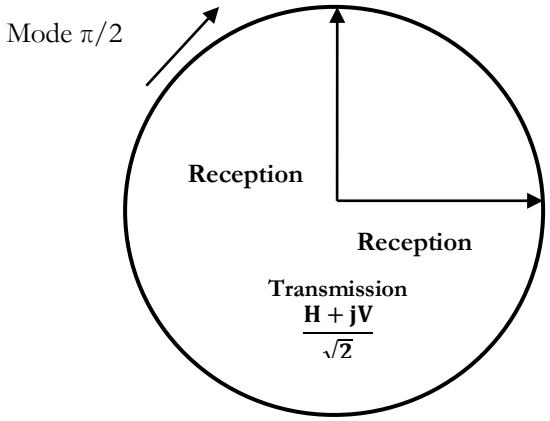

Figure 1-4 Compact polarimetry ($\pi/2$ mode)

Compact polarimetry involves the reconstruction of fully polarimetric quadrature polarized data from dual polarized mode. Compact polarimetric systems use fixed transmitter polarization state, while the dual channel coherent receiver configuration is maintained [4], whereas fully polarimetric systems allow transmission and reception in dual channel. The limitations of using fully-polarimetric data like data downloading, data volume, issue of pulse repetition frequency, complexity in system design and antenna technology can be reduced by using compact polarimetry technique. Studies have already been carried out in [10], [11], which reconstructs pseudo-quadrature polarized data from dual pol mode using the 2×2 covariance matrix obtained from the scattering vectors for compact polarimetry mode. The algorithm for reconstructing the fully-polarimetric information using 3×3 covariance matrix has already been developed in [11]. The complexity in the scatterer information present in a pixel, may lead to randomness in scattering which is represented as entropy values. Entropy indicates the degree of disorder of the polarimetric response. The value of entropy lies between 0 and 1. Entropy will be low, if there is a dominant scatterer and entropy values will reach maximum when there are different scattering mechanisms present in a single pixel and thereby making it difficult to extract a dominant fully polarized signature from the measurements [1].

Studies have been carried out in retrieving information on volume, surface and double-bounce scatterers from covariance matrix for compact polarimetry technique using different reconstruction algorithms and thereby assessing the performance of SAR compact polarimetry mode [10]. The extraction of quad-pol data using coherency matrix and its effect on volume scatterers from forest features like leaves, branches and tree trunk using Freeman-III component decomposition model has not been implemented and assessed. The coherency matrix accounts for local variations in the scattering matrix and it are suitable to extract the different polarimetric parameters [12] for distributed complex scatterers in the presence of speckle [13]. Moreover the coherency matrix is sensitive to orientation angle shift. These shifts produce higher cross-polarization intensity and makes coherency matrix reflection asymmetric [14]. Hybrid polarimetry technique can also be utilized for planetary science applications. Chandrayaan-1 mission

launched by ISRO in 2008, used Miniature SAR (MiniSAR) as the payload with hybrid polarimetry ($\pi/2$ mode) option for detecting water ice in the permanently shadowed regions on the lunar poles [15]. From a researcher's point of view, this technique using the coherency matrix approach can become an important subject of investigating the different aspects in forestry applications such as mapping of forest floods, forest cover types, deforestation aspects, mapping of fire scars and extraction of multilayer topographic information over forest areas using compact PolInSAR techniques.

1.7. Research identification

1.7.1. Research Objective

The prime focus of the present study is to explore the potential of compact polarimetry ($\pi/4$ mode) technique, to derive pseudo quad polarimetric information from dual polarimetric mode, using coherency matrix approach.

1.7.2. Sub-objectives

1. To reproduce 3×3 pseudo quad polarimetric coherency matrix from dual polarimetric mode using compact polarimetry techniques
2. To study and assess the backscatter contribution of volume scatterers (tree branches, leaves and stem) decomposed from 3×3 coherency matrices of compact polarimetric and fully polarimetric modes, using Freeman-III scattering model.

1.7.3. Research Questions

The research objectives and the associated sub-objectives have to be answered from the research questions framed below:

1. How, pseudo-quadrature polarimetric 3×3 coherency matrix can be derived and reproduced from dual polarimetric mode using compact polarimetric technique?
2. What is the relation between the entropy obtained from the fully polarimetric data and the entropy obtained from compact polarimetry mode?
3. How to validate the volume scatterer contribution of compact polarimetric data against the fully polarimetric data?
4. What is the accuracy of the estimated volume scatterer contribution obtained from compact polarimetry mode against to that obtained from fully polarimetric data, using Freeman-III model?

1.8. Thesis Structure

The whole thesis has been divided into eight chapters. The first chapter gives an overview of the major elements covered in this research work, problem statement, research objectives, sub-objectives and research questions. The second chapter on literature review presents information on the related works with respect to the research work. The third chapter gives information on the study areas chosen. The data used and the methodology has been detailed in the fourth chapter. The fifth chapter has been dedicated for explaining the modelling theory. The sixth chapter is devoted for explaining the results obtained from the methodology through different data analysis. The detailed discussion on the results obtained and observations from the research has been described in the seventh chapter. The thesis concludes with recommendations in a capsule in the last chapter.

2. LITERATURE REVIEW

2.1.1. Radar Remote Sensing

RADAR stands for Radio Detection and Ranging and it was developed to detect the presence of earth features using radio waves and to determine their distance and angular position [16]. Radar remote sensing utilizes microwave region of Electromagnetic spectrum from 1 mm to 1.3 m [1] wavelengths. The amount of signal received by the radar system from a particular earth feature is given by the radar equation [1].

$$W_R = \left(\frac{W_t G_t}{4\pi R^2}\right)\sigma\left(\frac{1}{4\pi R^2}\right)A_r$$

Here W_R is the received power, W_t is the transmitted power, G_t is the gain of the transmitting antenna, R is the distance from radar to the target, σ is the effective backscatter co-efficient and A_r is the effective aperture of the receiving antenna. The parameters which affect the radar return are related to system and target parameters [17]. The different target parameters are surface roughness, complex dielectric constant, slope angle and orientation. The different system parameters which influence the radar return are wavelength or frequency, look angle, look direction, polarization and resolution [4]. Among all the system parameters, wavelength and polarization are the two important principle components which affect the transmission characteristics.

Frequency or wavelength (Table 8 in Appendix I) is an important component since it influences the depth of penetration of the EM wave. As the wavelength increases the penetration level increases and helps to obtain information about the surface below the earth upto a particular depth [1]. When the wavelength factor combines along with different target parameters such as dielectric constant of the object, surface roughness, there will be variation in the radar backscatter depending on the remote sensing application [18].

2.1.2. SAR Polarimetry

The importance and potential of radar polarimetry for problems in remote sensing with real and synthetic aperture radar, inverse scattering, radar meteorology, target decomposition and classification were understood and investigated in the past few decades [19]. Electromagnetic waves, due to its intrinsic vector nature as its unique property, and which provides the complete description of propagation and scattering phenomena, requires the concept of wave polarization.

SAR polarimetry (PolSAR) is the technique that is concerned with the acquisition, synthesizing and analyzing the polarization state of an electromagnetic wave. Therefore, depending on the different modes of polarization, matrix formulation (scattering matrix) can be generated which can be used to synthesize the radar return with any transmit/receive polarizations and thereby measuring the complete information of target. The concept of scattering matrix as a fundamental descriptor for characterizing a coherent scatterer was developed by Sinclair [20], [21]. He studied the system properties which transmit polarized waves of different ellipticity and orientation angles and devised methods for measuring and assessing the

performance by defining a parameter which specifies the polarization specifications of the transmitting or receiving polarized wave.

Kennaugh [22], [23] introduced the concept of optimal polarizations and formulated a theory based on the backscattering of Eigen polarizations of the scattering matrix. Huynen [24] capitalized on exploited Kennaugh's optimal polarization concept developed in [23] and formulated the same concept to target radar phenomenology. He also developed the concept of "*orthogonal (group theoretic) target scattering matrix decomposition"* [24]. Boerner [25] pointed out the importance of polarization first in conceptualizing inverse scattering property of electromagnetic vector. He analyzed the work done in [23], [24] and also extended the theories formulated by them. Boerner et al. [26] summarized the concept formulation of the 2×2 coherent Sinclair matrix and the associated 4×4 Kennaugh power density matrix. Stokes introduced the concept of Stokes parameters in [27], where he described the partially polarized waves in terms of observable power instead of amplitude and phase

$$\begin{bmatrix} S_0 \\ Q \\ U \\ V \end{bmatrix} = \begin{bmatrix} |E_v|^2 + |E_h|^2 \\ |E_v|^2 - |E_h|^2 \\ 2Re\{E_v {E_h}^*\} \\ 2Im\{E_v {E_h}^*\} \end{bmatrix} = \begin{bmatrix} S_0 \\ S_0 \cos 2\psi \cos 2\chi \\ S_0 \sin 2\psi \sin 2\chi \\ S_0 \sin 2\chi \end{bmatrix} \quad (2\text{-}1)$$

Here S_0 in equation (2-1) is a measure proportional to the total intensity of the EM wave, E_v and E_h are the vertical and horizontal components of the electric field vector. Q is equal to the power in the horizontal linear or vertical linear polarization components of the plane wave vector [28]. U is equal to the power of the linearly polarized components with an orientation angle (ψ) of $45°$ or$135°$. V is equal to the power in the circular polarized component in the plane wave [28].

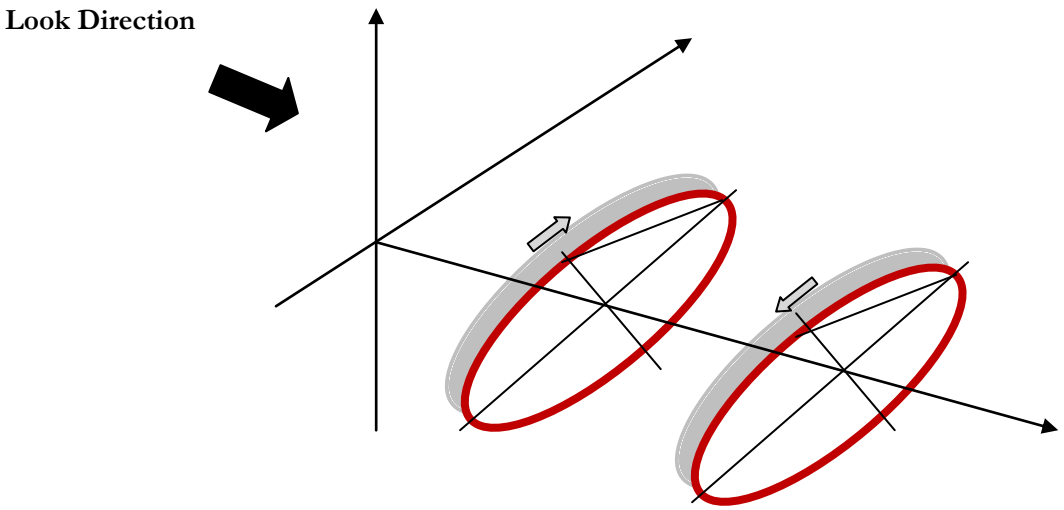

Figure 2-1: Polarization Ellipse- Rotation Sense

Pottier gave the concept of distinguishing characteristics of the polarization ellipse between right-handed (clockwise) and left-handed (counter-clockwise) when viewed in direction of the travelling wave for horizontal (H) and vertical (V) polarization states (figure: 2-1). Pottier also provided the conceptual idea of linear, elliptical and circular polarizations based on the ellipticity and orientation angle values in polarization ellipse.

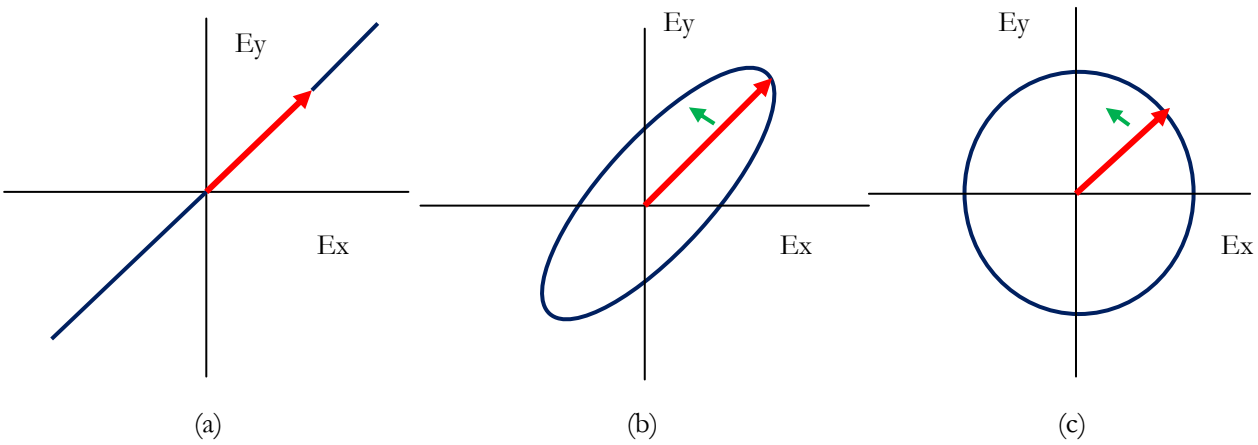

Figure 2-2: (a) Linear Polarization (b) Elliptical polarization (c) Circular polarization

The figures 2-2 (a) (b) and (c) represent linear, elliptical and circular polarizations, with the green arrow indicating the rotation of the electric field vector. The red arrow indicates the electric field vector and the locus traced by the tip perpendicular to the propagation direction represented by blue. The orientation angle of the EM wave (polarization ellipse) is the angle between the semi-major axes from the positive horizontal axis measured in the counter clockwise direction. The orientation angle ranges from 0° to 180°. Ellipticity or eccentricity represents the shape parameter, which describes the degree to which the shape of the polarization ellipse is oval and takes values between -45° to +45°. The polarization ellipse will become a straight line (0 ellipticity and polarization "linear"), when the phase angle between the horizontal and vertical components is 0 or π radians. If the orientation angle is 0° or 180° with 0 ellipticity, then the polarization is horizontal linear, while if the orientation angle is 90° with same ellipticity, then the polarization is vertical linear with zero horizontal component [3]. If there is a 90° phase angle between horizontal and vertical components, then the ellipse becomes a circle. Here the ellipticity is 45° even though the orientation angle is not defined. An ellipticity of +45° represents left circular polarization and -45° represents right circular polarization

In complex radar systems, the antennas are designed to transmit and receive EM waves for more than single polarization [5]. Since the object under study after backscattering can change the polarization state of the incident wave, radar systems are designed to receive different polarization components of the EM wave at the same time. Therefore, a radar system using H and V linear polarizations can have four different polarization channels [1].

- HH - Horizontal transmit, Horizontal receive
- VV - Vertical transmit, Vertical receive
- HV - Horizontal transmit, Vertical receive
- VH - Vertical transmit, Horizontal receive

HH and VV combinations are referred to as like-polarized while HV and VH are referred to as cross-polarized combinations. Based on the complexity, a radar system can be designed for different levels of polarizations.

- Single Polarized - HH or HV or VH or VV
- Dual Polarized - HH and HV or VV and VH or HH and VV
- Quad Polarized - HH and HV and VH and VV

2.1.3. Scattering Matrix, Covariance and Coherency Matrix

Fully-polarimetric radar transmits horizontal (H) and vertical (V) polarized waves which are orthogonal to each other and receives the backscattered portion of the electromagnetic wave in four polarization channels i.e. HH, VV, VH and HV where both the amplitude and relative phase values are measured. The measured values from these four channels represent all the information in the form of a 2×2 scattering matrix which is needed to measure the polarimetric scattering properties of the earth surface [1]. This matrix can be used to synthesize the radar return with any transmit/receive polarizations and thereby measuring the complete information of target. The scattering matrix is given by the expression

$$\begin{bmatrix} E_H^S \\ E_V^S \end{bmatrix} = \begin{bmatrix} S_{HH} & S_{HV} \\ S_{VH} & S_{VV} \end{bmatrix} \begin{bmatrix} E_H^I \\ E_V^I \end{bmatrix} \tag{2-2}$$

Here E_H^S and E_V^S in equation (2-2) represents the horizontal and vertical components to describe the backscatter properties of the target, whereasE_H^I and E_V^I represents the same for an incident wave. The elements of the scattering matrix are known as the complex scattering amplitudes. In case of monostatic radar (system where the receiving antenna is co-located with the transmitting antenna), the reciprocal property is assumed. This means that $S_{HV} = S_{VH}$. The scattering matrix now becomes symmetrical and has only 3 independent elements [4]. The incident and the scattered wave field can be represented by the scattering matrix [29]. The scattering matrix can only be used effectively to obtain information in case of pure or coherent targets which doesn't contribute in complex scattering mechanisms. In case of presence of complex or multiple targets in a single resolution cell, the radar cross section which is the effective area of backscatter is by contributed by complex scattering mechanisms [29]. Therefore the partially polarized waves cannot be used for characterizing the information content in a scattering matrix. Thus the second order derivatives [1] of scattering matrix - covariance matrix and coherency matrix has to be used [30].

In order to extract the physical information from the polarization description of the earth feature, a new formalism was developed by constructing target vector of the scatterer which is the vectorized form of the scattering matrix given by:

$$k = V([S]) = \frac{1}{2} Trace\ ([S]\varphi) \tag{2-3}$$

Here $V(.)$ is the vectorization operator, φ is a set of 2×2 complex basis matrices which are orthonormal under a Hermitian inner product and $Trace\ (.)$ is the sum of the diagonal elements of the argument. Pauli and Lexicographic basis sets are two among the several basis sets which can be formulated using the above principle. Lexicographic basis set is given by the expression

$$\varphi_L : 2\left\{\begin{bmatrix} 1 & 0 \\ 0 & 0 \end{bmatrix}, \begin{bmatrix} 0 & 0 \\ 1 & 0 \end{bmatrix}, \begin{bmatrix} 0 & 1 \\ 0 & 0 \end{bmatrix}, \begin{bmatrix} 0 & 0 \\ 0 & 1 \end{bmatrix}\right\} \tag{2-4}$$

Pauli basis set is given by the expression

$$\varphi_P : \sqrt{2}\ \{[\sigma_i]\}, i = 0, 1, 2, 3$$

Where in

$$[\sigma_0] = \begin{bmatrix} 1 & 0 \\ 0 & 1 \end{bmatrix}, [\sigma_1] = \begin{bmatrix} 1 & 0 \\ 0 & -1 \end{bmatrix}, [\sigma_2] = \begin{bmatrix} 0 & 1 \\ 1 & 0 \end{bmatrix}, [\sigma_3] = \begin{bmatrix} 0 & -j \\ j & 0 \end{bmatrix} \tag{2-5}$$

The lexicographic format assuming reciprocity condition $S_{HV} = S_{VH}$ is given by

$$K_L = \begin{bmatrix} S_{HH} \\ \sqrt{2}\, S_{HV} \\ S_{VV} \end{bmatrix} \tag{2-6}$$

The Pauli format assuming reciprocity condition is given by

$$K_P = \frac{1}{\sqrt{2}} \begin{bmatrix} S_{HH} + S_{VV} \\ S_{HH} - S_{VV} \\ 2\,S_{HV} \end{bmatrix} \tag{2-7}$$

The covariance and coherency matrices are obtained from Pauli and Lexicographic basis scattering vectors which are generated from scattering matrix [31]. The covariance matrix is generated by multiplying the Lexicographic scattering vector form of scattering matrix with its transpose, while the coherency matrix using Pauli basis vector form [32]. The covariance matrix can be converted to coherency matrix using a unitary similarity transformation matrix [33]. These matrices represent the mathematical description of the complex state of the scatterer and provide information about the geometrical characteristics of the earth feature acquired by the radar [34]. The target vector is then used to generate the 3×3 Hermitian coherency matrix [33]. The coherency matrix is obtained by multiplying the Pauli basis vector with its complex conjugate transpose represented by $\mathrm{T} = K_P . K_P{}^{\dagger}$.

$$[T] = \begin{bmatrix} 2A_0 & C - jD & H + jG \\ C + jD & B_0 + B & E + jF \\ H - jG & E - jF & B_0 - B \end{bmatrix} \tag{2-8}$$

Here $A_0, B_0, B, C, D, E, F, G$ and H are the Huynen parameters which reflect the physical source of correlation effects in the earth feature [13]. The nine parameters of the 3×3 coherency matrix are essential for general feature analysis without any model reference and are thereby useful for obtaining real physical target information [24]. The parameters $A_0, B_0 + B \; and \; B_0 - B$ called as the target generators. They are directly related to the symmetry, irregularity and non-symmetrical physical characteristics in case of a pure coherent scatterer or related to the surface, the double-bounce and the volume scattering mechanisms in case of distributed scatterers present in natural media [13].

2.1.4. Compact Polarimetry

The different polarimetric configurations, the single polarimetric mode (HH or VV), dual (HH/HV or VV/VH), alternating (HH/VV), and quadrature or full (HH/HV/VH/VV) polarimetric modes are recognized as the *classical* modes, since all the past and present SAR systems for earth observation purpose have been operating in one or more of these modes. A more general concept of polarimetry has emerged based on the transmission and/or reception of polarization states different from the usual H or V state [11]. There are three classes defined for the new concept. The first class is referred to as *Hybrid polarimetry* where the transmission is circular; with a linear reception [35]. The Hybrid mode comprises of circular compact polarimetry and with interleaved left and right transmission, which leads to the quad-hybrid mode reception [35]. The second class of this special case of compact SAR architectures is the *circular polarimetric mode*, whose transmission and reception is circular polarized. The third class referred to as *Compact Polarimetry* or *Partial polarimetry*, is a special case of dual polarized mode in which the transmitted polarization is either right circular or left circular with 90° phase angle between vertical and horizontal components and the ellipticity $\chi = \pm 45°$ or linearly polarized with an orientation angle of $\psi = 45°$ and both vertical and horizontal polarizations were received simultaneously [8].

Table 1: Compact SAR modes vs. Classical Modes

		RECEPTION					
		H	V	H,V	Linear 45°	Circular	Circular L,R
TRANSMISSION	H	Single	-	Dual	-	-	-
	V	-	Single	Dual	-	-	-
	H,V	Alternating		Full or Quad	-	-	-
	Linear 45°	-	-	Compact	-	-	-
	Circular	-	-	Compact-Hybrid	-	-	Dual-Circular
	Circular L,R	-	-	Quad-Hybrid	-	-	Quad-Circular

Table 1 shows the classification of compact SAR modes in contrast with the classical SAR modes. The classical modes are shown in cream colour, compact-polarimetry modes shown in green colour, hybrid polarimetry modes shown in red colour and circular polarimetric modes shown in yellow colour. In Radar meteorology, experiments involving inventive dual polarimetry started 40 years ago which included transmitting "slant" linear polarization at an angle of 45° relative to horizontal direction or circular polarization and receiving orthogonal linear polarizations [38].

The first impression of the compact polarimetry concept which appeared in SAR literature was in 2002 when Souyris and Mingot [11], assessed polarization duality in reception for a SAR which transmits only single polarization. They developed an algorithm for reproducing the fully-polarized data using the covariance matrix. A procedure was developed to estimate the fully polarimetric information of distributed earth features using the compact polarimetric approach, where they assumed that the correlation between co-polarized and cross-polarized terms is equal to zero.

The extent to which pseudo-quad pol data can be reconstructed from the covariance matrix using the different compact polarimetry modes was studied by Souyris et al. [10]. They assumed reflection symmetry and a mathematical relationship between linear coherence and cross-polarized (S_{HV}) ratio to reconstruct the pseudo quad-polarized ($S_{HH}, S_{HV}, S_{VH}, S_{VV}$) data, using the polarization state extrapolation algorithm. While comparing the performance of reconstructed data and the fully polarimetric data for analysis of point targets in Landes forest area in France and Flevoland in USA using L-band SIR-C/XSAR and JPL AIRSAR images, the classification accuracy of $\pi/4$ mode was found to be comparable with fully-polarimetric mode. The study proposed future improvements including proper calibration scheme which includes Faraday rotation, system channel cross-talk, amplitude imbalance corrections, refinement of power budget and detailed signature studies for $\pi/4$ mode [10].

Raney [35] proposed Hybrid-polarity architecture which consists of transmitting circular polarization and receiving orthogonal linear polarizations on mutually-coherent channels, given a dual polarized antenna and a spaceborne SAR. He suggested that using the resultant data from the system is sufficient to derive all four Stokes parameters from which the circular-polarization ratio may be calculated along with several other quantitative image domain characterizations. It also helps to characterize the backscattering

mechanism under circular polarized condition completely. The hybrid polarity architecture proposed was meant for planetary applications thereby leading to simpler and capable radar hardware in comparison with contemporary dual polarized (circular) system**.** Through sensitivity analysis, he also showed that circular-polarization ratio calculated from hybrid polarimetry was less sensitive to channel imbalance by a factor of two when compared to traditional calculation. The architecture was characterized by several advantages such as Stokes parameter data products, comparable signal levels, error sensitivity and less risk of cross talk [36]. Raney also concluded that $\pi/2$ mode is advantageous over $\pi/4$ mode due to target rotational invariance and system optimization factors.

Nord et al. [37] studied on reconstructing quad-pol data using $\pi/2$ mode (Circular transmit, linear receive). They compared the performance of different compact polarimetric modes using the covariance matrix. They also modified the reconstruction algorithm proposed in [11] to show enhancements in the generated pseudo-quadrature polarised data. It was concluded that of the three compact polarimetric modes, $\pi/4$ mode showed improved results in terms of relative error and standard deviation parameters [37]. The data analysis from all the three compact polarimetric modes suggested that the assumption of reflection symmetry removes all possibilities of estimating orientation angle of the scatterers. Compact polarimetry is also useful for terrain classification roles where spatial averaging becomes a less difficult problem and the results of the statistical properties of large homogeneous regions are desirable.

Lavalle [9] investigated the potential of the compact polarimetric and interferometric SAR for estimating forest height. His main objective was to develop a general framework for comparison between full and compact PolInSAR data over forest areas using fully polarimetric data. He demonstrated the RVoG inversion model (two layer inversion model used for estimating the vegetation height using PolInSAR data) using ALOS PALSAR data through a systematic approach starting from detailed processing of raw data and then performing the complete basic SAR polarimetric and interferometric algorithms for subsequent ingestion in model-based inversion procedures [9]. He debated that compact polarimetry may not represent a substitute for fully polarimetric mode, especially not for all earth based applications. He showed that the reconstruction of the HH, VV and HV polarimetric channels is almost well preserved satisfying the reflection symmetry condition. He also investigated based on the increased accuracy of height retrieval based on coherence region enlargement by PolInSAR reconstruction in the complex plane.

Ainsworth et al. [7] inter-compared the polarimetric content of dual-polarimetric imaging modes and dual-polarimetric imaging extended by polarimetric scattering models. They compared Wishart classifications [4] for both the partial polarimetric and the fully-polarimetric datasets. From the analysis of different polarimetric modes, the study concluded that true quad-polarimetric data produced the most accurate Wishart classifications, while standard linear dual-polarimetric data yielded the poorest results. In between these two extremes are the compact polarimetric modes (the CTLR and $\pi/4$ modes) and the pseudo-quadrature polarimetric data generated from polarimetric scattering models. The analysis of the study done in [7] showed degradation of the method for mixtures of the volume, the dihedral and the surface scattering mechanisms. It was found from the classification results that the hybrid dual-polarimetric modes (CTLR and $\pi/4$ modes) perform better (not always) than the standard linear dual-polarimetric modes.

Charbonneau et al. [38] evaluated the compact polarimetry mode configuration for different applications such as soil moisture estimation, crop identification, ship detection, and sea-ice classification conducted by Government of Canada. The implications of the results obtained after evaluation were also discussed for future SAR missions such as the Canadian RADARSAT Constellation Mission, the American DESDynI, and India's RISAT [38]. From the study based on different scattering mechanisms affected by the compact

polarimetric mode, the main conclusion drawn was that radar must transmit circular polarization, if the backscattered field has to be rotationally robust related to the geometric aspects of the image scene under study provided the objectives of the image analysis include feature discrimination between single and double bounce scatterers that have random orientations. The data from quadrature-polarized radar can be transformed to any form of compact polarization which follows directly from the fundamental principle of polarization synthesis. The analysis revealed that the compact polarimetric combinations could not achieve the accuracy of Cloude-Pottier or Freeman-Durden decomposition parameters, with Stokes parameters as the exception. The four Stokes parameters produced early season crop classification accuracy for any fully-polarimetric or compact polarimetric dataset [38]. The study from the crop classification concluded that, a compact polarimetric mode capable data acquisition with large swath width is able to produce accurate early season and end-of-season crop classifications [38]. For ship detection application, the quadrature-polarimetric system provided the best detection among all the other systems considered, while the dual-polarimetric and simulated left circular polarimetric mode provided better detection than the single-channel systems. A dual-polarized system such as left circular-polarimetric mode should provide wider swath coverage than a quad-polarized system for ship detection application.

Raney [39] obtained patent for synthetic aperture radar hybrid-quadrature polarity architecture and method by transmitting both left and right circular polarizations with minimum Nyquist sampling rate, orthogonal linear feeds simultaneously by two identical waveforms $\pm$ 90° out of phase and receiving two orthogonal linear polarizations [39]. He suggested that for $\pi/4$ and circular polarization modes are useful for important applications such as planetary geology including lunar surface characterization in which the decomposition should be able to classify dihedral like scattering features irrespective of orientation. The study added the advantages of the resultant hybrid polarity architecture, which included minimizing sensitivity to relative errors and cross-talk, amplitude and phase calibration, simpler system with less RF hardware, low mass and low power consumption, increased swath width when compared to the fully-polarimetric system, minimized level of range ambiguities which helps in extending range swath and incident angle of the system [39].

2.1.5. Polarimetric Decomposition

The polarimetric information from an earth feature may contain the geometric and physical characteristics of the feature under observation. The polarimetric target decomposition theorems express the average scattering mechanism as a sum of individual and independent scattering mechanisms [4]. These theorems exploit the phase information contained in the data and may be used for classification and target recognition purposes. The two types of decomposition techniques are coherent decomposition, which deals with the scattering matrix and incoherent decomposition, which works on coherency or covariance matrices [40].

The radiative transfer theory developed by Karam and Fung [41] assumed that the particles scatter independently. The canopy was modelled as a two layered medium above the rough interface, where the upper layer stands for forest crown with the leaves are modelled as randomly oriented distributed discs and needles for deciduous and coniferous forests and the branches modelled as randomly oriented finite length dielectric cylinders [41]. The lower layer which contained the tree trunks were modelled as vertical cylinders, positioned randomly above the rough soil. The total backscattering coefficients were conveyed in terms of the backscattering amplitude tensors of leaves, branches, trunks and soil [41].

Kroagager decomposition [4] which is another type of coherent decomposition, asserted that scattering matrix, which is altered by a rotation operator to balance the misalignment between the antenna and the target orientation, can be modelled as a combination of sphere, oriented diplane and a right or left wound

helix [42]. The simulated feature consisted of uniformly spaced and evenly strong single scatterers in the form of spheres, diplanes, wires and helices with different orientation angles [42].

Cloude and Pottier [43] employed Eigen value analysis of the coherency matrix and employed a three level Bernoulli statistical model which generated the average target scattering matrix parameter estimates from the radar data. The study assumed that there will always be a dominant average scattering mechanism present in every imaged pixel and from there; the parameter estimation was carried out. The Eigen value is basis invariant and therefore these estimates give the statistical independence between the target vectors [43]. The advantage of this decomposition technique was that, it gave a formal connection between the signal processing concepts and that the noise can be estimated from the covariance matrix [43].

Durden et al. [44] developed a model for L-band microwave backscattering from a forest area, where they modelled the forest surface as rough dielectric surface above which, there was a layer of tree trunks represented by vertical dielectric cylinders. The tree branches were represented by randomly oriented cylinders and using these assumptions, several scattering mechanisms were identified and calculated the corresponding Stokes matrices, which in turn combined to give the total Stokes matrix and resulting polarization signature [44].

Freeman and Durden [45], [46] suggested that polarimetric radar backscatter models which were developed for naturally occurring terrains and man-made features are highly complex and require large number of input parameters such as tree height and diameters, tree density, leaf size and angular distribution, ground roughness, trunk dielectric constants to predict the observed radar backscatter. The study described a new technique which fit a model using three scattering mechanisms: the volume scattering, modelled from a cloud of randomly oriented dipoles, the even or double-bounce scattering, modelled from a pair of orthogonal surfaces with different dielectric constants and the odd or single bounce scattering, modelled from a Bragg scatter from a moderately rough surface [45]. The new model was able to estimate the overall contribution for each of the three scattering mechanisms for every SAR imaged pixel. The number of input parameters (radar backscatter measurements) and the output parameters (backscatter contributions from all the three scattering components and the two additional parameters) were the same. It was assumed that for all the backscatter components, the co-polarized and cross-polarized radar returns were uncorrelated and the backscatter is reciprocal. The model used in [45] study predicted that, for upland forest areas, the dominant scattering mechanism was volume scattering for P, L and C-band frequencies. There is only less than 20% contribution from double-bounce scattering mechanism at P-band, none at L and C-bands. In case of the surface scattering, it was found that it was very low at P-band, but with ~20% contribution for C-band return. The model employed in [46] fitted well for tropical rain forest over a wide range of incidence angles. The study showed that there is an increase in the surface scattering contribution for L and P-band at lower incidence angles. There was a slight decrease in the even-bounce scattering contribution at P-band for incidence angles either side of 40°.

Yamaguchi et al. [47] extended the three component decomposition model proposed by Freeman and Durden [45], [46], by adding a fourth component, the helix scattering to take in account of the co-polarized and cross-polarized correlations which normally appears in complex urban scattering and lacking for natural terrains. The reflection symmetry condition which was assumed for three component model does not hold for helix scattering, since there is a major presence of the co-polarized and the cross-polarized correlations in case of urban scattering.

Zhang et al. [48] proposed multiple component scattering model (MCSM) which was the expansion of three and four component scattering model developed in [45], [46] and [47] described the single-bounce, the double-bounce, the volume and the helix scattering mechanisms. The MCSM was developed by adding an additional scattering mechanism, the wire scattering. The wire scattering was described by a characteristic scattering matrix of the canonical thin wire target represented as a function of the orientation angle around the radar line of sight [48].

2.1.6. Polarimetric Scattering Entropy

The complexity in the scatterer information present in a pixel may lead to randomness in scattering which is represented as entropy values. Entropy indicates the degree of disorder of the polarimetric response. The value of entropy lies between 0 and 1. Entropy will be low, if there is a dominant scatterer and entropy values will reach maximum when there are different scattering mechanisms present in a single pixel and thereby making it difficult to extract a dominant fully polarized signature from the measurements [1]. Entropy (H) provides a resourceful and appropriate basis-invariant parameter in order to define the degree of statistical disorder of each distinct scattering mechanism present in the ensemble and is given by [28].

$$H = -\sum_{k=1}^{N} P_k \log_N P_k$$

Here P_k represents the pseudo-probabilities obtained from Eigen values λ_k and N is the logarithmic basis which depends on the polarimetric dimension (N=3 in case of monostatic and N=4 for bistatic case). If polarimetric entropy H is low (H<0.3), then the system can be considered as weakly depolarizing and the dominant scattering mechanism in terms of a specifically identifiable coherent scatterer may be found [28]. When entropy becomes high, the number of feature classes which can be distinguished from the SAR observations get reduced and even the target scattering may become a truly random noise process.

2.1.7. Polarization Signature

The radar backscatter from a particular area may consist of superposition of number of waves from different polarizations [49]. Since the incident wave can take up different polarizations and the scattering matrix consists of complex numbers, it may be helpful to have a graphical or visual method to plot the response of the earth feature as a function of incident and received polarizations. One such method is using "polarization signature" of the earth feature.

The scattering power from the earth feature can be calculated as a function of incident orientation angle ψ and ellipticity χ and backscattered orientation angle ψ and ellipticity χ. In order to simplify this graphical method using too many variables, the backscattered polarization was restricted to the calculation of co-polarized and cross-polarized responses for each incident polarization, represented in two surface plots called co-pol and cross-pol signatures [3]. The incident electromagnetic wave can have an electric field vector with orientation angle ψ between 0° to 180° and ellipticity between -45° to +45°. These variables are plotted in a 3D graph with synthesized radar cross section as a function of orientation angle along the y-axis and ellipticity along the x-axis [50]. For incident polarization with unit amplitude, the co-polarized or cross-polarized power of the backscattered wave is represented along the z-axis. The polarization signature plot is often normalized to a peak value of one.

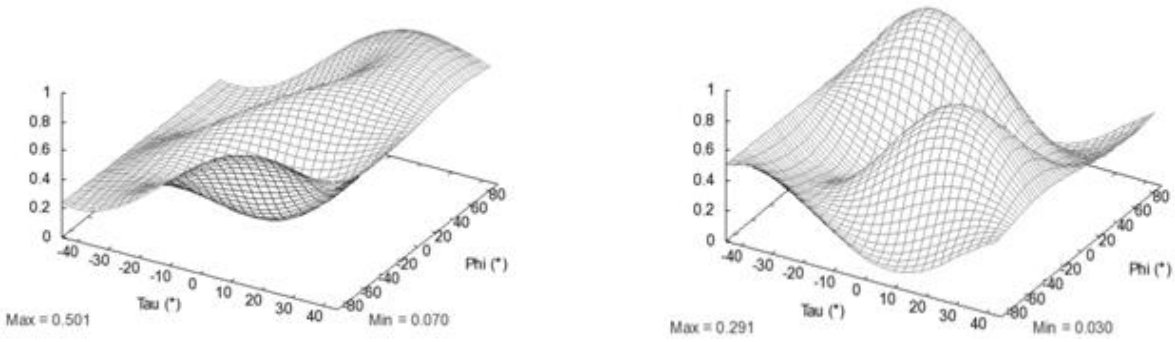

(a) (b)

Figure 2-3: Polarization signature (a) Co-polarization channel (b) Cross-polarization channel

The figures 2-3 (a) and (b) represents an example for polarization signature for co-polarized and cross-polarized channels from a SAR imaged pixel representing a particular earth feature. The values represented in "Max" and "Min" tags shows the minimum and maximum received power useful for calculating the co-efficient of variation parameter, which is the ratio of minimum received power to the maximum received power. The polarization signature takes different shapes for different earth scatterers depending on their complexity in scattering mechanism. The pedestal height is an important parameter that is obtained from polarisation signature. It is defined as the minimum value of the backscattered intensity, when the maximum response is normalized to unity [3]. The height of the pedestal indicates the presence of unpolarized scattering component present in the backscatter. This can be related to degree of polarization of the backscattered wave. If the radar backscatter is from a discrete scatterer with the fully-polarized backscatter, then the value of the pedestal is zero or close to it. If there are more scattering mechanisms present in a single pixel, then unpolarized component will be more and therefore the value of the pedestal becomes non-zero.

Evans *et al.* [49] studied that, small co-efficient of variation results in large difference between maximum and minimum received powers and therefore the scattering mechanisms of the averaged pixels are relatively similar and also the signal to noise ratio also becomes high. The presence of multiple scatterers in a single pixel can also increase co-efficient of variation thereby increasing randomness in scattering mechanism which causes a "pedestal" in polarisation signature [50]. The study also proved that, in forest areas with high randomness, the co-efficient of variation increases with increase in vegetation height and density, which happens due to increased scattering from randomly oriented vegetation.

2.2. Literature Review Conclusion

The past major study done on compact polarimetry has been reviewed in this chapter. The main works involved reconstruction of the pseudo-quad polarized data from the dual-polarized mode based on covariance matrix and various classification techniques employed on different study areas after reconstruction procedure. Most of the works have not concentrated on decomposition techniques after reconstruction. After reviewing the works done by eminent researchers on compact polarimetry, it was found that there is still a research gap especially in exploring the possibility of reproducing the pseudo-quad polarized data from the dual-polarized mode using coherency matrix approach. The potential of compact polarimetry to reproduce based on coherency matrix will be explored in this research.

3. STUDY AREA

3.1. Barkot Forest Area

3.1.1. Introduction

The first site chosen for the study swathes a part of Uttarakhand State, located in North India. The total area of around 1800 km^2 lies between 30.45 Northern latitude, 29.81 south latitude and 78.34 east longitude, 77.94 west longitudes. The major towns Haridwar, Rishikesh, Thano and Dehradun lie within this extent. The other small towns Bulawala, Jwalapur, Lal Dhang etc. have their own contributory impact for the overall development of the state.

3.1.2. Attributes and Scientific Importance of this area

This region falls under the Shivalik range of Himalayas. River Ganges emerges from the mountains to touch this region. Hence, due to the presence of agricultural patches of wheat, sugarcane, maize and bajra, the region has gained national importance due to their large scale crop production. The terrain of Rajaji National park is almost hilly at an elevation range of 100 to 450 m. This park which is a part of Shivaliks contains tropical and subtropical moist broadleaf forests. The area proposed for this study is embedded with dense cover of Sal forests, sub-tropical pine forests, trees of West Gangetic plain which are moist and dry northern Decidous and Kair-Sissoo forests, which makes up the Barkot forest range in the northern slopes. The southern slopes consist of mixed vegetation including bamboo, grasses and shrubs. The ecosystem of this area is quite diverse and varied.

The presence of dense Sal forests in the forest area acts as a strong source for volume scattering. The agricultural lands present in the area also contribute in volume scattering during crop growing season and contributes for surface scattering during non-crop growing season. Water bodies having smooth surface act as specular reflectors. Permanent scatterers like buildings and mountains act as corner reflectors responsible for double-bounce scattering. These all factors make this region a complete package for this study. The proposed study concentrates in volume scattering from the forest features such as tree trunks, leaves and branches.

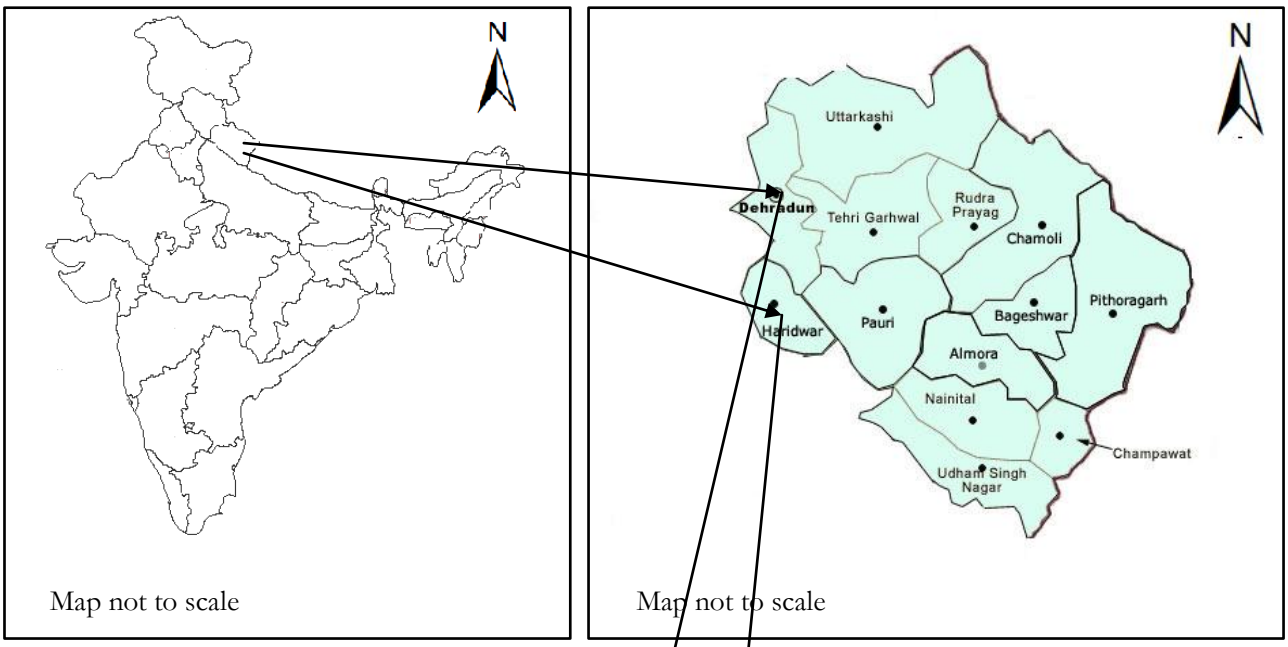

(a) (b)

(c)

Figure 3-1: (a) India Map (b) Uttarakhand State map (c) Study area I - Geoeye-I Sensor, Source: Google Earth

3.2. The Sundarbans

3.2.1. Introduction

The second study area chosen covers a part of Sundarbans forest area, a part of West Bengal state, in Eastern India. Sundarbans forest area which is located close to the meeting point of Ganges pure water and salt water of Bay of Bengal is the largest block formation of mangrove in the world [51] and is the world's largest coastal wetland and covers an area of almost 5000 km^2. Formed by Ganges, Meghna and Brahmaputra rivers, the Sundarbans are of a part of the World's largest delta and also the World's largest estuarine mangrove forest, 40% in India and 60% in Bangladesh [52]. In 1997, UNESCO recognized the Sundarbans as a World heritage site. The region lies between 22.02 North latitude 21.37 South latitude and 88.77 East longitude 88.40 West longitudes. The region is bounded by Bagerhat, Khulna and Satkhira districts in the North and the Bay of Bengal in the south. The western region is bounded by Raimangal and Hariabhanga rivers which forms the Bangladesh border with West Bengal in India.

3.2.2. Attributes and Scientific Importance of this area

3.2.2.1. Geography of the area

The region extends over almost 200 small islands separated by 15 distributaries of major rivers flowing north-south and almost 400 tidal estuaries, canals and creeks, which are interconnected. These form an impenetrable saltwater swamp reaching 100-130 km inland which supports the largest tidal mangrove forest in the world [52]. The Sundarbans are an excellent example of Monsoon rain flooding, plant colonization, tidal influence and delta formation [52]. The area lies within a World Wildlife Fund (WWF) Global Eco-region, and is contained by UNESCO Biosphere Reserve, which contains the Tiger reserve, a National Park and three wildlife sanctuaries and a Ramsar Wetland [52]. The soil type of the region is clay loam with alternate layers of sand, silt and clay.

3.2.2.2. Flora and Fauna

The dominant flora species are Sundari *(Heritiera Fomes),* Gewa *(Exoecaria Agallocha),* Goran *(Ceriops Decandra) and* Keora *(Sonneratia Apetala)* [52]. The Sundarbans forest area is classified as moist tropical seral forests, comprising of a mosaic succession of four types of tidal forest communities: low mangrove forest, tree mangrove forest, freshwater Heritiera swamp forest and salt-water Heritiera forest [52].

The Sundarbans supports one of the largest populations of the famous Royal Bengal Tiger *(Panthera Tigris Tigris)*, in the sub-continent, which is famous for swimming and man-eating. 48 other mammal species have been recorded including Leopard Cat, Jungle Cat, Indian spotted Deer and Wild Boar to name a few. A total of 315 bird species have also been recorded from this area.

3.2.2.3. Reasons for Selection of area

The presence of dense Mangrove forests in the area acts as a strong source for volume scattering. The agricultural lands present in human habitats also contribute in volume scattering Water bodies in the form of canals, distributaries, tidal estuaries and creeks having smooth surface act as specular reflectors, responsible for surface scattering. Permanent scatterers like buildings in townships act as corner reflectors responsible for double-bounce scattering. The presence of swamps also contributes to significant variation in scattering mechanisms due to surface roughness and moisture content.

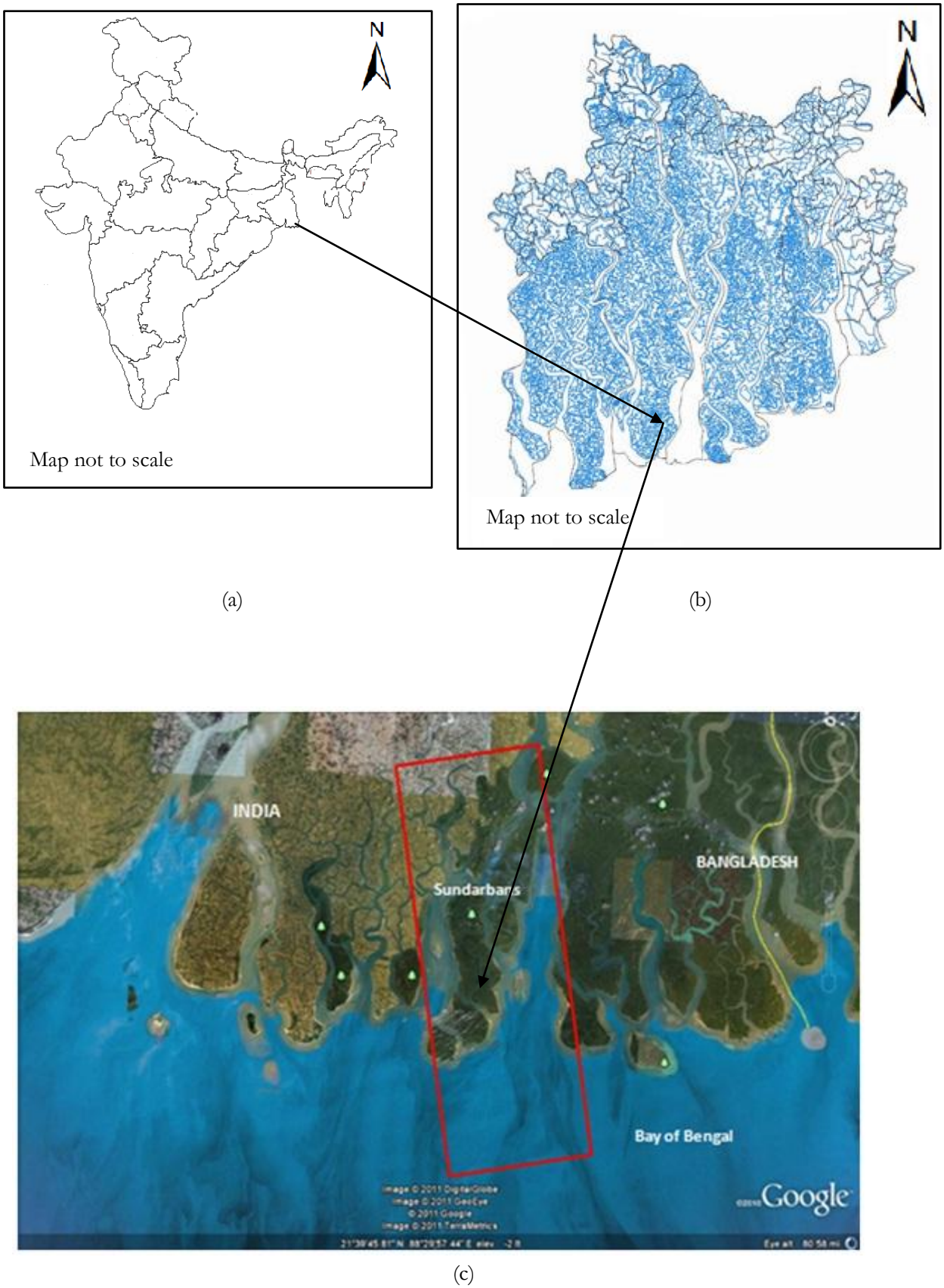

Figure 3-2: (a) India Map (b) Part of Sundarbans (c) Study area I - Geoeye-I Sensor, Source: Google Earth

3.3. Why different Study Areas?

The first study area, Barkot forests contains tropical and subtropical broadleaf forests embedded with dense cover of Sal and sub-tropical pine forests. Even though the forest canopy area is small, the size of the tree leaves in tropical forests has bigger size (10-25 cm long and 5-10 cm broad) which makes the radar waves to undergo volume scattering from multiple scatterers such as the large tree leaves, tree trunk and the ground.

The second study area in Sundarbans is a coastal wetland, embedded with very dense cover of mangrove forests such as *Rhizophora apiculata, Rhizophora mucronata* (Red Mangrove), Sundari, Gewa, Goran, Keora etc., whose tree height is very small (3-5 m)when compared to Sal and Pine trees(~35 m). The forest canopy area is very large when compared to the trees from Barkot area. Due to the moist and swampy conditions, the backscatter reflectance may be higher when compared to that from Barkot forests. Even though volume scattering may not be prominent from tree trunks due to low tree height, the effect of large forest canopy area and moist ground shall influence volume scattering mechanism and may be different when compared to that from the first study area.

The terrain of the two study areas also holds key importance for the research. Barkot forest range lie in a hilly terrain for almost 75% of the total area at an elevation upto 300 m. Therefore the effect of volume scattering may vary due to undulating slopes where the volume scatterers are physically located. On the other side, Sundarbans lie in a relatively plain area where undulations are much less thereby reducing variations in volume scattering from volume scatterers located in plain smooth surfaces.

Therefore in order to study the variations in volume scattering mechanism from different types of terrains and forest areas and thereby affecting the volume scattering component after reconstruction of pseudo-quadrature polarized data, these two study areas having different geographical features and climate behaviour are selected for the research.

4. MATERIALS AND METHODOLOGY

This section is divided into two sub sections; the first subsection provides in-depth description on the used datasets while the second subsection the method which has been adopted for this research work. The explanation on the methodology will then give a detailed outline to the innovation carried out in this work which will be explained in the following chapters. The figure 4-1 shown below shows the procedure to derive pseudo-quadrature polarized data in the form of 3×3 coherency matrix, based on compact polarimetric techniques followed by decomposing the volume scattering contribution using three component incoherent decomposition model from both compact and fully polarimetric modes.

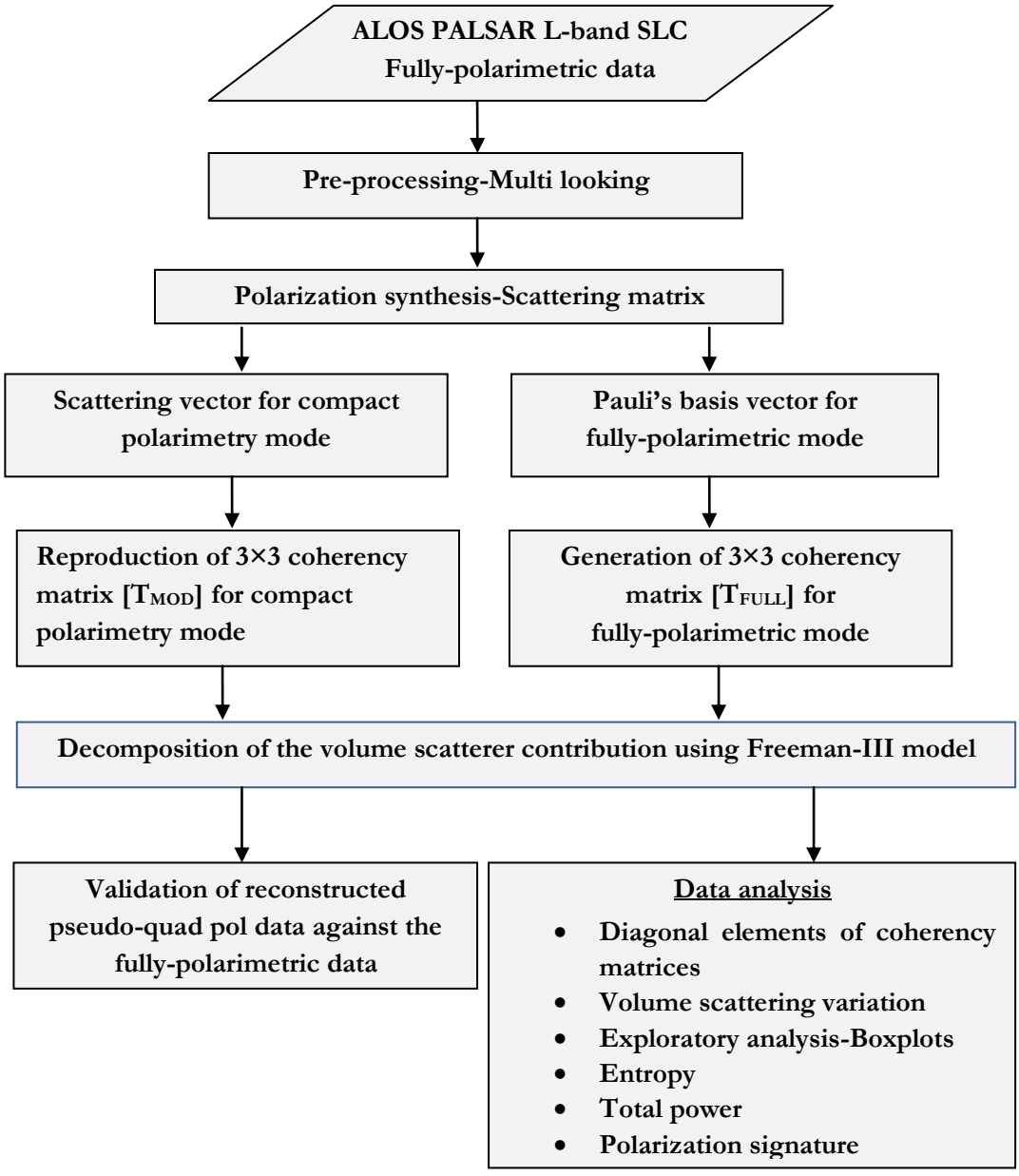

Figure 4-1 Methodology Flow Diagram

4.1. Data

The data used in this project is ALOS PALSAR fully polarimetric L-band SLC data. The Advanced Land Observing Satellite (ALOS), a satellite developed by Japan Aerospace Exploration Agency (JAXA) uses Polarimetric Phased Array L-band Synthetic Aperture Radar (PALSAR) as one of the remote sensing instruments which operates in single, dual and full polarization modes [53], [54], [55].

The wavelength for this data is 23.5 cm. L-band data, due to its longer wavelength than C and X-bands, has the capability to partially penetrate through the forest cover and can reach the ground. Therefore, L-band data gives the volume scattering information from tree trunks, tree leaves and ground, double and triple bounce scattering from corner reflectors, especially from man-made structures. L-band data also gives surface scattering information from the ground, creeks, canals and distributaries especially for Sundarbans study area, depending on the surface roughness and soil moisture content. The proposed study areas fall under tropical forest region. The size of the tree leaves in tropical forests has large size, which is greater than the wavelength of C and X-band SAR systems. L-band wavelength is having the capability to penetrate through tropical forest vegetation and ALOS-PALSAR is the only space-borne SAR system, which has acquired fully polarimetric data in L-band. The dataset description and characteristics (resolution, swath width and wavelength details) for both study areas is shown in table 9 and 10 in Appendix-I.

The data supplied was in single look complex (SLC), Level 1.1 format, in fully polarimetric mode. The datasets were later converted in multi looked format (ML). The dataset used for the research which was provided in level 1.1, SLC format contains an ALOS product file in .txt format, 4 SAR image files in SLC format and associated .PAR files of the corresponding image files of all four polarizations, one Meta file in .meta format and a KML file of the dataset representing the area covered by the sensor on that date of acquisition.

4.2. Method

The methodology is divided into four main steps. The first step involves pre-processing of SAR data including conversion of slant range to ground range - multi looking process and polarization synthesis. The latter step involves generating 2×2 scattering matrix which can be used to synthesize the radar return with any transmit/receive polarizations and thereby measuring the complete information of the earth feature. From this stage, the work is carried out in two phases. In the first phase, the pseudo-quadrature polarized data in the form of 3×3 coherency matrix is derived using the dual polarized scattering vectors, based on polarization state extrapolation algorithm which works on the concept of compact polarimetry. In the next phase, 3×3 coherency matrix from fully polarimetric mode is also generated using Pauli basis vectors. After completion of this phase, both the coherency matrices from fully polarimetric and compact polarimetric modes were decomposed for estimating the volume scattering contribution using three-component incoherent decomposition model. After decomposition, detailed data analysis like Entropy, polarisation signature analysis was carried out followed by the final step of validating the reconstructed pseudo-quadrature polarized data against fully polarimetric mode.

4.2.1. Multi look setup

The SLC format of the dataset used in fully polarimetric mode contains information from all four polarizations. The actual spatial resolution of a SAR system has two dimensions namely: azimuth resolution and range resolution. Azimuth resolution is measured along track, while range resolution in

across-track direction. Radar data is created in slant range geometry [5]. It has to be projected into ground range plane. This is because the uncorrected radar image is displayed in slant-range geometry which is the actual distance from the radar to the feature in the scene under observation. Due to the slant range distortion, the earth objects which are in the near range appears to be compressive when compared to objects at far range which results in different azimuth and range resolution. Therefore slant-range was converted into ground range by multi looking process. The first step in multi looking process was to calculate the pixel spacing in ground range which is done by dividing pixel spacing in slant-range by sine of look angle (30° in this case). Here the pixel spacing in ground range after calculation becomes 18.737 m. After this step, pixel spacing in ground range is compared with pixel spacing in azimuth of 3.792 m. Therefore 6 looks in azimuth direction and 1 look in range direction is considered to obtain a resolution of 18 m thereby increasing the resolution in azimuth direction and with equal range and azimuth resolutions.

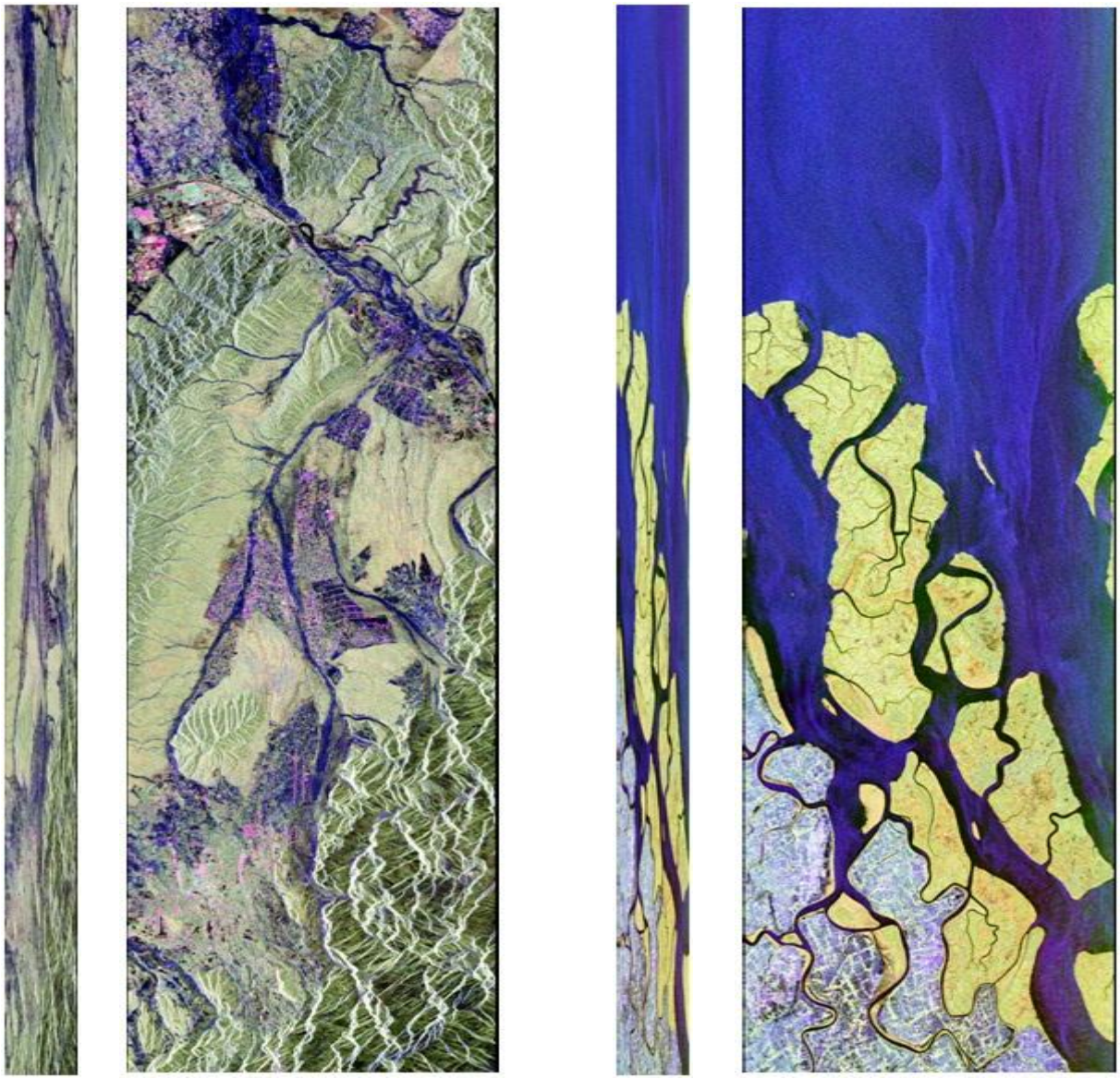

(a) (b) (c) (d)

Figure 4-2: (a) SLC image-Study area I (b) Multi look image-Study area I (c) SLC image-Study area II and (d) Multi look image- Study area II.
Red channel: HH polarization, Green channel: HV Polarization and Blue channel: VV polarization

4.2.2. Polarization synthesis-Scattering matrix

The next step was to obtain the scattering matrix which can be used to combine the radar return with any transmit/receive polarizations and thereby measuring the complete information of the earth feature.

$$[S] = \begin{bmatrix} S_{HH} & S_{HV} \\ S_{VH} & S_{VV} \end{bmatrix} \tag{4-1}$$

4.2.3. Target Vectors for fully polarimetric and compact polarimetric modes

The vectorized formulation of scattering matrix in the form of Pauli basis vector for fully polarimetric mode and dual-polarimetric target vector for compact polarimetric (π/4) mode were generated for deriving the pseudo-quadrature polarimetric information in the form of 3×3 coherency matrix for the compact polarimetric (π/4) and the fully-polarimetric modes.

$$K_P = \frac{1}{\sqrt{2}} \begin{bmatrix} S_{HH} + S_{VV} \\ S_{HH} - S_{VV} \\ 2\,S_{HV} \end{bmatrix} \tag{4-2}$$

$$K_{\pi/4} = \frac{1}{\sqrt{2}} [S_{HH} + S_{HV} \quad S_{VV} + S_{VH}]^T \tag{4-3}$$

Here K_P represents the Pauli basis vector for the fully polarimetric mode whereas $K_{\pi/4}$ represents the scattering vector for the compact polarimetric (π/4) mode.

4.2.4. Derivation of 3×3 coherency matrices from fully polarimetric and compact polarimetric modes

The scattering matrix and the basis vectors cannot give complete feature information on complex distributed earth scatterers present in every imaged SAR pixel. This is because; presence of different scattering mechanisms in each pixel, due to complexity of the features (e.g. forest features, man-made features) makes it difficult to obtain information of individual features. Therefore, 3×3 coherency matrix which represents a more expandable form of scattering matrix is derived from basis vectors of both the fully polarimetric and the compact polarimetric (π/4) modes.

The 3×3 coherency matrix for fully polarimetric mode was reproduced by multiplying the Pauli basis vector with its complex conjugate transpose represented by $\mathrm{T_{FULL}} = K_P \times K_P{}^{\dagger}$. Therefore,

$$[T_{FULL}] = \frac{1}{2} \begin{pmatrix} \langle |S_{HH} + S_{VV}|^2 \rangle & \langle (S_{HH} + S_{VV})(S_{HH} - S_{VV})^* \rangle & 2\langle (S_{HH} + S_{VV}) \times S_{HV}^* \rangle \\ \langle (S_{HH} - S_{VV})(S_{HH} + S_{VV})^* \rangle & \langle |S_{HH} - S_{VV}|^2 \rangle & 2\langle (S_{HH} - S_{VV}) \times S_{HV}^* \rangle \\ 2\langle S_{HV} \times (S_{HH} + S_{VV})^* \rangle & 2\langle S_{HV} \times (S_{HH} - S_{VV})^* \rangle & 4\langle |S_{HV}|^2 \rangle \end{pmatrix} \tag{4-4}$$

The pseudo-quadrature polarimetric information in the form of 3×3 coherency matrix$[T_{MOD}]$, based on the polarization state extrapolation algorithm for the compact polarimetric (π/4) mode was also derived. The detailed theory and mathematical calculations are explained in the following chapter.

4.2.5. Decomposition of the volume scattering contribution using three-component incoherent decomposition model.

The coherency matrices reproduced for the fully-polarimetric and the compact polarimetric (π/4) modes were then decomposed using three component incoherent decomposition model for estimating the contributions of fundamental scattering mechanisms such as the single-bounce, the double-bounce and the volume scattering. The coherency matrices derived from the both modes were decomposed into the surface, the double-bounce and the volume scattering components and their respective contributions to every imaged SAR pixel were estimated from both study areas.

4.2.6. Validation

The volume scattering contribution of tree leaves, tree trunk and from the ground estimated from the reproduced compact polarimetric data was validated against the fully polarimetric data. For this research, the multi looked single polarized imagesS_{HH}, S_{VV} or S_{HV} of the respective study areas were used as the reliable reference data. The validation procedure was to use the concept of Pauli matrix basis of the individual polarizations. This matrix basis was obtained as the elements of the resulting scattering vector obtained from the vectorization of the scattering matrix which is associated with the theory of wave scattering allowing the explanation of the three basic scattering mechanisms [3], [56]. These three mechanisms are the odd-bounce, the double-bounce and the volume scattering. The Pauli matrix basis is given by

$$K_P = \frac{1}{\sqrt{2}} [S_{HH} + S_{VV} \quad S_{HH} - S_{VV} \quad 2\,S_{HV}]^T \tag{4-5}$$

Here $S_{HH} + S_{VV}$ gives physical interpretation on the odd-bounce scattering, $S_{HH} - S_{VV}$ on the double-bounce scattering and $2\,S_{HV}$ on the volume scattering mechanisms respectively [3]. Therefore, these matrix elements were calculated from the single polarized images from both study areas and used as reference data for validation.

4.2.7. Sampling plan for data analysis and validation

In this study, the sampling plan employed is stratified random sampling which involves defining a population which consists of number of units for a particular feature out of which a sample consisting of fixed number of units shall be selected from the population using simple random sampling or systematic random sampling. All the pixels representing the backscatter from the different features responsible for the single-bounce, the double-bounce and the volume scattering mechanisms were considered as the population. The population was then divided into three groups or strata representing pixels from these three scattering mechanisms. The next step involves choosing the sampling size. Here, a sample size of 300 is taken, out of which 100 points are taken from areas responsible for the odd-bounce scattering, 100 points from areas responsible for the double-bounce scattering and 100 points are from areas responsible for the volume scattering mechanisms. The selection of points also depends on the feature from which the points are taken for every set of sample. Therefore to maintain homogeneity of features while selection and for the ease of mathematical computation during data analysis, 100 points were randomly selected from each set of sample for studying the performance of reconstruction of the pseudo-quadrature polarized data against the fully-polarimetric data.

4.2.8. Data analysis

Different data analysis was carried out to study the performance of the reproduced pseudo-quadrature polarized data against the fully-polarimetric data. The

a) Boxplots or box and whisker plot is a type of graph used in exploratory data analysis used to show the shape of the distribution of values along with descriptive statistics like median, upper and lower quartiles and minimum and maximum values. The box part in the boxplot contains 50% of the values. That means 50% of the data values lies between the upper and the lower edges (hinge) of the box i.e. between the first and the third quartiles. The vertical line inside the box represents the central value or the median of the dataset sample. The boxplot also gives information on the inter-quartile range which is the difference of the third quartile and the first quartile. It gives information on the spread of the 50% of the values which are not affected by outliers. The whiskers or the dotted vertical lines of the boxplot extending from the box edges represent the maximum and minimum power values of the sample data, excluding the outliers which are present if the whiskers extend to a maximum of 1.5 times the inter-quartile range. The boxplot also provides idea on the skewness depending on the concentration of dataset towards a particular direction.

b) The entropy values calculated from the sampled points from the forested areas responsible for the volume scattering, for both the modes are analyzed using graphical and modelling approaches to study the variation in randomness from the forested areas after reconstruction.

c) The diagonal elements of the coherency matrix are related with the physical properties in terms of symmetrical and non-symmetrical factors in case of discrete features, while more importantly it is related to surface, double-bounce and the volume scattering in case of distributed scatterers especially in natural media [13]. In case of the fully-polarimetric mode, the first diagonal element $T_{11} = \langle |S_{HH} + S_{VV}|^2 \rangle$ is sensitive to surface or odd-bounce backscatter return while the second diagonal element $T_{22} = \langle |S_{HH} - S_{VV}|^2 \rangle$ represents the double-bounce scattering especially from corner reflectors. The third diagonal element $T_{33} = \langle |S_{HV}|^2 \rangle$ which is the cross-polarized power is sensitive to the volume scattering especially from natural media such as forests. In order to achieve this, the first and second diagonal elements are multiplied by a factor 2 and the third diagonal element of $[T_{FULL}]$ divided by 2. This is done since the coherency matrix $[T_{FULL}]$ contains a constant ½ as a multiplier the matrix elements.

d) The total power of the fully-polarimetric SAR system represents the total power from all the four channels namely HH, HV, VH and VV. In terms of scattering matrix, the total power or span is represented by the sum of $|S_{HH}|^2$, $|S_{HV}|^2$, $|S_{VH}|^2$ and $|S_{VV}|^2$. In terms of coherency matrix, the total power in the four channels is proportional to the sum of the diagonal elements or trace of the matrix [12]. Even though the total power or the span is polarimetrically invariable (i.e, it doesn't contain any polarimetric information), the total power symbolize the multi-polarized information from all the elements of the scattering matrix into a single SAR image. The total power was calculated using the formula

$$T_p = \mathrm{T}_{11} + \mathrm{T}_{22} + \mathrm{T}_{33} \tag{4-6}$$

e) Polarization signature analysis was done to study the backscattering behaviour of the earth feature under study. Since this research used two study areas, it was imperative to understand the scattering mechanisms from these areas and to infer the type of scattering which have taken place in the area. The pedestal height is an important parameter that is obtained from polarisation signature. The height of the pedestal indicates the presence of unpolarized scattering component present in the backscatter, which can

be related to degree of polarization of the backscattered wave. The polarization signature also gives information on the maximum and minimum received power, which useful for calculating the co-efficient of variation parameter, which is the ratio of minimum received power to the maximum received power.

4.2.9. Accuracy assessment

The different measures used as parameters in the different data analysis, measures the accuracy of the reproduction of the pseudo-quadrature polarized data when compared to the fully-polarimetric data. The different measures employed in this study for accuracy assessment are

a) Relative error-It is defined as the ratio of the absolute error to the magnitude of the fully-polarimetric data, where the absolute error is calculated as the difference between the backscattered power from the fully-polarimetric data and the reconstructed pseudo-quadrature polarized data. The expression for the relative error is given by

$$RE = \frac{\mathrm{FP}-\mathrm{CP}}{\mathrm{FP}} \tag{4-7}$$

Here FP represents the backscattered power from the fully-polarimetric data; CP represents the backscattered power from the pseudo-quadrature polarized data. Therefore, in case of calculating the relative error in single-bounce scattering occurred after reconstruction in the first diagonal element of the coherency matrix, the relative error is calculated as

$$RE_{T_{11}} = \frac{T_{11_x}-T_{11_y}}{T_{11_x}} \tag{4-8}$$

Here T_{11_x} represents the backscattered power in fully-polarimetric data from the first diagonal element T_{11}, while T_{11_y} represents the same from the compact polarimetric mode. Similarly the relative errors from the remaining diagonal elements were also calculated and interpreted. The median values from the relative errors shows the bias in the pseudo-quadrature polarized values from the factual fully-polarimetric values, expected for a perfect reproduction. Negative medians show that the reconstructed values are larger than the fully-polarimetric values. Standard deviation from the relative errors measures the width of the relative error distribution.

2) Correlation coefficient (r)-The linear correlation coefficient is used to measure the strength and direction of linear relationship between the fully-polarimetric data and the reconstructed pseudo-quadrature polarized data. Correlation explains how well both these data vary together, whereas the correlation coefficient quantifies the direction and the magnitude of the correlation between them. The value of the sample correlation coefficient is given by

$$r = \frac{\mathrm{N}\sum_{1=1}^{100}\mathrm{xy}-((\sum_{1=1}^{100}\mathrm{x})(\sum_{1=1}^{100}\mathrm{y}))}{\sqrt{\mathrm{N}(\sum_{1=1}^{100}\mathrm{x}^2)-(\sum_{1=1}^{100}\mathrm{x})^2}\sqrt{\mathrm{N}(\sum_{1=1}^{100}\mathrm{y}^2)-(\sum_{1=1}^{100}\mathrm{y})^2}} \tag{4-9}$$

Here x represents the backscattered power from fully-polarimetric data and y represents the same from the reproduced pseudo-quadrature polarized data. N represents the total number of observations in the sample. The value of r ranges from $-1 \leq r \leq +1$, where + and – signs indicate positive and negative linear correlations.

3) Coefficient of determination (r^2)-This measure gives the amount of variation of the pseudo-quadrature polarized data that was predicted from the fully-polarimetric data. It gives a measure of

how well the regression line modelled using linear or non-linear models, represents the data. The value of coefficient of determination ranges from$0 \leq r^2 \leq 1$. The value is calculated using the formula

$$r^2 = 1 - \frac{\mathrm{CP}_{\text{predicted}}}{\mathrm{CP}_{\text{original}}} \tag{4-10}$$

Here $\mathrm{CP}_{\text{predicted}}$ measures the deviations of the original pseudo-quadrature polarized values from their predicted values obtained after regression analysis and $\mathrm{CP}_{\text{original}}$ measures the deviations of the pseudo-quadrature polarized values from their sample mean.

4) Root mean square error (RMSE)-In order to get the measure of the spread of the pseudo-quadrature polarized values around that average, root mean square error is calculated. First, the difference between the actual pseudo-quadrature polarized values and the predicted pseudo-quadrature polarized values also called as residuals are calculated. This value can either be positive or negative as the predicted value might over estimate or under estimate the actual values. The residual values are then squared, averaged and then square root of this average is calculated. The RMSE of the regression line is also known as the RMS error of the residuals. The final value obtained after this step gives the root mean square error (RMSE). The value of RMSE is calculated using the formula

$$RMSE = \sqrt{\frac{\sum_{i=1}^{100}(y-x)^2}{100}} \tag{4-11}$$

Here y represents the predicted pseudo-quadrature polarized values obtained from regression analysis, while x represents the actual pseudo-quadrature polarized values obtained after reconstruction from the fully-polarimetric mode.

5) Residual analysis-The regression analysis using linear and non-linear models has to be assessed for its quality. Sometimes the regression line does not pass through all the data which entails some error in the model fit. The vertical amount by which the regression model fit fails to fit the data is called a residual. The graphical plot between the residuals and the fully-polarimetric data values is called as the residual plot.

4.3. Tools

This research work used different software tools such as PolSARpro v4.2.0, ENVI 4.8, MS Excel 2007 and R 2.14.1.

PolSARpro is a polarimetric data processing and educational tool [57]. The tool facilitates the provision of processing and exploiting SAR datasets of multiple polarizations. The source code of this tool which is made freely available by ESA made it even more useful in modifying the tool for this work.

ENVI 4.8 tool was used for data visualization, basic features like geo linking multiple data which is useful for taking points from sample, for comparison of power values.

R 2.14.1 statistical tool and MS Excel 2007 were used for exploratory data analysis like Boxplots and for quantification of results. The dataset processing, analysis and quantification of results, using the above mentioned tools were implemented in a standard desktop PC.

5. Derivation of 3×3 coherency matrix (π/4 mode) and three-component decomposition modelling theory

This chapter is divided into two main sections. The first section gives the flow diagram which derives a pseudo-quadrature polarized data from a dual-polarimetric mode using the polarization extrapolation algorithm, based on a coherency matrix approach. The second section describes the decomposition process of 3×3 coherency matrices obtained from a fully-polarimetric mode and the reconstructed pseudo-quadrature polarized data, using a polarization state extrapolation algorithm, for estimating the individual contributions of the basic three scattering mechanisms - the surface-bounce, the double-bounce and the volume scattering, which may be present as an individual contribution or a combination in an imaged SAR pixel. The basic algorithm developed for compact polarimetry for (π/4) mode [10] is used here. The pseudo-quadrature polarized data obtained represented by 3×3 coherency matrix after derivation has been used for decomposing volume scattering contribution using three-component incoherent decomposition model, which is explained in the ensuing subsection 6.1.

5.1. Polarization State Extrapolation Algorithm

Compact polarimetric techniques involve reconstruction pseudo-quadrature polarized data from dual-polarized modes. The flow diagram shows the procedure for reproducing the pseudo-quadrature polarized data from the dual-polarimetric mode using coherency matrix approach.

2×2 scattering matrix

$$\begin{bmatrix} S_{HH} & S_{HV} \\ S_{VH} & S_{VV} \end{bmatrix}$$

⇨ Target vector for compact polarimetry (π/4 mode)

$$\frac{1}{\sqrt{2}}[S_{HH} + S_{HV} \quad S_{VV} + S_{VH}]^T$$

⇩

2×2 covariance matrix for π/4 mode

$$\frac{1}{2} \times \begin{bmatrix} |S_{HH}|^2 & S_{HH}\, S_{VV}^* \\ S_{VV}\, S_{HH}^* & |S_{VV}|^2 \end{bmatrix} + \frac{1}{2} \times \begin{bmatrix} |S_{HV}|^2 & |S_{HV}|^2 \\ |S_{HV}|^2 & |S_{HV}|^2 \end{bmatrix} + \frac{1}{2} \times \begin{bmatrix} 2\mathrm{Re}\,(S_{HH}\, S_{HV}^*) & S_{HH}\, S_{HV}^* + S_{VV}^*\, S_{HV} \\ S_{HH}^*\, S_{HV} + S_{VV}\, S_{HV}^* & 2\mathrm{Re}(S_{VV}\quad S_{HV}^*) \end{bmatrix}$$

Using Polarization State Extrapolation algorithm ⇩

Estimates for fully-polarimetric quad-pol data in the form of 3×3 covariance matrix

$$[\bar{\bar{C}}] = \begin{bmatrix} j_{11} - \hat{X}^{(n)} & 0 & j_{12} - \hat{X}^{(n)} \\ 0 & 2\hat{X}^{(n)} & 0 \\ j_{12}^* - \hat{X}^{(n)} & 0 & j_{22} - \hat{X}^{(n)} \end{bmatrix}$$

Conversion of covariance matrix to coherency matrix using similarity transformation matrix $[A]$

$$[A] = \begin{bmatrix} \frac{1}{\sqrt{2}} & \frac{1}{\sqrt{2}} & 0 \\ 0 & 0 & 1 \\ \frac{1}{\sqrt{2}} & -\frac{1}{\sqrt{2}} & 0 \end{bmatrix}$$

$$[T_{MOD}] = [A] \times [\bar{\bar{C}}] \times [A^T]$$

Estimates for fully-polarimetric quad-pol data in the form of 3×3 coherency matrix $[T_{MOD}]$

$$[T_{MOD}] = \begin{bmatrix} \frac{1}{2}(J_{11} - \hat{X}^{(n)}) + \frac{1}{\hat{X}^{(n)}} & \frac{1}{\sqrt{2}}(J_{12} - \hat{X}^{(n)}) & \frac{1}{2}(J_{11} - \hat{X}^{(n)}) - \frac{1}{\hat{X}^{(n)}} \\ \frac{1}{\sqrt{2}}(J_{12} - \hat{X}^{(n)}) & J_{22} - \hat{X}^{(n)} & \frac{1}{\sqrt{2}}(J_{12} - \hat{X}^{(n)}) \\ \frac{1}{2}(J_{11} - \hat{X}^{(n)}) - \frac{1}{\hat{X}^{(n)}} & \frac{1}{\sqrt{2}}(J_{12} - \hat{X}^{(n)}) & \frac{1}{2}(J_{11} - \hat{X}^{(n)}) + \frac{1}{\hat{X}^{(n)}} \end{bmatrix} \quad (5\text{-}1)$$

The value of $[T_{MOD}]$ in equation: (5-1) shows the 3×3 coherency matrix representing the reconstructed pseudo-quadrature polarized data, derived using the polarization state extrapolation algorithm. The technical explanation of the algorithm including explanation of the terms has been explained in Appendix-II.

5.2. Three-component incoherent decomposition model

The main objective of incoherent decomposition is to separate these second order derivatives of scattering matrix-covariance and coherency matrices as a combination of simpler scattering mechanisms for easier physical interpretation.

Freeman and Durden [6] developed a physically based three component decomposition model to fit the polarimetric SAR observations without utilizing reference data. They modelled the second order covariance matrix/coherency matrix as a combination of three different scattering mechanisms the surface-bounce, the double-bounce and the volume scattering.

In case of volume scattering, it is assumed that the backscattered radar return, which occurs in forest canopies, was modelled from randomly oriented thin cylinder like scatterers [6]. The coherency matrix for ensemble of dipoles was given by

$$\langle [T_{FULL}] \rangle_{\text{volume}} = \frac{f_v}{4} \times \begin{bmatrix} 2 & 0 & 0 \\ 0 & 1 & 0 \\ 0 & 0 & 1 \end{bmatrix} \quad (6\text{-}1)$$

Here f_v represents the volume scattering contribution to the $|S_{VV}|^2$ component (VV cross-section).

The double-bounce scattering component is modelled by scattering from dihedral corner reflector, made from a pair of vertical and horizontal surfaces of different dielectric constants [6]. The coherency matrix for double-bounce scattering was given by

$$\langle [T_{FULL}] \rangle_{\text{Double}} = f_d \times \begin{bmatrix} |\alpha|^2 & \alpha & 0 \\ \alpha^* & 1 & 0 \\ 0 & 0 & 0 \end{bmatrix} \quad (6\text{-}2)$$

Here α is given by

$$\alpha = e^{j2(\gamma_h - \gamma_v)} \frac{R_{\text{gh}}\, R_{\text{th}}}{R_{\text{gv}}\, R_{\text{tv}}}$$

Here R_{th} and R_{tv} represent Fresnel reflection co-efficients of vertical surface (e.g. tree trunk) for horizontal and vertical polarizations respectively and R_{gh} and R_{gv} represent Fresnel reflection co-efficients of horizontal surface (e.g. ground) for both horizontal and vertical polarizations respectively. Additional term f_d represents the double-bounce contribution to the $|S_{VV}|^2$ component (VV cross-section).

The single-bounce or surface scattering component, which is the direct backscatter from earth surface is modelled by a first-order Bragg surface scatterer [6]. The coherency matrix for single-bounce scattering is given by

$$\langle [T_{FULL}] \rangle_{\text{surface}} = f_s \times \begin{bmatrix} 1 & \beta^* & 0 \\ \beta & |\beta|^2 & 0 \\ 0 & 0 & 0 \end{bmatrix} \tag{6-3}$$

Here f_s represent the surface scattering contribution to the $|S_{VV}|^2$ component (VV cross-section).

For all these backscattering components, under assumption of reciprocity condition and there is a complete decorrelation between the co-polarized and the cross-polarized terms. Along with these assumptions, it is assumed that there is no correlation between the surface-bounce, the double-bounce and the volume scattering mechanisms. Therefore the total second-order statistics is equal to the sum of the total of the individual scattering mechanisms. As a result the three-component decomposition model expresses the coherency matrix for fully-polarimetric mode $[T_{FULL}]$ as

$$[T_{FULL}] = \langle [T_{FULL}] \rangle_{\text{volume}} + \langle [T_{FULL}] \rangle_{\text{double}} + \langle [T_{FULL}] \rangle_{\text{surface}} \tag{6-4}$$

Substituting values of $\langle [T_{FULL}] \rangle_{\text{volume}}$, $\langle [T_{FULL}] \rangle_{\text{doub le}}$ and $\langle [T_{FULL}] \rangle_{\text{surface}}$ from equations: (6-1), (6-2) and (6-3) in (6-4), $[T_{FULL}]$ becomes

$$\frac{1}{2}\begin{pmatrix} \langle |S_{HH} + S_{VV}|^2 \rangle & \langle (S_{HH} + S_{VV})(S_{HH} - S_{VV})^* \rangle & 2\langle (S_{HH} + S_{VV}).S_{HV}^* \rangle \\ \langle (S_{HH} - S_{VV})(S_{HH} + S_{VV})^* \rangle & \langle |S_{HH} - S_{VV}|^2 \rangle & 2\langle (S_{HH} - S_{VV}).S_{HV}^* \rangle \\ 2\langle S_{HV}.(S_{HH} + S_{VV})^* \rangle & 2\langle S_{HV}.(S_{HH} - S_{VV})^* \rangle & 4\langle |S_{HV}|^2 \rangle \end{pmatrix} =$$

$$\frac{f_v}{4} \times \begin{bmatrix} 2 & 0 & 0 \\ 0 & 1 & 0 \\ 0 & 0 & 1 \end{bmatrix} + f_d \times \begin{bmatrix} |\alpha|^2 & \alpha & 0 \\ \alpha^* & 1 & 0 \\ 0 & 0 & 0 \end{bmatrix} + f_s \times \begin{bmatrix} 1 & \beta^* & 0 \\ \beta & |\beta|^2 & 0 \\ 0 & 0 & 0 \end{bmatrix} \tag{6-5}$$

From equation: (6-5), the volume scattering contribution is estimated directly and the value of f_v was used for simplifying the other equations, making it three equations and four unknowns. The values of α and β were also assumed to be $\alpha = -1$ and $\beta = 1$, depending on whether the surface scattering or the double-bounce scattering are dominant [6]. With the help of these assumptions, f_d, f_s and α or β were estimated [6]. In the last step, the contribution of all the three scattering mechanisms can be estimated to the span or the total power, which is equal to the sum of diagonal elements T_{11}, T_{22} and T_{33} of the 3×3 coherency matrix$[T_{FULL}]$. Therefore the total power P_T is

$$P_T = P_S + P_D + P_V$$

Here P_V, P_D and P_S represents the scattering powers with respect to the volume scattering, the double-bounce scattering and the surface scattering respectievely.

Therefore,
$$P_S = f_s(1 + |\beta|^2)$$
$$P_D = f_D(1 + |\alpha|^2) \text{ and}$$
$$P_V = f_v$$

The estimates of the volume scattering contribution for the fully-polarimetric mode has been derived above. In the similar way the pseudo-quadrature polarized data, dervied using the polarization state extrapolation algoirthm was decomposed for estimating the single-bounce, the double-bounce and the volume scattering contributions. Therefore the three-component decomposition model expresses the 3×3 coherency matrix, decribing pseudo-quadrature polarized data, for compact polarimetric mode $[T_{MOD}]$ as

$$[T_{MOD}] = \langle [T_{MOD}] \rangle_{volume} + \langle [T_{MOD}] \rangle_{double} + \langle [T_{MOD}] \rangle_{surface} \quad (6\text{-}6)$$

In a similar way for the fully-polarimetric mode, substituting the values of $\langle [T_{MOD}] \rangle_{volume}$, $\langle [T_{MOD}] \rangle_{double}$ and $\langle [T_{MOD}] \rangle_{surface}$ from equations: (6-1), (6-2) and (6-3) into (6-4), $[T_{MOD}]$ leads to

$$[T_{MOD}] = \begin{bmatrix} T_{11} & T_{12} & T_{13} \\ T_{21} & T_{22} & T_{23} \\ T_{31} & T_{32} & T_{33} \end{bmatrix} = \begin{bmatrix} \frac{1}{2}\left(C_{11} - \hat{X}^{(n)}\right) + \frac{1}{\hat{X}^{(n)}} & \frac{1}{\sqrt{2}}\left(C_{12} - \hat{X}^{(n)}\right) & \frac{1}{2}\left(C_{11} - \hat{X}^{(n)}\right) - \frac{1}{\hat{X}^{(n)}} \\ \frac{1}{\sqrt{2}}\left(C_{12} - \hat{X}^{(n)}\right) & C_{22} - \hat{X}^{(n)} & \frac{1}{\sqrt{2}}\left(C_{12} - \hat{X}^{(n)}\right) \\ \frac{1}{2}\left(C_{11} - \hat{X}^{(n)}\right) - \frac{1}{\hat{X}^{(n)}} & \frac{1}{\sqrt{2}}\left(C_{12} - \hat{X}^{(n)}\right) & \frac{1}{2}\left(C_{11} - \hat{X}^{(n)}\right) + \frac{1}{\hat{X}^{(n)}} \end{bmatrix} =$$
$$\frac{f_v}{4} \times \begin{bmatrix} 2 & 0 & 0 \\ 0 & 1 & 0 \\ 0 & 0 & 1 \end{bmatrix} + f_d \times \begin{bmatrix} |\alpha|^2 & \alpha & 0 \\ \alpha^* & 1 & 0 \\ 0 & 0 & 0 \end{bmatrix} + f_s \times \begin{bmatrix} 1 & \beta^* & 0 \\ \beta & |\beta|^2 & 0 \\ 0 & 0 & 0 \end{bmatrix} \quad (6\text{-}7)$$

The contribution of all the three scattering mechanisms can be estimated to the span or the total power, which is equal to the sum of diagonal elementsT_{11}, T_{22} and T_{33} of the coherency matrix$[T_{MOD}]$.

Therefore the total power P_T is

$$P_T = P_S + P_D + P_V \quad (6\text{-}8)$$

Equating the total power P_T with corresponding diagonal terms T_{11}, T_{22} and T_{33},

$$P_T = \frac{f_v}{2} + |\alpha|^2 f_d + f_s + \frac{f_v}{4} + f_d + |\beta|^2 f_s + \frac{f_v}{4}$$

After simplification,

$$P_D = f_D(1 + |\alpha|^2)$$
$$P_S = f_s(1 + |\beta|^2) \text{ and}$$
$$P_V = f_v = 4T_{33} \quad (6\text{-}9)$$

The equation: (6-9) was used to estimate the volume scattering contribution from the reproduced pseudo-quadrature polarized data (3×3 coherency matrix$[T_{MOD}]$) from both study areas, dervied based on the polarization state extrapolation algorithm. The volume scattering contributions estimated from both the modes from both study areas was then analyzed which are explained in Chapter 6.

6. ANALYSIS, RESULTS AND VALIDATION

This chapter presents the results obtained from the method adopted for this research work. It starts with the presentation of results, different data analysis used for studying the results obtained, followed by discussions on interpreting the various results obtained.

6.1. Derivation of pseudo-quadrature polarized data, using Polarization state extrapolation algorithm based on π/4 mode.

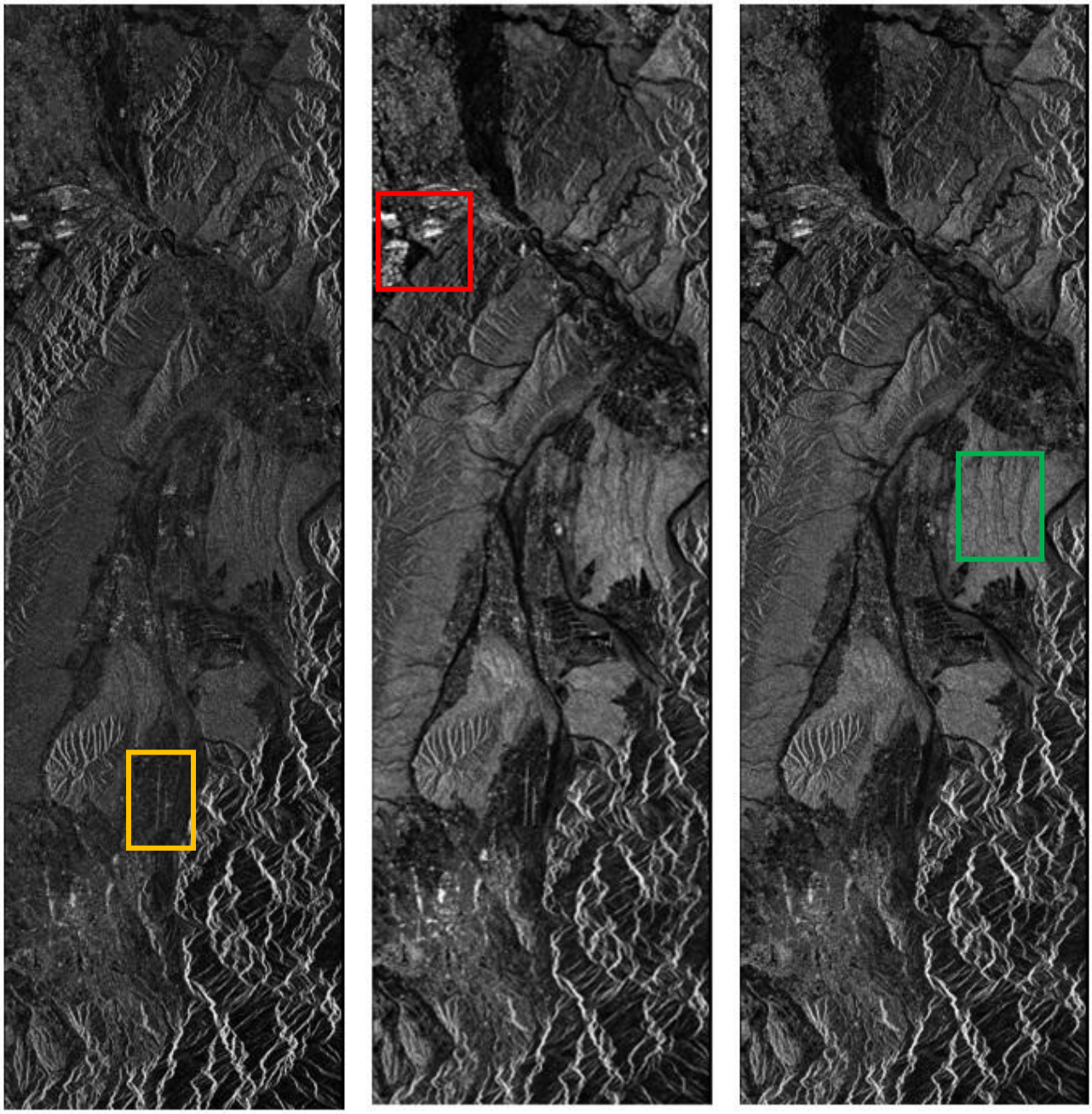

(a) (b) (c)

Figure 6-1: (a) Coherency matrix element T_{11} (b) T_{22} (c) T_{33} - Study area I

(a) (b) (c)

Figure 6-2: (a) Area sensitive to Surface-bounce scattering (b) Double-bounce scattering (c) Volume scattering

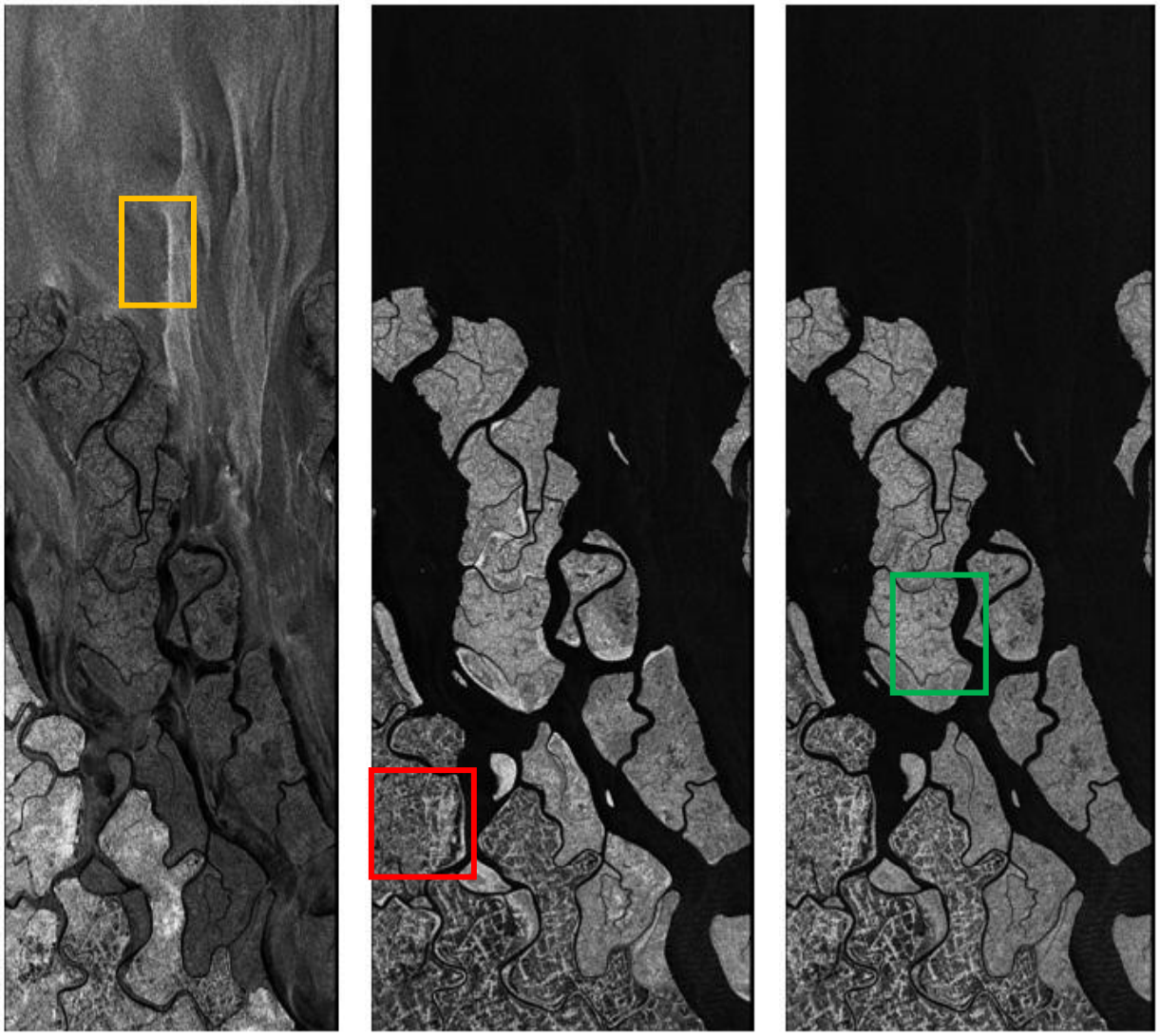

(a) (b) (c)

Figure 6-3: (a) Coherency matrix element T_{11} (b) T_{22} (c) T_{33} - Study area II

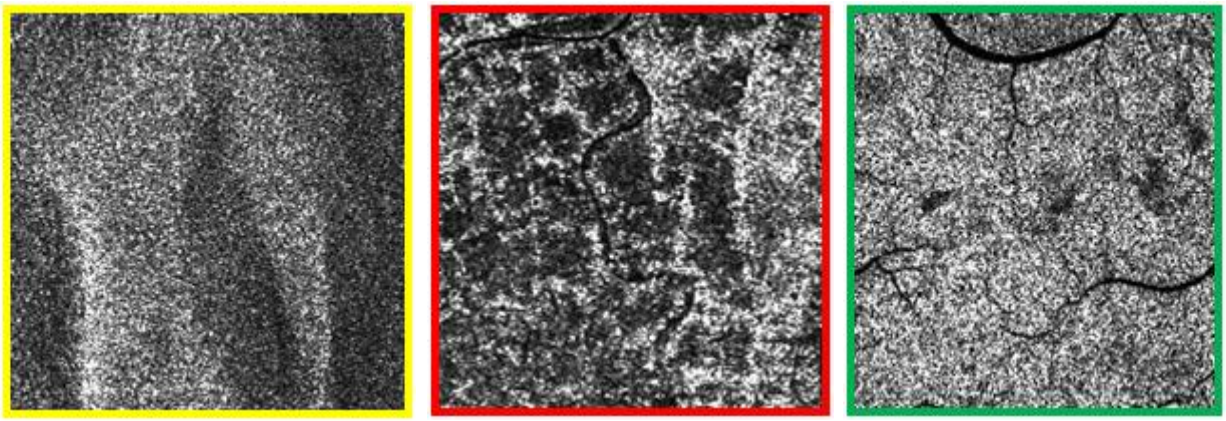

(a) (b) (c)

Figure 6-4: (a) Area sensitive to Surface-bounce scattering (b) Double-bounce scattering (c) Volume scattering

The figures 6-1 (a),(b),(c) and 6-3 (a),(b),(c) represents the diagonal elements T_{11}, T_{22} and T_{33} of 3×3 coherency matrix $[T_{MOD}]$ which represents the pseudo-quadrature polarized data for both study areas reproduced using polarization state extrapolation algorithm, based on compact polarimetry ($\pi/4$ mode) technique.

The next set of images (subsets) figures 6-2 (a), (b), (c) and 6-4 (a), (b), (c) in different colour borders represent the areas contributing to the basic three scattering mechanisms. The locations selected from figures: 6-1 (a) and 6-3 (a) represented (by yellow border) in subsets figure: 6-2 (a) and 6-4 (a) show high backscatter from plain surface (Runway-Dehradun Airport) and calm sea surface (Bay of Bengal) which gives clear understanding that T_{11} is responsible for surface-bounce scattering, contributed by HH polarization. The locations selected from figure: 6-1 (b) and 6-3 (b) represented (by red border) in subsets Figure: 6-2 (b) and 6-4 (b) show high backscatter from urban scatterers (Haridwar city-Study area I) and sea surface (Kishoripur Town-Study area II) which gives clear idea that T_{22} is responsible for double-bounce scattering, contributed by VV polarization. The locations selected from figures: 6-1 (c) and 6-3 (c) represented (by green border) in subsets figures: 6-2 (c) and 6-4 (c) show high backscatter from dense forests from both study areas which gives clear understanding that T33 is sensitive to volume scattering, contributed by HV polarization.

6.2. Analysis of backscattered power on diagonal elements of 3×3 coherency matrices

The diagonal elements T_{11}, T_{22} and T_{33} of the 3×3 coherency matrices for both the fully-polarimetric $[T_{FULL}]$ and the compact polarimetric $[T_{MOD}]$ modes contain information from different polarizations separately and the addition of these elements give the total backscattered power which is important to analyze the change in the total power for every imaged SAR pixel for both modes. In this analysis, in order to identify and quantify the changes in the backscattered power which might have occurred after reproducing the pseudo-quadrature polarized data using compact polarimetry technique, 100 points were taken from a sample from T_{11}, T_{22} and T_{33} reproduced using fully-polarimetric and compact polarimetric modes.

6.2.1. Analysis of T_{11} elements

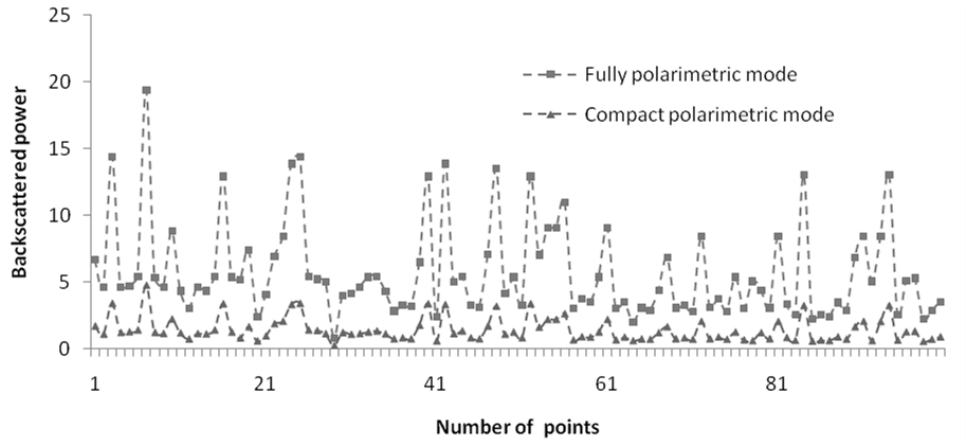

Figure 6-5: Variation of T_{11} elements for Study area I:
The lines are added to assist interpretation

The figure 6-5 represents the variation of 100 values plotted from runway (road surface) of Dehradun airport (figure: 6-6) responsible for the surface-bounce scattering from T_{11} element, for both the fully-polarimetric and the compact polarimetric (π/4) modes. The line with square markers represents the backscattered power from the fully-polarimetric mode while that in circular markers from the compact polarimetric (π/4) mode. From the graph, it is clear that there is reduction in surface scattering power in the reproduced pseudo-quadrature polarized data, when compared to the fully-polarimetric mode.

Figure 6-6: Dehradun airport runway (Road surface)

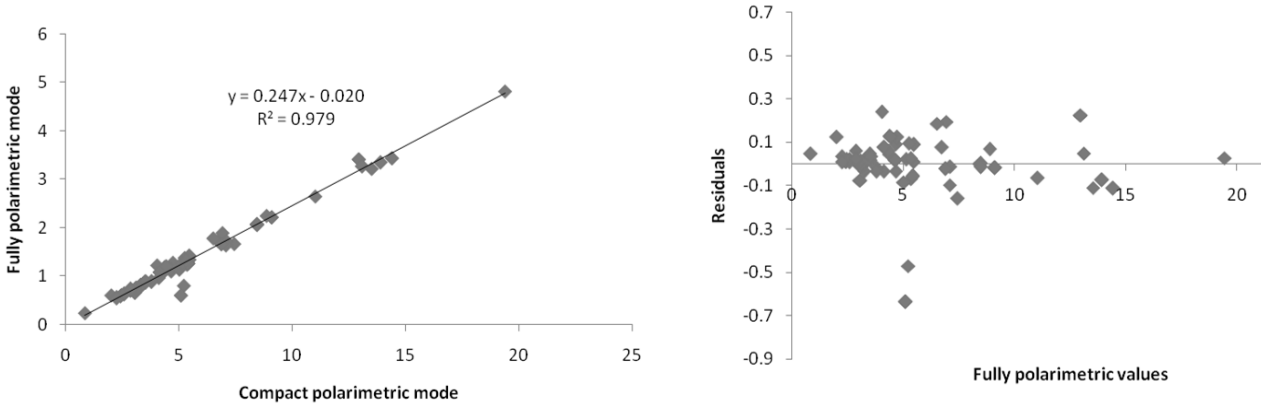

(a) (b)

Figure 6-7: Regression analysis-Study area I - (a) Linear model (b) Residual plot

The relative error was calculated using the formula shown in equation: (4-7). From the relative error calculated for T_{11} sample, the median error was found to be 0.738, which is positive error, which meant that the reconstructed values are lower than that of original fully-polarimetric values. The value of r was found to be 0.985. The relationship between the compact polarimetric data reproduced and the fully-polarimetric data was also analyzed using regression analysis using linear model to check for the best fit model, shown in figure: 6-6 (a). A comparative analysis of coefficient of determination or R^2 value was used from which it was found that the R^2 value of the model was 0.979 with RMSE value of 0.128.

It was observed that there is high correlation between the reconstructed pseudo-quadrature polarized data and the fully-polarimetric data, using linear regression model, with low RMSE and the linear model fits T_{11} elements. Even then the quality of the regression line has to be assessed. On analyzing the residual graph (figure: 6-7(b)) plotted against the residuals with the fully-polarimetric values, the mean absolute error of the residuals calculated from the residual plot was 0.12 and the correlation coefficient between the residuals the fully-polarimetric values was 0.023, with a negative correlation. The residuals shown in the plot appears to have a random structure without any fixed trend, which means in theory that the linear model fits well for the data.

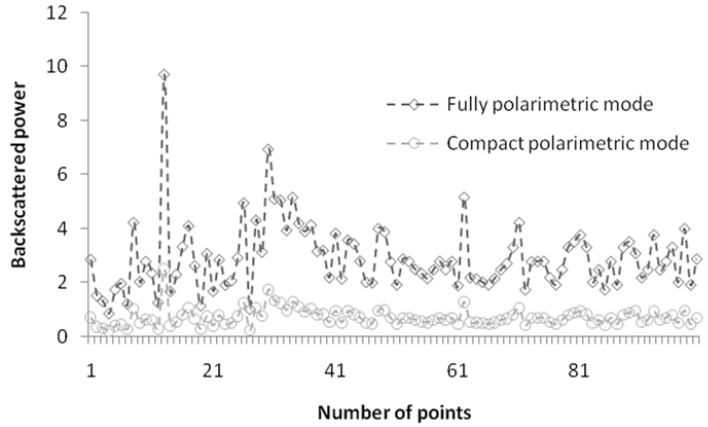

Figure 6-8: Variation of T_{11} elements - Study area II. The lines are added to assist interpretation

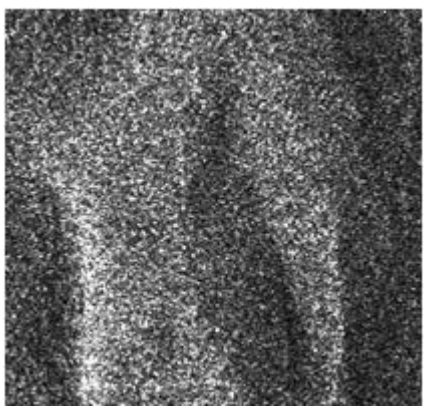

Figure 6-9: Portion of sea surface (Bay of Bengal)

The figure 6-8 represents graph showing variations from a sample of 100 values plotted from sea surface (Bay of Bengal) (figure: 6-9) responsible for surface-bounce scattering, from T_{11} element of second study area for both the fully-polarimetric and the compact polarimetric ($\pi/4$) mode. The line with square marker represents the backscattered power from the fully-polarimetric mode while that with circle marker from the compact polarimetric ($\pi/4$) mode. From the graph it is clearly evident that, there is a decrease in surface scattering power in the reproduced pseudo-quadrature polarized data when compared to the fully-polarimetric mode.

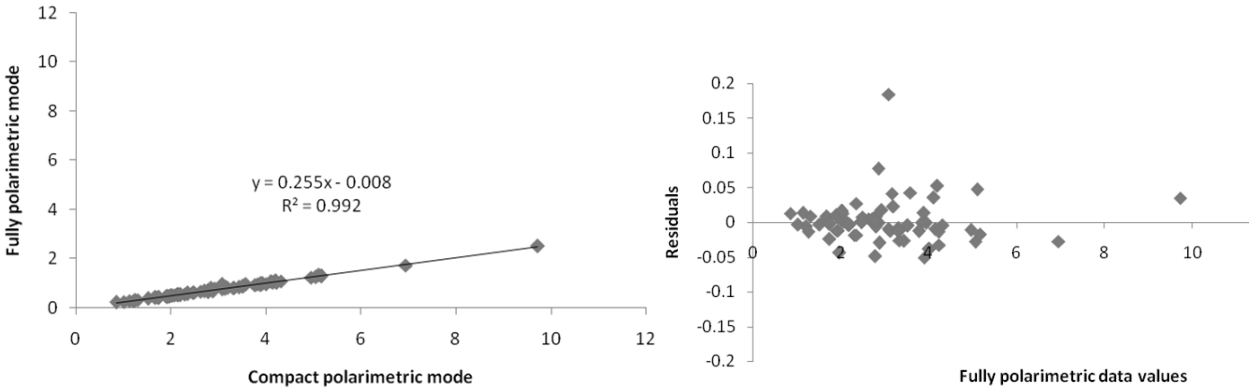

(a) (b)

Figure 6-10: Regression analysis-T_{11} element-Study area II-(a) linear model (b) Residual plot

The relative error of T_{11} in compact polarimetric ($\pi/4$) mode was calculated and the median error was found to be 0.756, which is positive error, which meant that the reconstructed values are lower than that of original fully-polarimetric values. The correlation coefficient was calculated and found to be 0.996. The R^2 value for linear model (figure 6-10 (a)) came out as 0.992 with RMS error of 0.027. There is high correlation and low RMSE between the reconstructed pseudo-quadrature polarized data and the fully-polarimetric data using linear model, even though there is a decrease in single-bounce scattering power in the compact polarimetric ($\pi/4$) mode. The mean absolute error of the residuals (figure: 6-10 (b)) was found to b 0.01 with negative correlation of -1.9×10^{-9} which proved that the regression equation fits well for the data and the residuals showed a random trend with the fully-polarimetric values.

6.2.2. Analysis of T_{22} elements

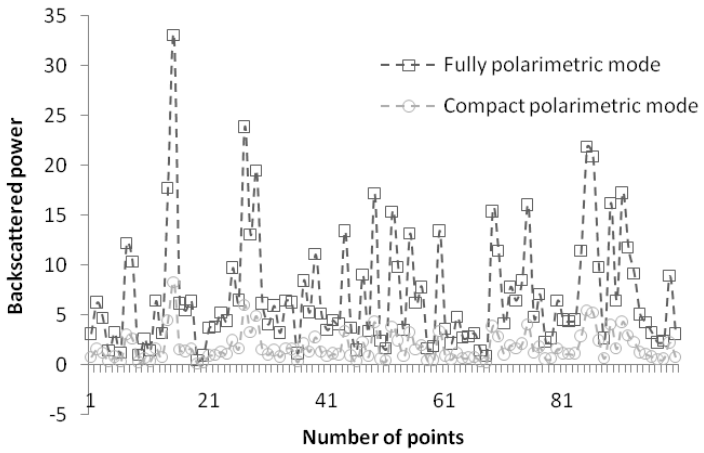

Figure 6-11: Variation of T_{22} elements for Study area I. The lines are added to assist interpretation

The figure 6-11 represents graph showing variations from a sample of 100 values plotted from the urban areas of Haridwar (figure: 6-12), responsible for double-bounce scattering from T_{22} element, for both the fully-polarimetric and the compact polarimetric ($\pi/4$) modes. The line with square markers represents the backscattered power from fully-polarimetric mode while that in circular marker from compact polarimetric mode. It is visually evident from the graph that there is decrease in double-bounce scattering power in the reproduced pseudo-quadrature polarized data when compared to the fully-polarimetric mode.

Figure 6-12: Portion of Urban areas of Haridwar city

The median error calculated from the relative error was found to be 0.75, which is positive error. The value of r was found to be 0.999. The relationship between compact polarimetric data reproduced and fully-polarimetric data was analyzed using the regression analysis (figure: 6-13 (a)), with the coefficient of determination calculated as 0.998 between the reconstructed pseudo-quadrature polarized data and the fully-polarimetric data, with a very low RMSE value of 0.001. The residual plot was analyzed from figure: 6-13 (b) for assessing the quality of the model fit. The mean absolute error of the residuals was found to be 0.003, with a negative correlation coefficient of -5.34×10^{-5}. This meant that the regression line plotted fits the data. The residual trend was reported to be a non-random trend, which according to theory works well for a non-linear model.

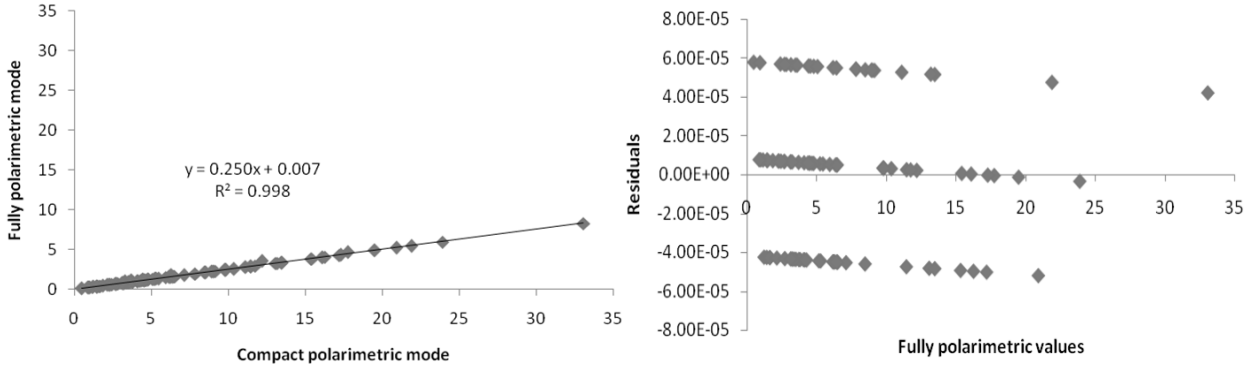

(a) (b)

Figure 6-13: Regression analysis for T_{22} element-Study area I - (a) Linear model (b) Residual plot

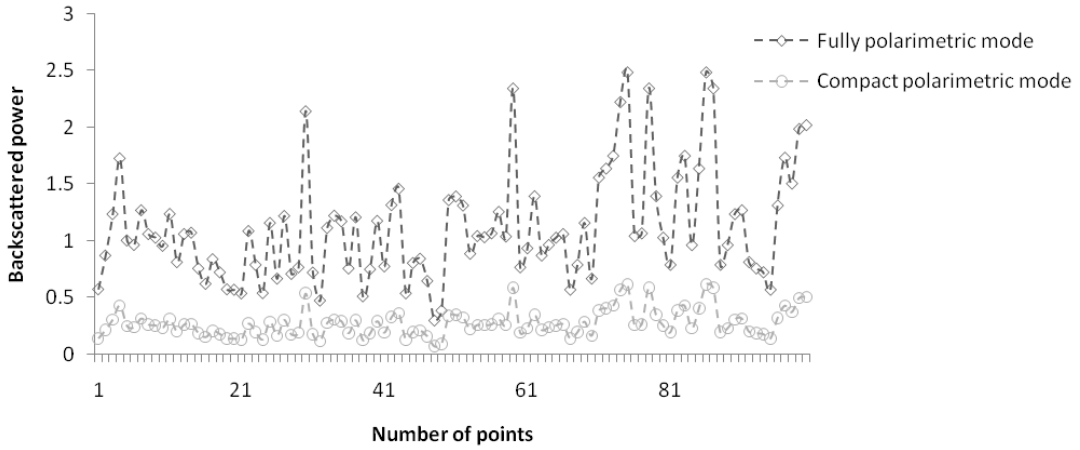

Figure 6-14: Variation of T_{22} elements for Study area II. The lines are added to assist interpretation

The figure 6-14 represents graph showing variations from a sample of 100 values plotted from the man-made features from Kishoripur town near Sundarbans (figure 6-16), responsible for double-bounce scattering, from T_{22} element, for both the fully-polarimetric and the compact polarimetric ($\pi/4$) modes. The line in square markers represents the backscattered power from fully-polarimetric mode while that in circular markers from compact polarimetric mode. It is visually evident from the graph that there is decrease in the double-bounce scattering power in the reproduced pseudo-quadrature polarized data, when compared to the fully-polarimetric mode.

Figure 6-15: Portion of Urban areas of Sundarbans

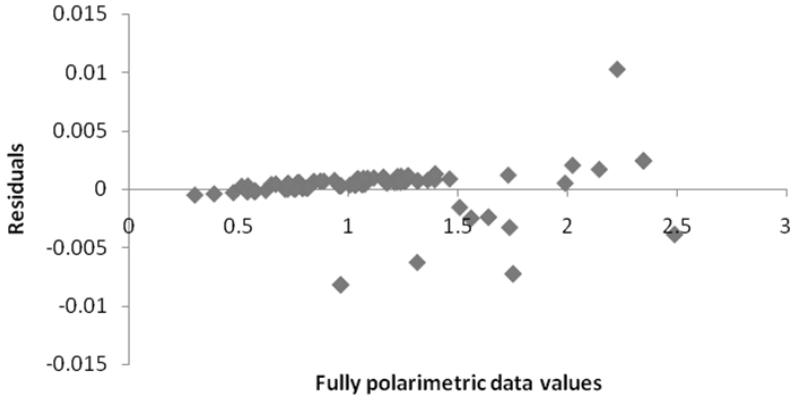

Figure 6-16: Regression analysis for T_{22} element- Study area II - Residual plot

The relative error of T_{22} in compact polarimetric mode was calculated with the median error calculated as 0.751, which is positive error. The value of r was found to be 0.999. The correlation between compact polarimetric data reproduced and fully-polarimetric data for the second study area was found to be similar to that of the first study area with the coefficient of determination to be 0.999 between the reconstructed pseudo-quadrature polarized data and the fully-polarimetric data and a very low RMSE value of 0.001. Using residual analysis from figure: 6-16 (b), the mean absolute error of the residuals was calculated and found to be 0.001 with a very low positive correlation of 9.673×10^{-15} which means that the linear model used for regression analysis fits well for the T22 data. The residual error from the plot through visual interpretation was also found to be very low close to zero, but with a linear trend throughout the residuals and with a random trend at the end.

6.2.3. Analysis of T_{33} elements

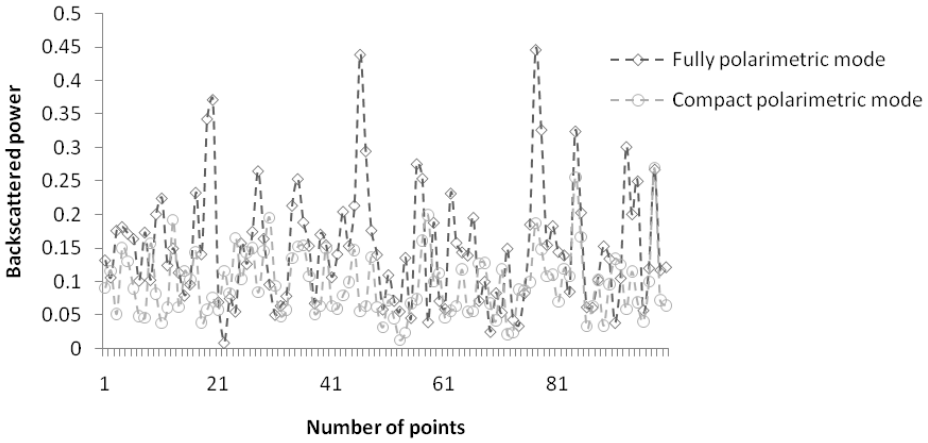

Figure 6-17: Variation of T_{33} elements for Study area I. The lines are added to assist interpretation

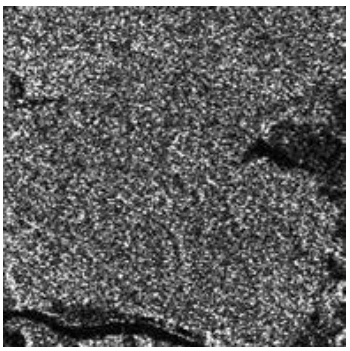

Figure 6-18: Portion of Barkot forest area

The figure 6-17 represents graph showing variations from a sample of 100 values plotted from the Barkot forest area (figure: 6-18), responsible for the volume scattering, from T_{33} element, from the fully-polarimetric and the compact polarimetric modes. The line in square markers represents the backscattered power from the fully-polarimetric mode while that in circular markers from the compact polarimetric mode. It is visually evident from the graph that there is an uneven decrease in volume scattering power in the reproduced pseudo-quadrature polarized data, when compared to the fully-polarimetric mode.

The relative error of T_{33} in the compact polarimetric mode was calculated and the median error was found to be 0.692, which is positive error, which meant that the reconstructed values are lower than that of the original fully-polarimetric values. The standard deviation of the volume scattering power in the compact polarimetric (π/4) mode was also calculated as 0.087 while that of the fully-polarimetric mode was 0.049. The value of correlation coefficient was found to be 0.231.

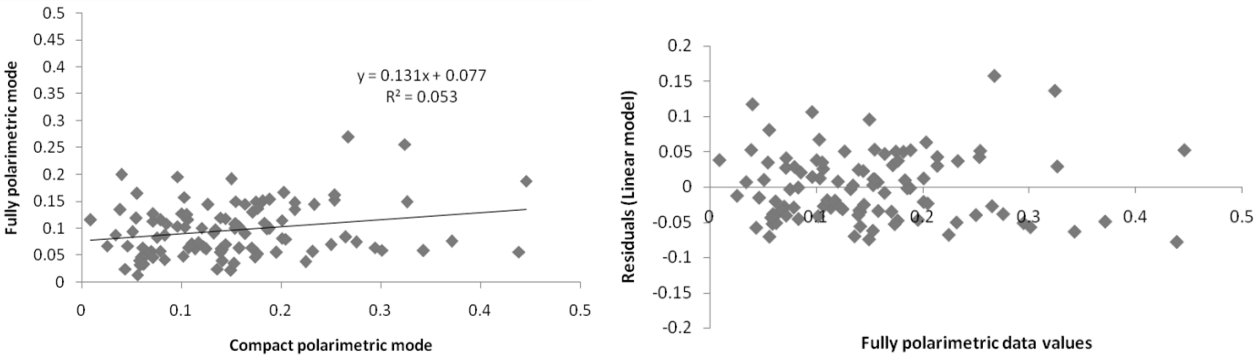

(a) (b)

Figure 6-19: Regression analysis for T_{33} element Study area I-(a) Linear model (b) Residual plot

Using linear model, shown in figures: 6-19 (a) it was found that there is extremely low correlation $(R^2 = 0.053)$ between the reconstructed pseudo-quadrature polarized data and fully-polarimetric data, with RMSE value of 0.048. The high variation in the volume scattering power in both the fully-polarimetric and the compact polarimetric modes might have caused the correlation to decrease. The residual plot for the linear model represented in figures: 6-19 (b) show random trend in the distribution of residual errors. The mean absolute error of the residuals was calculated and found to be 0.039, with a low positive correlation of 0.017. Therefore, taking residual plot to assess the quality of the regression line, it can be concluded that the regression line fits using the linear model fit well for the T_{33} data from Barkot area.

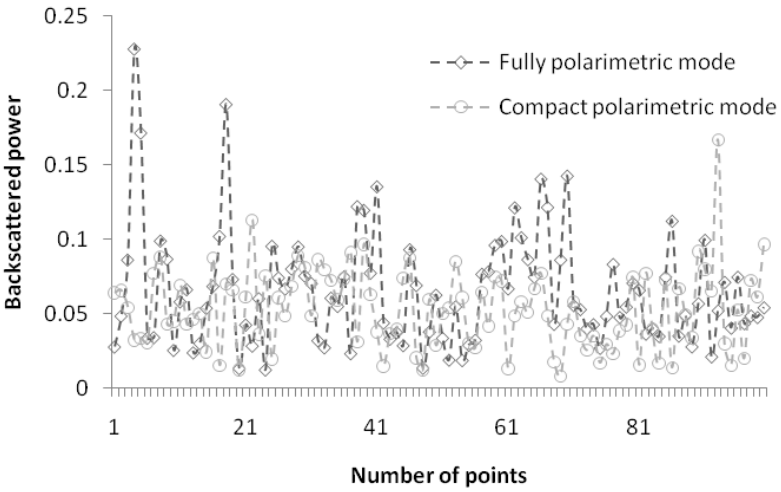

Figure 6-20: Variation of T_{33} elements for Study area II. The lines are added to assist interpretation

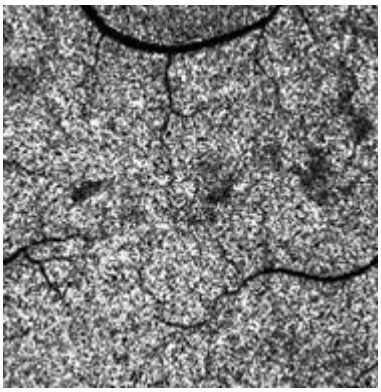

Figure 6-21: Portion of Mangrove forests, Sundarbans

The figure 6-20 represents graph showing variations from a sample of 100 values plotted from Mangrove forests of Sundarbans (figure 6-21), responsible for volume scattering from T_{33} element, from both modes. The line in square markers represents the backscattered power from the fully-polarimetric mode while that in circular markers from the compact polarimetric ($\pi/4$) mode. Even for this area, there is an uneven decrease in volume scattering power in the reproduced pseudo-quadrature polarized data, when compared to the fully-polarimetric mode.

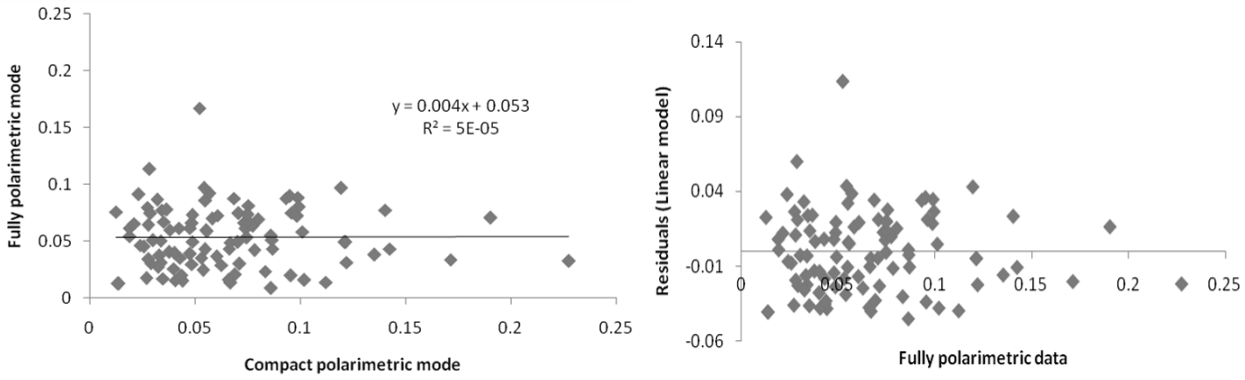

(a) (b)

Figure 6-22: Regression analysis - T_{33} element Study area II - (a) Linear model (b) Residual plot

The relative error of T_{33} in the compact polarimetric mode was calculated and the median error was found to be 0.06, which is positive error, which meant that the reconstructed values are lower than that of the original fully-polarimetric values. The value of r was found to be 0.006. The relationship between the compact polarimetric data reproduced and the fully-polarimetric data was also analyzed using linear model, to check for the best fit model, shown in figure: 6-22 (a). It was found that there is extremely low correlation $(R^2 = 0.00005)$ with RMSE value of 0.026 between the reconstructed pseudo-quadrature polarized data and the fully-polarimetric data. The residual plot for the linear model represented in figures: 6-22 (b) show random trend in the distribution of residual errors. The mean absolute error of the residuals found to be 0.021 with a higher negative correlation of 0.027. Similar to the Barkot area, the linear model fits for the cross-polarized power from the Sundarbans area.

The RMSE value, R^2, the mean absolute error and the residual pattern for all the three diagonal elements has been summarized in a tabular form in Appendix-III.

6.3. Estimation of volume scattering contribution from both modes, using three-component decomposition model.

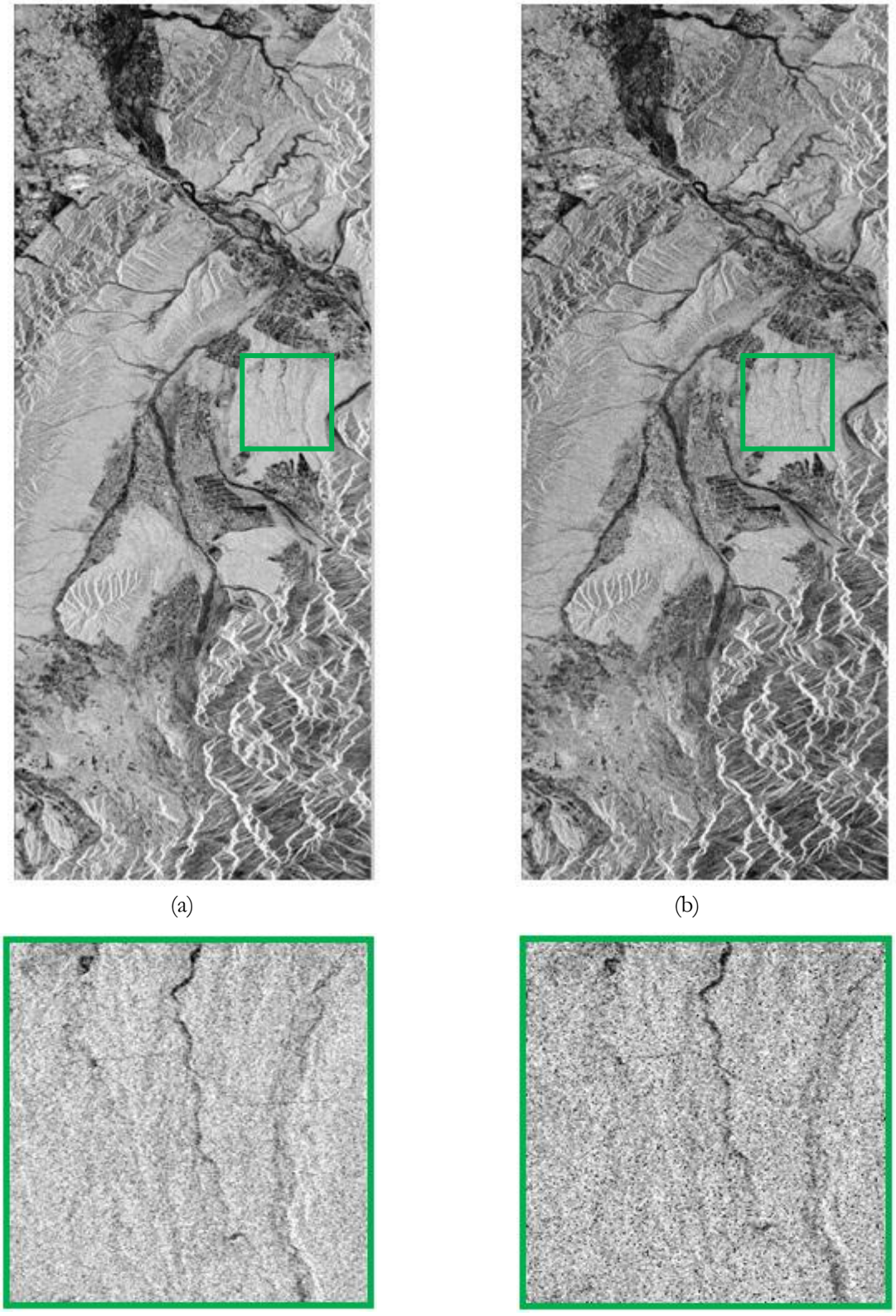

(a) (b)

(c) (d)

Figure 6-23: (a) - Volume scattering contribution Study area I - FP mode (b) CP mode (c) - Zoomed image - FP mode(d) CP mode

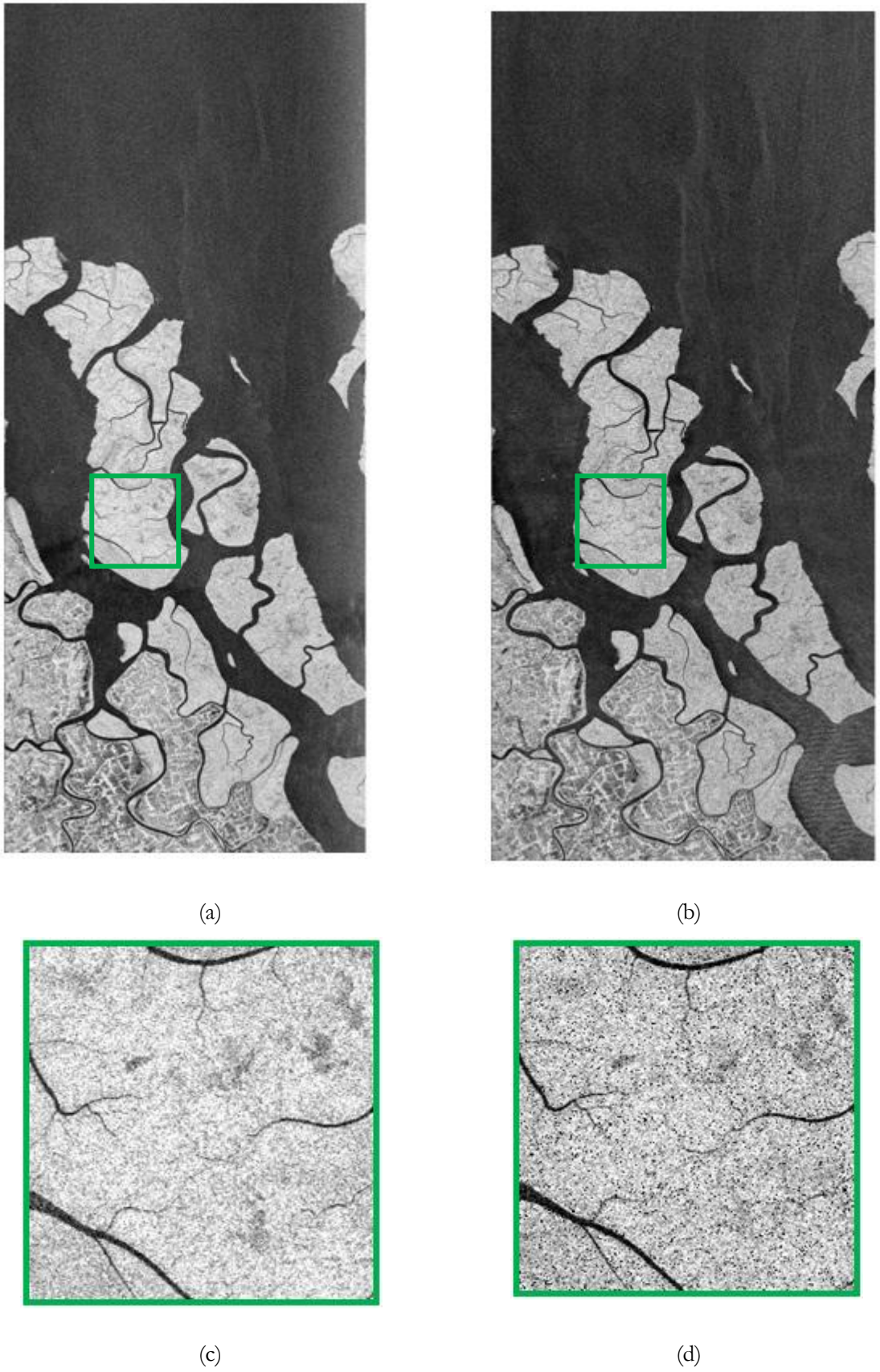

Figure 6-24: Volume scattering contribution Study area II – FP mode (b) CP mode (c) Zoomed image-FP mode(d) CP mode

The estimated volume scattering contribution obtained after decomposing the reproduced pseudo-quadrature polarized data and the fully-polarimetric data using the three-component decomposition model, for both study areas is shown in the Figures. The figures 6-23 (a),(b) represent the volume scattering images of the fully-polarimetric and compact polarimetric data, of the first study area, while figures 6-24 (a),(b) represent the same for the second study area, for both the modes respectively. The next set of images (subsets) figures 6-23 (c), (d), bordered in green represent the forest area from Barkot, Dehradun from the first study area, contributing to the volume scattering mechanism, while figures 6-24 (c), (d) represent a region of the Mangrove forests of Sundarbans from the second study area.

6.3.1. Box plot analysis

In this research work, it is important to understand the variation of volume scattering power, in the compact polarimetric (π/4) mode (CP mode) when compared to the fully-polarimetric (FP) mode. 100 points were taken from a sample from volume scattering images from both study areas. Boxplots were used to study the spread of power values for both the modes, indication on skewness and symmetry of the data and to compare volume scattering contribution of both the modes from both study areas.

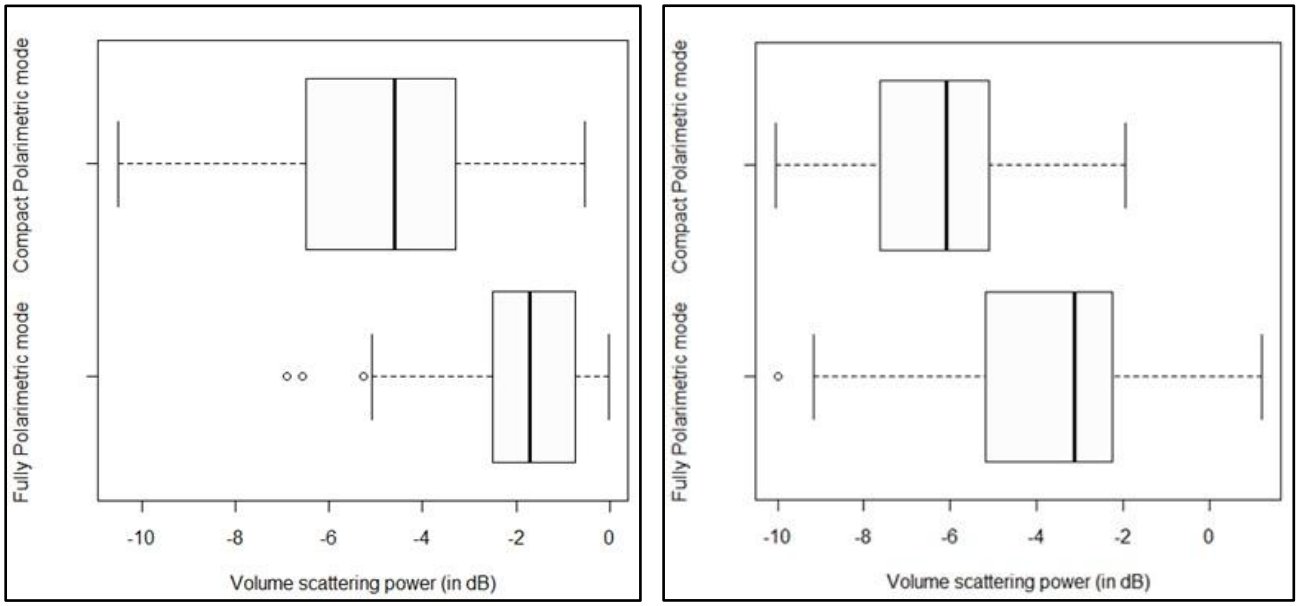

(a) (b)

Figure 6-25: Boxplots (a) Study area I (b) Study area II

Table 2: Boxplot parameters - Study area I

Parameter	Fully-polarimetric mode	Compact polarimetric mode
Range (Min)	-6.898 dB	-10.51 dB
Range (Max)	-0.029 dB	-0.537 dB.
Median	-1.714 dB	-4.594 dB
First Quartile	-2.507 dB	-6.648 dB
Third Quartile	-0.735 dB	-3.304 dB
Inter-quartile range (IQR)	1.771 dB	3.163 dB
Skewness	Left	symmetric

Table 3: Boxplot parameters - Study area II

Parameter	Fully-polarimetric mode	Compact polarimetric mode
Range (Min)	-9.988 dB	-10.054 dB
Range (Max)	1.214 dB	-1.932 dB.
Median	-3.133 dB	-6.1 dB
First Quartile	-5.182 dB	-7.627 dB
Third Quartile	-2.231 dB	-5.127 dB
Inter-quartile range (IQR)	2.95 dB	2.499 dB
Skewness	Symmetric	Symmetric

The figure 6-25 (a) and (b) shows the boxplots representing the distribution of volume scattering power for 100 pixels taken from a sample of volume scattering decomposition images of both fully and compact polarimetric (π/4) modes from both study areas. The boxplot represented in the first half of the window shows the distribution of the volume scattering power from the compact polarimetric (π/4) mode, while that in the second half represents the distribution of the same in the fully-polarimetric mode.

The boxplot was interpreted by taking two cases, first for fully-polarimetric mode and the second for compact polarimetric (π/4) mode. In case of fully-polarimetric mode the 50% of the volume scattering power lies between -2.507 dB to -0.735 dB for Barkot area and -5.182 dB to -2.231 dB for Sundarbans. In case of the compact-polarimetric (π/4) mode the 50% of the volume scattering power lies between -6.468 dB to -3.304 dB for Barkot area and -7.627 dB to-5.127 dB for Sundarbans.

For Barkot area, With regard to skewness factor, in case of the fully-polarimetric mode, most of the observations are concentrated towards the left which means the distribution of volume scattering power in fully-polarimetric is skewed left. In case of compact polarimetric (π/4) mode, most of the observations are split almost evenly at the median, which means the distribution of volume scattering power in the compact-polarimetric (π/4) mode is symmetric. For Sundarbans area, in case of the fully-polarimetric mode, most of the observations are split almost evenly at the median which means the distribution of volume scattering power in fully-polarimetric is approximately symmetric. Majority of the observations are split almost evenly at the median, which means the distribution of volume scattering power in the compact-polarimetric (π/4) mode is nearly symmetric.

6.3.2. Analysis of decomposed volume scattering power

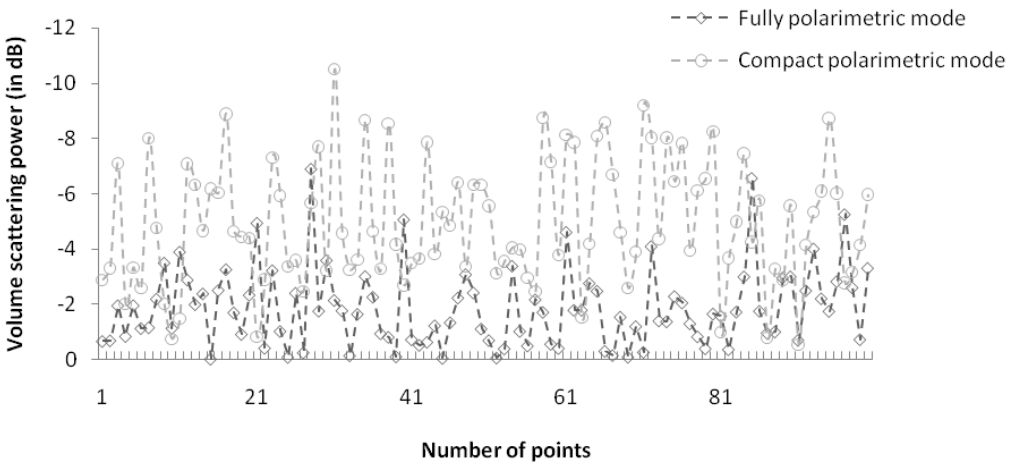

Figure 6-26: Variation of volume scattering power-FP and CP modes - Study area I
The lines are added to assist interpretation

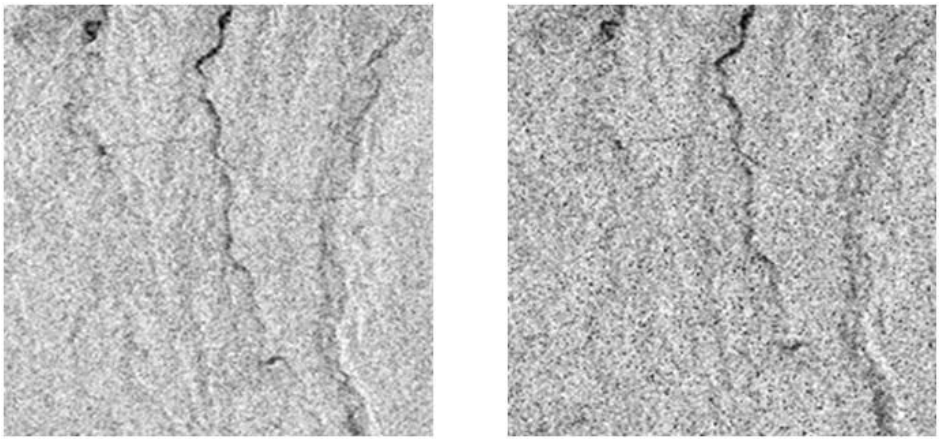

(a) (b)

Figure 6-27: Portion of Barkot area – Volume scattering (a) FP mode (b) CP mode

The graph represented in figure: 6-26 graphically shows the variation of the volume scattering power, obtained after decomposing the coherency matrices derived for both the fully-polarimetric and the compact polarimetric ($\pi/4$) modes using the three-component decomposition model, from Sal forests of Barkot (figure 6-27 (a) and (b)). It is clearly evident from the graph that there is decrease in the estimated volume scattering power from the reproduced compact polarimetric ($\pi/4$) mode, when compared to the fully-polarimetric mode

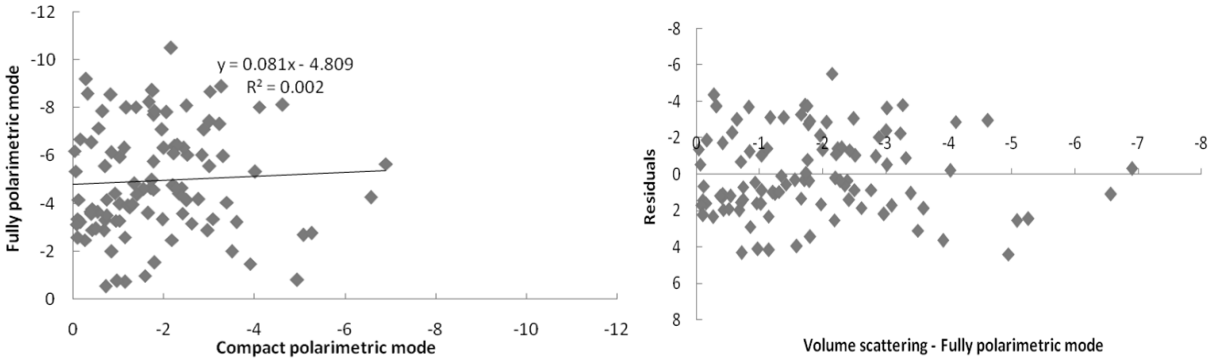

(a) (b)

Figure 6-28: Regression analysis- Study area I - (a) Linear model (b) Residual plot

The figure: 6-28 (a) represents the regression analysis between the volume scattering contribution of tree leaves, trunk and ground obtained after decomposition of coherency matrices reproduced from both the fully-polarimetric and the compact polarimetric ($\pi/4$) modes. The correlation coefficient was found to be 0.05 After, fitting the points for estimating the best fit line using linear model, the R^2 value was found to be very low with correlation equal to 0.002 and with a high RMSE of 2.24. The correlation coefficeint calculated shows high variation in the volume scattering power obtained for the compact polarimetric mode when compared to the fully-polarimetric mode.

The quality of the regression line fitted was assessed using residual plot (figure 6-28 (b)) between the residuals calculated after modelling and the corresponding volume scattering power values from the fully-polarimetric mode. The mean absolute error of the residuals was calculated and was found to be 1.893, which is greater than zero which indicates that, the linear model does not fit for the data. Even though, the correlation coefficient between the volume scattering power values from the fully-polarimetric mode and the residuals was found to be very low with a negative correlation of -8.152×10^{-17} and the residual trend showed randomness, non-linear model may be used to fit the values.

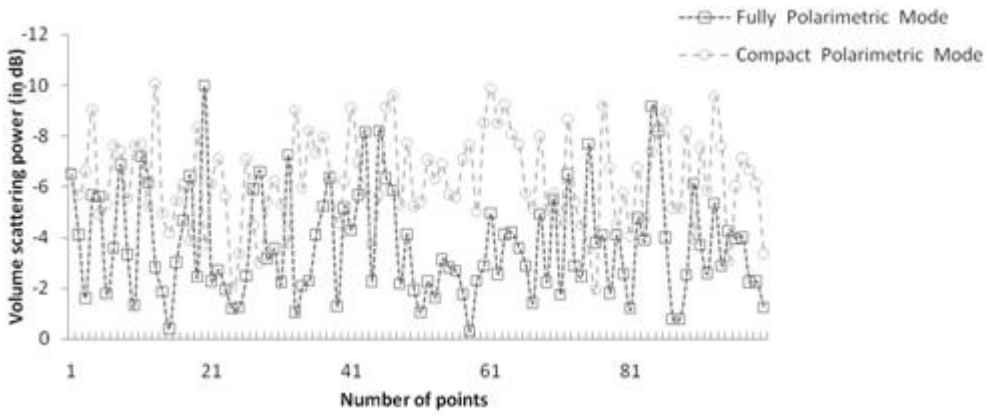

Figure 6-29: Variation of volume scattering power-FP and CP modes - Study area II.
The lines are added to assist interpretation

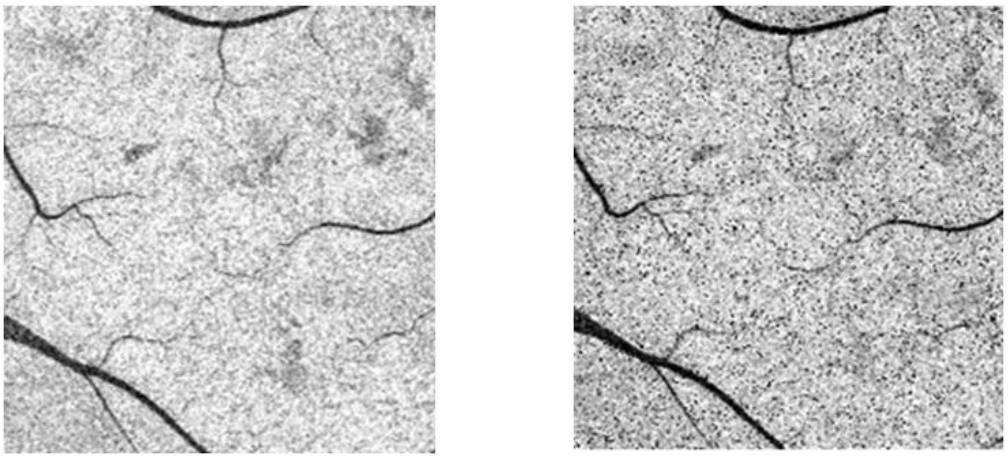

(a) (b)

Figure 6-30: Portion of Mangrove forests, Sundarbans-Volume scattering
(a) FP mode (b) CP mode

The graph represented in figure: 6-29 shows the variation of the volume scattering power, obtained after decomposing the coherency matrices derived for both the fully-polarimetric and the compact polarimetric (π/4) modes, using three-component decomposition model, from the Mangrove forests of Sundarbans (figure: 6-30 (a) and(b)). With the help of graphical interpretation, it can be inferred similar to the volume scattering variation from Sal forests of Barkot that there is decrease in volume scattering power from the compact polarimetric (π/4) mode, when compared to the fully-polarimetric mode.

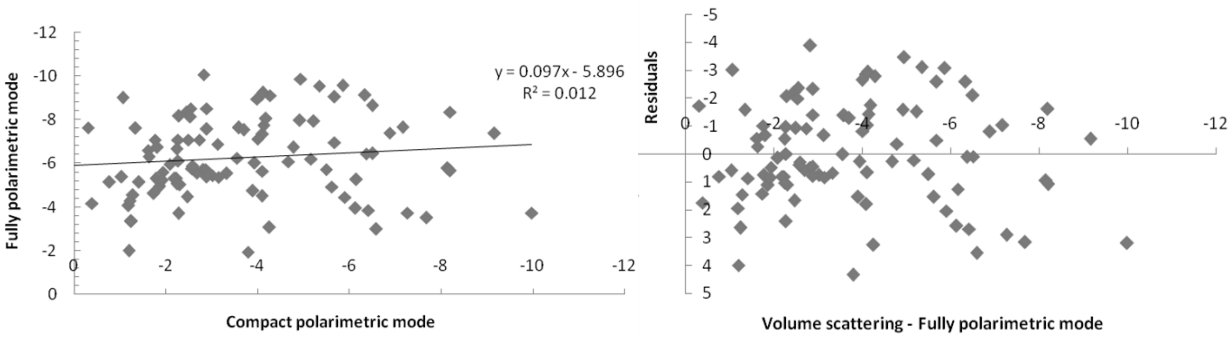

(a) (b)

Figure 6-31: Regression analysis-Volume scattering- Study area II - (a) Linear model (b) Residual plot

The value of correlation coefficient was found to be 0.122. After, fitting the points for estimating the best fit line, using linear model (figure: 6-31 (a)), the R^2 value was found to be very low with correlation equal to 0.012, with an RMSE of 1.81. The residual plot represented in figure: 6-31 (b), shows random trend in the residual values calculated from the linear model. The correlation coefficient was found to be very low with a negative correlation of -5.7×10^{-17} and the mean absolute value of the residuals was found as 1.486, which is close to the standard error of 1.83 calculated while predicting the volume scattering power in the compact polarimetric mode. Even though the correlation coefficient is very low close to zero with a random trend of residuals, the linear model may not be suitable for fitting the volume scattering values to predict the volume scattering power in the compact-polarimetric mode from the forested areas.

6.3.3. Polarization Signature Analysis

In this analysis, the areas from of the volume scattering decomposed images, responsible for this mechanism were considered and its signature in co-polarized and cross-polarized channels were portrayed for both the fully-polarimetric and the compact polarimetric (π/4) modes.

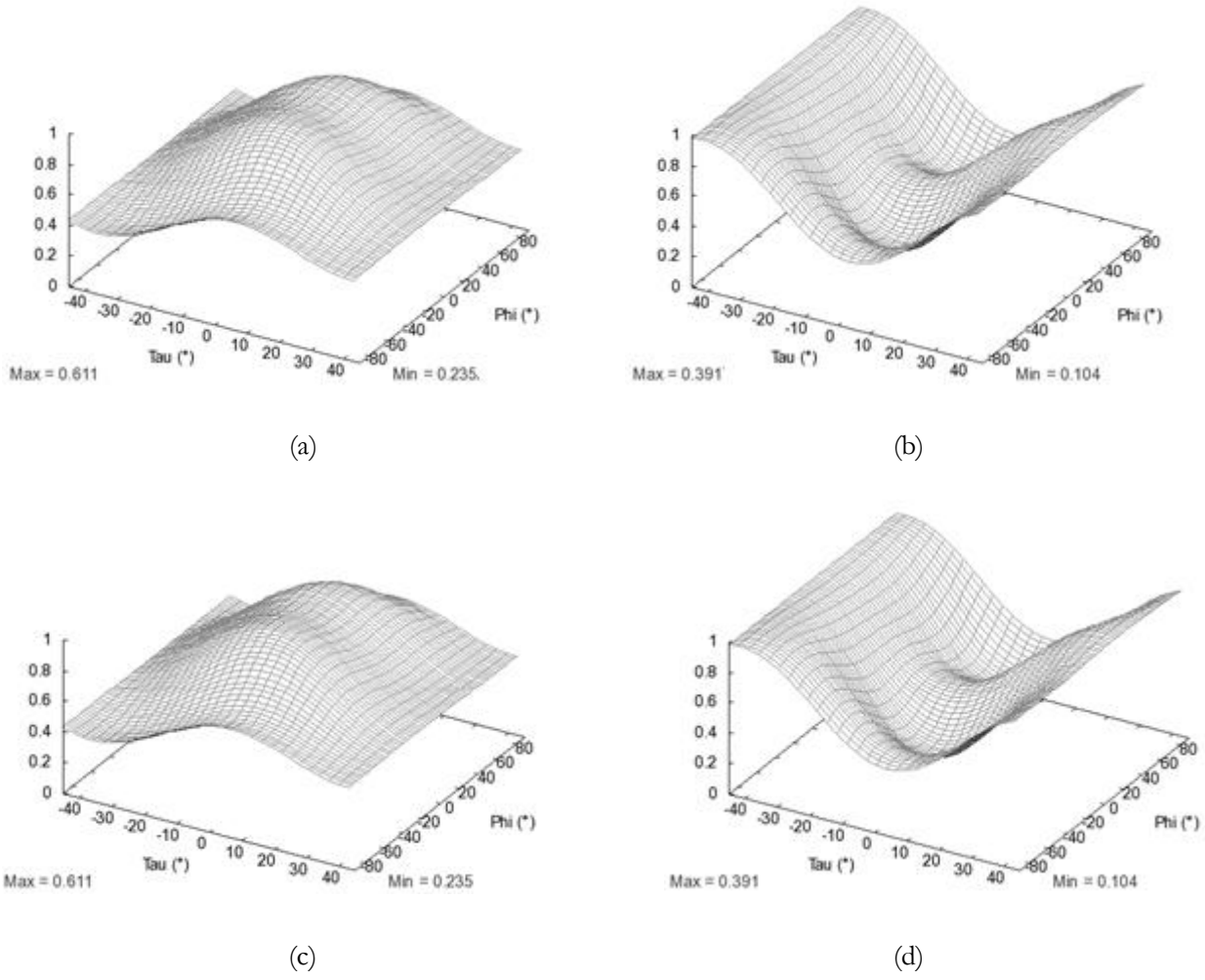

Figure 6-32: Normalized signature (a) Co-pol channel -FP mode(b) Cross-pol channel -FP mode (c) Co-pol channel -CP mode (d) Cross-pol channel -CP mode -Study area I

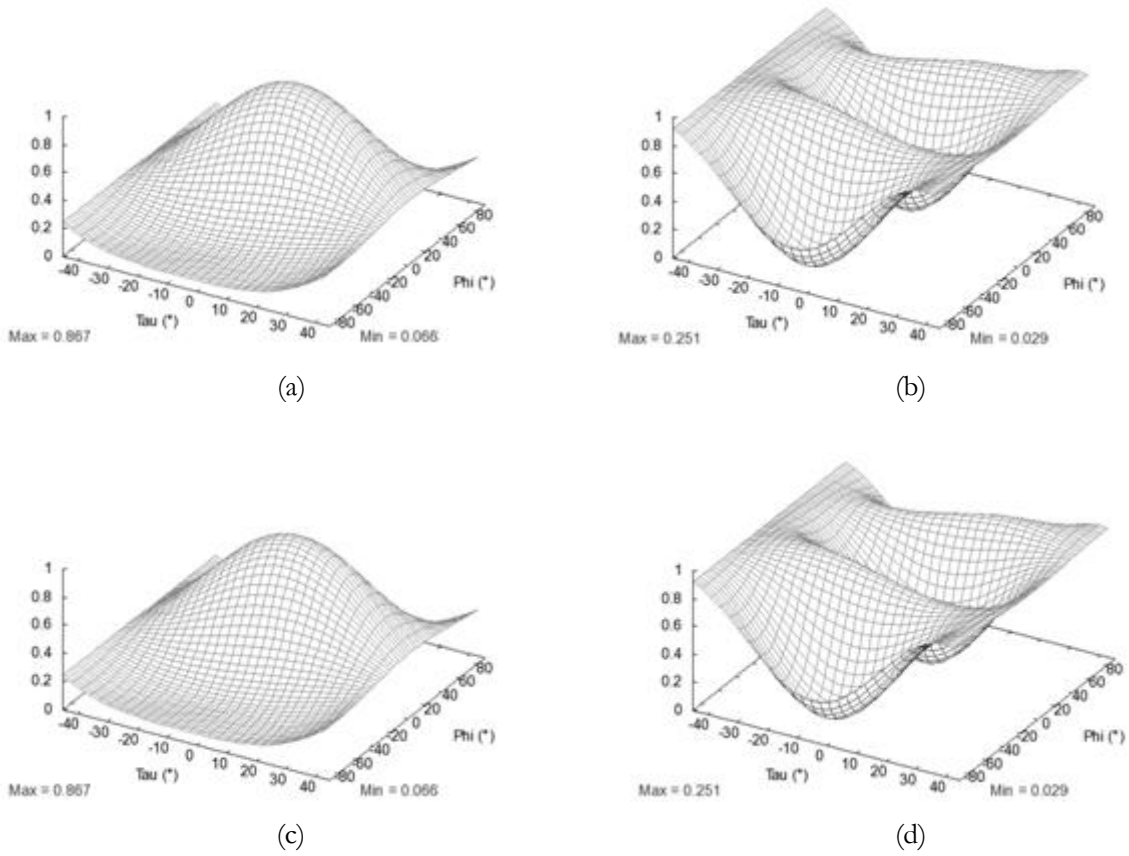

Figure 6-33: Normalized signature (a) Co-pol channel -FP mode(b) Cross-pol channel -FP mode (c) Co-pol channel -CP mode (d) Cross-pol channel -CP mode -Study area II

The figures 6-32 (a) and (c) represent the normalized polarization signatures, in co-polarized channel, from the volume scattering images of both the fully-polarimetric and the compact polarimetric (π/4) modes, from Sal forests of Barkot area. Similarly, figures 6-33 (b) and (d) represent the same in cross-polarization channels of both the modes. The maximum and the minimum received power are denoted in red colour. It can be clearly analyzed from the shape of the signature that, for both co-polarized and cross-polarized channels, there is no change in the pedestal height, maximum and minimum received powers in both the fully-polarimetric and the compact polarimetric (π/4) modes. The value of coefficient of variation for cross-polarized channel signature for both the modes was found to be 0.734.

The figures 6-33 (a) and (c) represent the normalized polarization signatures, in co-polarized channel, from the volume scattering images of both the fully-polarimetric and the compact polarimetric modes, from Mangrove forests in Sundarbans, while figures 6-33 (b) and (d) represent the same in cross-polarization channels of both the modes. Similar to the analysis done on the signatures from the first study area, it can be clearly analyzed that there is no change in the pedestal height, maximum and minimum received powers in both the fully-polarimetric and the compact polarimetric modes. The value of coefficient of variation for cross-polarized channel signature for both the modes was found to be 0.884.

6.3.4. Analysis of Total Power

In this research, it was crucial to study the variation in the total power, which might have happened after reproducing the pseudo-quadrature polarized data, using the compact polarimetric (π/4) mode technique. The total power from both the modes was calculated by taking the sum of the diagonal elements of the coherency matrix $[T_{FULL}]$ and $[T_{MOD}]$. Similar to the analysis of diagonal elements, 100 pixels

representing the total power were taken from a sample, from both the modes and analyzed. The pixels were taken from the areas responsible for volume scattering mechanism.

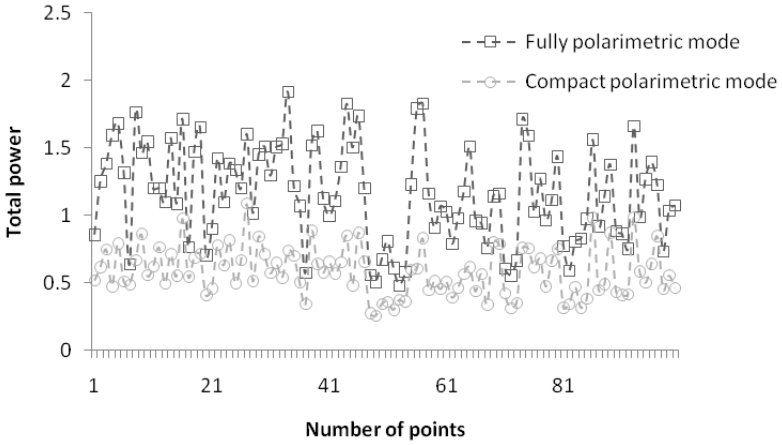

Figure 6-34: Variation of total power FP and CP modes-Study area I.
The lines are added to assist interpretation

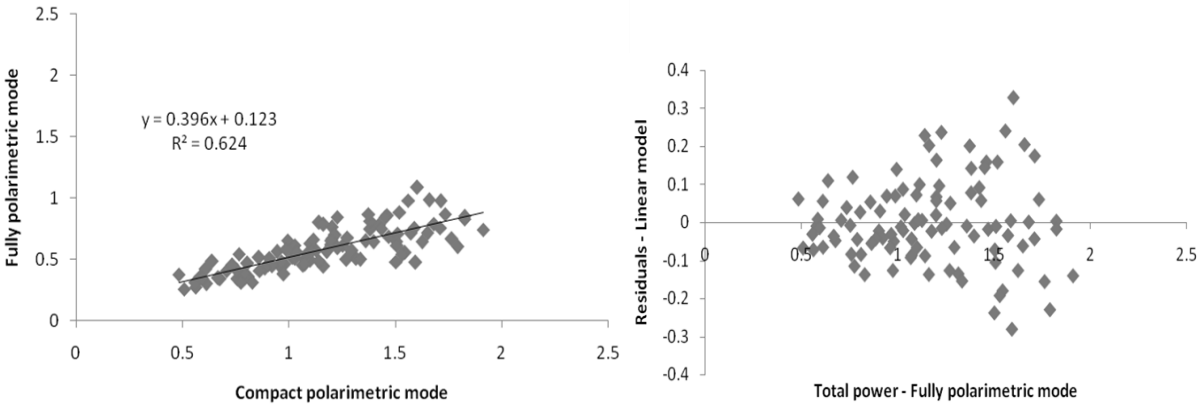

(a) (b)

Figure 6-35: Regression analysis-Total power- Study area I - (a) Linear model (b)Residual plot

The relationship between the total power received from the fully-polarimetric mode and the reproduced pseudo-quadrature polarized mode, from the Sal forests of Barkot has been analyzed using linear model, in figure: 6-35 (a). The value of correlation coefficient was found to be 0.79. The coefficient of determination was found to be 0.624 with a low RMSE of 0.110 between the predicted total power and the actual total power after reconstruction of pseudo-quadrature polarized values. After inspection of the variation graph (Figure 6-34**)** and the model fit, the compact polarimetric ($\pi/4$) mode tends to under estimate the total power, which has supported the fact of under estimating the single, double and the volume scattering powers from the data, after reproduction.

The residual analysis shown in figure 6-35 (b) shows an increasing trend which means the error variance increases with the total power in the fully-polarimetric mode from the Barkot forests. The correlation coefficient between the residuals and the total power of the fully-polarimetric data was found to be negative for linear model. The mean absolute error was also found to be close to zero for the linear model. Since there is an increasing trend in the residuals, the regression line does not fit the data.

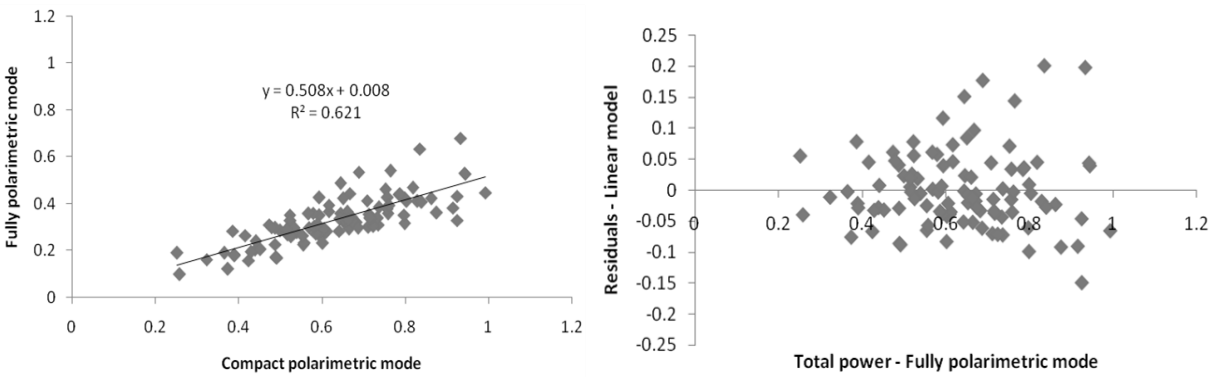

(a) (b)

Figure 6-36: Regression analysis-Total power-Study area II - (a) Linear model (b) Residual plot

The graphs represented in figures 6-36 (a) symbolize the relationship between the total power received from Mangrove forests of Sundarbans, for both the fully polarimetric and the compact polarimetric ($\pi/4$) modes, from a sample of 100 pixels, taken from the forested areas. The correlation coefficient was found to be 0.788. The regression analysis performed using linear model attained a coefficient of determination of 0.621 with a very low RMSE of 0.062 for total power. Similar to the result from Sal forests of Dehradun implemented (from the variation graph in figure 6-35), the compact polarimetric ($\pi/4$) mode tends to reduce the total power, which has supported the fact of reducing the single, double and volume scattering powers from the data, after reproduction.

Similar to the Barkot forests, the residuals (figure 6-36 (b)) show an in increasing trend, which means the error variance is increasing with the total power of the fully-polarimetric data from the Mangrove forests of Sundarbans. Similarly, the mean absolute error and the correlation coefficient is also very less in case of the linear model, Due to the increasing trend of the residual values, the regression line does not fit the total power data from both the modes for Mangrove forests of Sundarbans.

6.3.5. Entropy Analysis

The variation of entropy values from the forested areas from both study areas were analyzed, for both the fully-polarimetric and the compact polarimetric ($\pi/4$) modes.

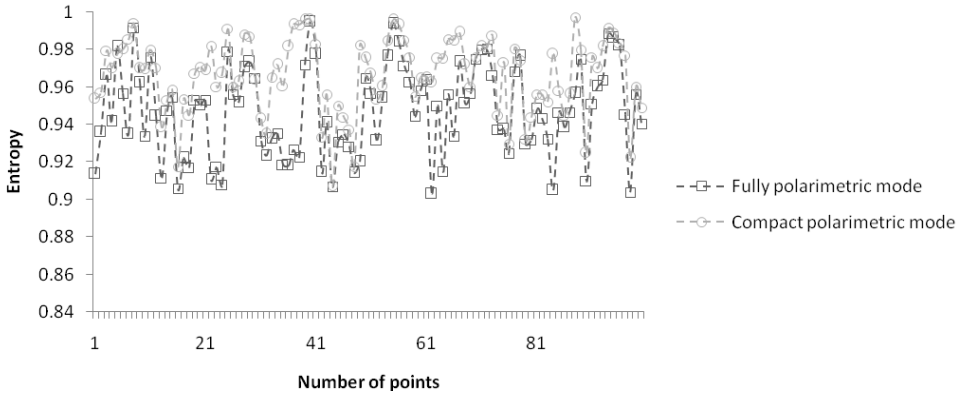

Figure 6-37: Variation of entropy- FP and CP modes - Study area I.
The lines are added to assist interpretation

The graph represented in figure: 6-37 represents the variation in the randomness in the volume scattering mechanism after reproduction of pseudo-quadrature polarized data, in comparison with fully-polarimetric mode, from Sal forests of Barkot area. From visual comparison, it can be concluded that there is a slight increase in the entropy from the forested areas, in the compact polarimetric mode, which meant that there is more randomness in the volume scattering mechanism in the reconstructed mode, when compared to the fully-polarimetric mode. The mean entropy value (sample) obtained from the fully-polarimetric mode was 0.947, while that from the compact polarimetric ($\pi/4$) mode was 0.966. The correlation coefficient was found to be 0.488.

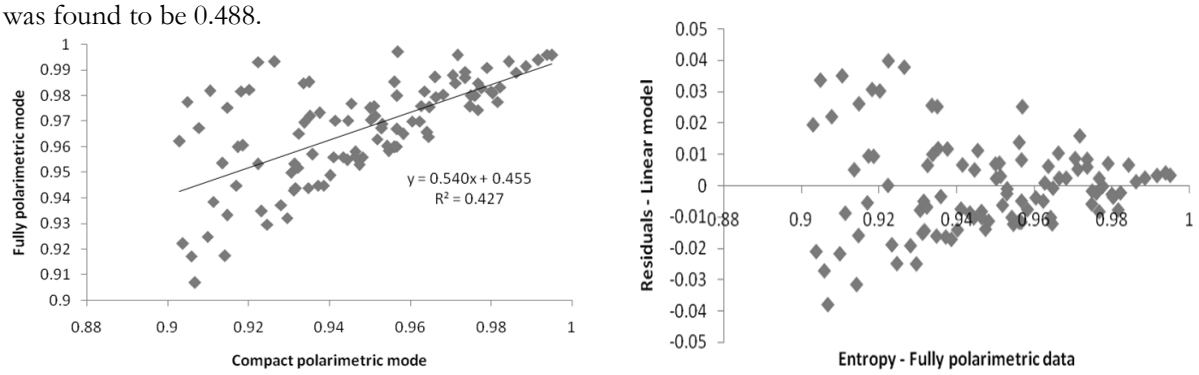

(a) (b)

Figure 6-38: Regression Analysis-Entropy - Study area I - (a) Linear model (b) Residual plot

In order to obtain the relationship between the entropy of the fully-polarimetric and the compact polarimetric ($\pi/4$) mode, regression analysis was performed using linear to estimate the model fit. The coefficient of determination, from the linear model (figure: 6-38 (a)) was found to be 0.427 with an RMSE of 0.01 between the estimated entropy value and the true entropy value obtained after reconstruction. The residual plot shown in figure: 6-38 (b) shows decreasing trend of residuals which means that, the error variance of the entropy values decreases with the entropy values calculated from the fully-polarimetric mode. Even though the mean absolute error was found to be low as 0.47 and the correlation coefficient between the residuals and the entropy values of the fully-polarimetric mode was negative close to zero, it has to be presumed that, a non-linear model may be used to estimate the best line fit for the data.

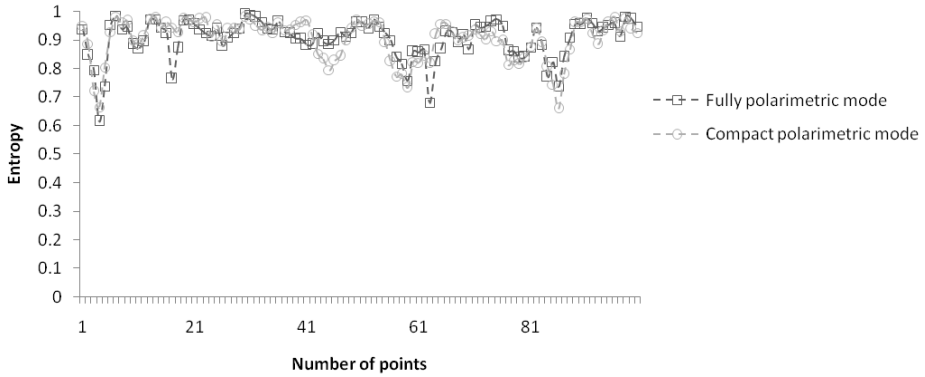

Figure 6-39: Variation of entropy-FP and CP modes - Study area II.
The lines are added to assist interpretation

The graph represented in figure: 6-39 represents the variation in the randomness in the volume scattering mechanism after reproduction of pseudo-quadrature polarized data from the Mangrove forests of

Sundarbans. Similar to the analysis implemented on Sal forests from the first study area, from the graph it can be inferred that the compact polarimetric (π/4) mode tends to over estimate the entropy from the Mangrove forests, which means that there is more randomness in the volume scattering mechanism in the reconstructed mode, when compared to the fully-polarimetric mode. The value of correlation coefficient was found to be 0.579.

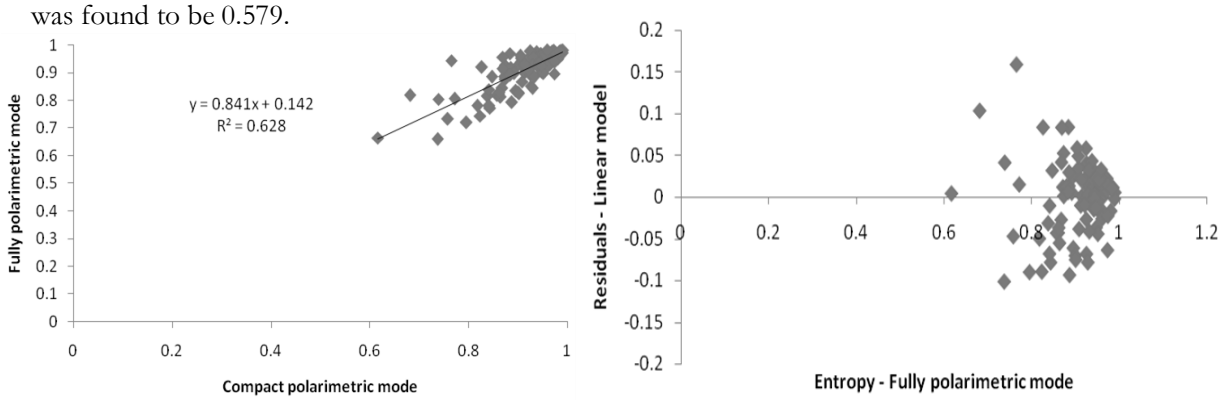

(a) (b)

Figure 6-40: Regression analysis-Entropy-Study area II - (a) Linear model (b) Residual plot

In order to obtain the relationship between the entropy of the fully-polarimetric and the compact polarimetric (π/4) mode, regression analysis was performed using linear model (figure: 6-40 (a)). The coefficient of determination was found to be 0.628 with an RMSE of 0.04 between the estimated entropy value and the true entropy value obtained after reconstruction. Similar to the entropy variation from Barkot forest, the residual plot shown in figure: 6-40 (b) shows decreasing trend of residuals for Mangrove forests, which almost converges to 0.9904 with an error of 0.057. The mean absolute error and the correlation coefficient were also found to be very low and negative close to zero.

6.4. Validation

The volume scattering contribution from tree trunk, leaves and from the ground from both the forested areas, decomposed using the three-component decomposition model, were validated against the multi looked single polarized data $2S_{HV}$, which was assumed to be the reliable reference data.

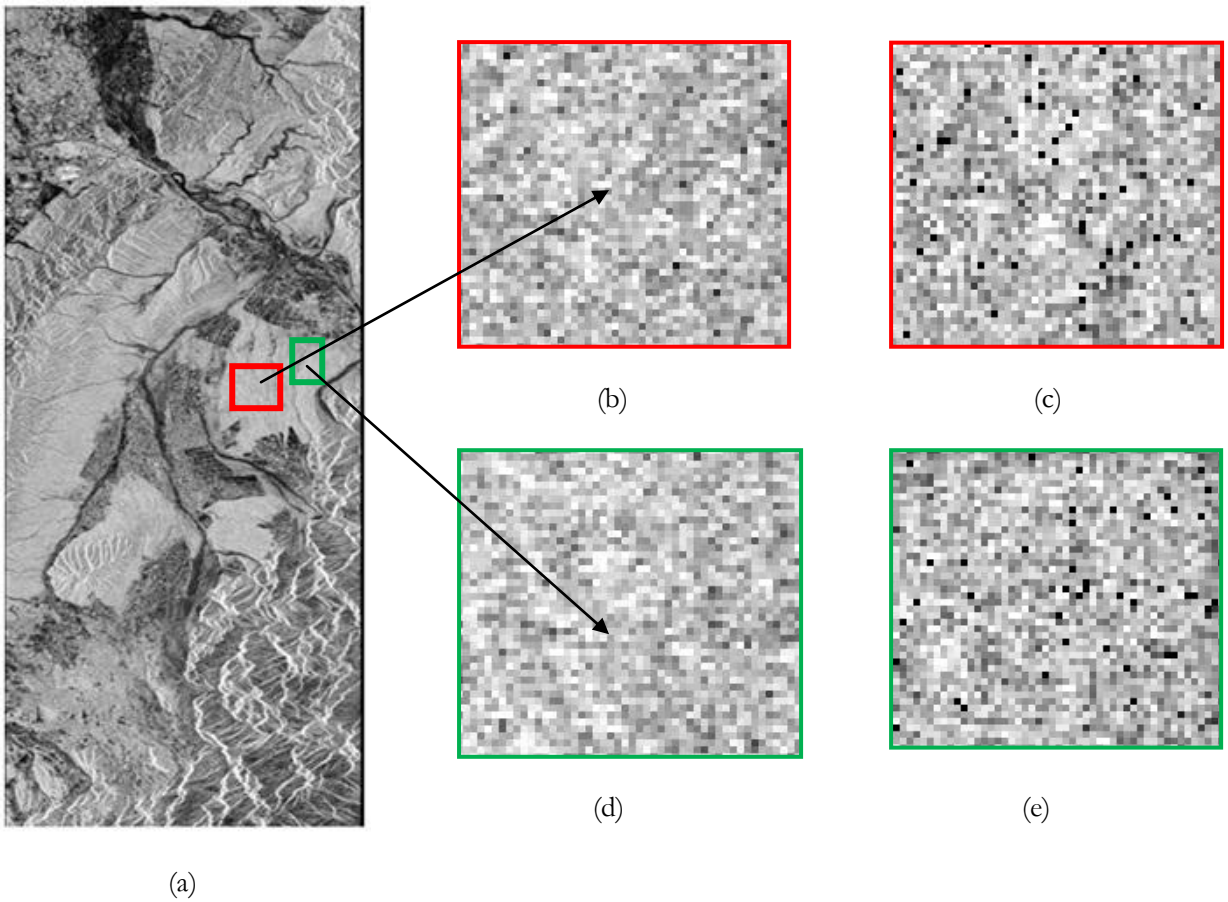

Figure 6-41: (a) Reference data $2S_{HV}$ - Barkot area (b) Forest area subset - reference data (c) - Forest area subset - volume scattering decomposed image-CP mode (d) Sample subset - reference data (e) Validation subset - volume scattering decomposed image-CP mode

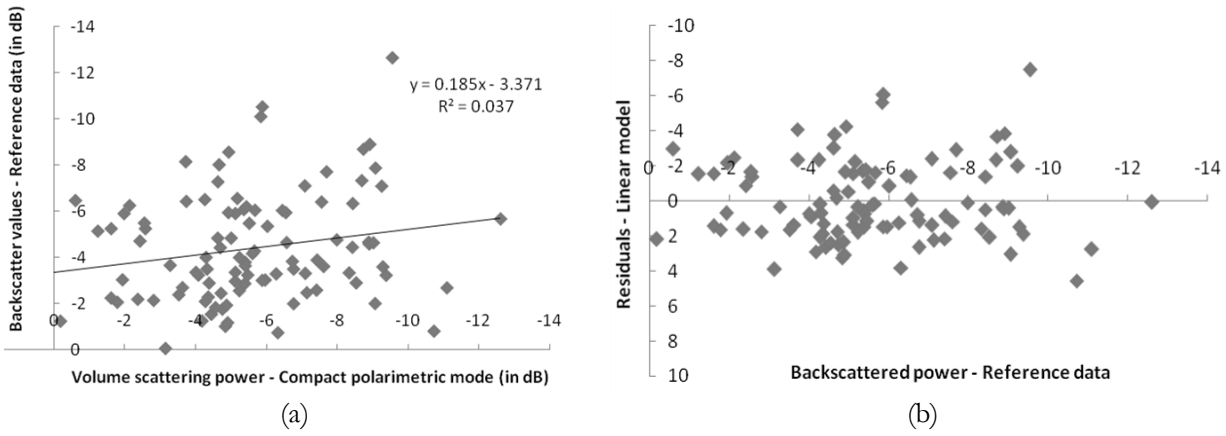

Figure 6-42: Regression analysis – Validation - Study area I - (a) Linear model (b) Residual plot

The figure: 6-42 (a) shows the model fit using linear model between the volume scattering power from Barkot forest area, of 100 points taken from the sample subset shown in figure: 6-41 (c) against the backscattered power values from the same pixels from the sample subset of the reference data $2S_{HV}$ shown in figure: 6-41 (b). The residual graph (figure: 6-42 (b)) showing the relation between the backscattered power values from the reference data and the difference between the predicted value and the original pseudo-quadrature polarized data, shows random trend with negative and low correlation coefficient and mean absolute error, close to zero. Therefore it can be presumed that the linear model fits the data. This model was used in another sample consisting of 100 pixels from the same population of forested areas shown in figures: 6-41 (b) and (d), in order to validate the volume scatterer contribution of tree leaves, trunk and from the ground of the Barkot forest area.

Table 4: Statistical summary for accuracy measures after validation-Study area I

Statistical Measure	**Regression from first sample**			**Regression from the validated sample**		
	Reference data	**$\pi/4$ mode**	**Predicted value ($\pi/4$ mode)**	**Reference data**	**$\pi/4$ mode**	**Predicted value ($\pi/4$ mode)**
Mean	-5.631 dB	-4.41 dB	-4.41 dB	-6.19 dB	-4.60 dB	-4.51 dB
Standard deviation	2.424 dB	2.338 dB	0.44 dB	2.889 dB	3.188 dB	0.534 dB
RMS error of regression	2.282 dB			3.192 dB		
Average Residual	4.44×10^{-19} dB			-0.087 dB		
Mean absolute error (MAE)	1.869 dB			2.192 dB		
Correlation coefficient (Residuals)	4.935×10^{-13} dB			-0.125 dB		

Table 5 shows the summary of different statistical parameters used for validating the volume scatterer contribution from the compact polarimetric mode against the fully-polarimetric mode. The mean of the backscattered power from the sample of the reference data from both the samples are almost identical with suggests homogeneity in the selection of forest class sample from the population. The mean of the decomposed volume scattering power from the reconstructed pseudo-quadrature polarized mode also is identical, however the volume scattering power has increased when compared to the backscattered power from the reference data. The mean of the predicted value of the reconstructed mode after using the build model also remains identical. RMS error, being considered as a robust measure for accuracy assessment was also used for validation. The RMS error of regression obtained after modelling from the first sample was found to be 2.282 dB. While validating the test sample, which represents the population of forest class, the linear model produced the RMS error of 3.192 dB, almost identical to the RMS error from the first sample. The average value of residuals was calculated and found to be identical and close to zero. The mean absolute error was also found to be identical and close to the standard errors of 2.058 dB and 2.21 dB. Finally the correlation coefficient between the reference data and the residuals obtained after modelling was also found to be negative with identical values close to zero.

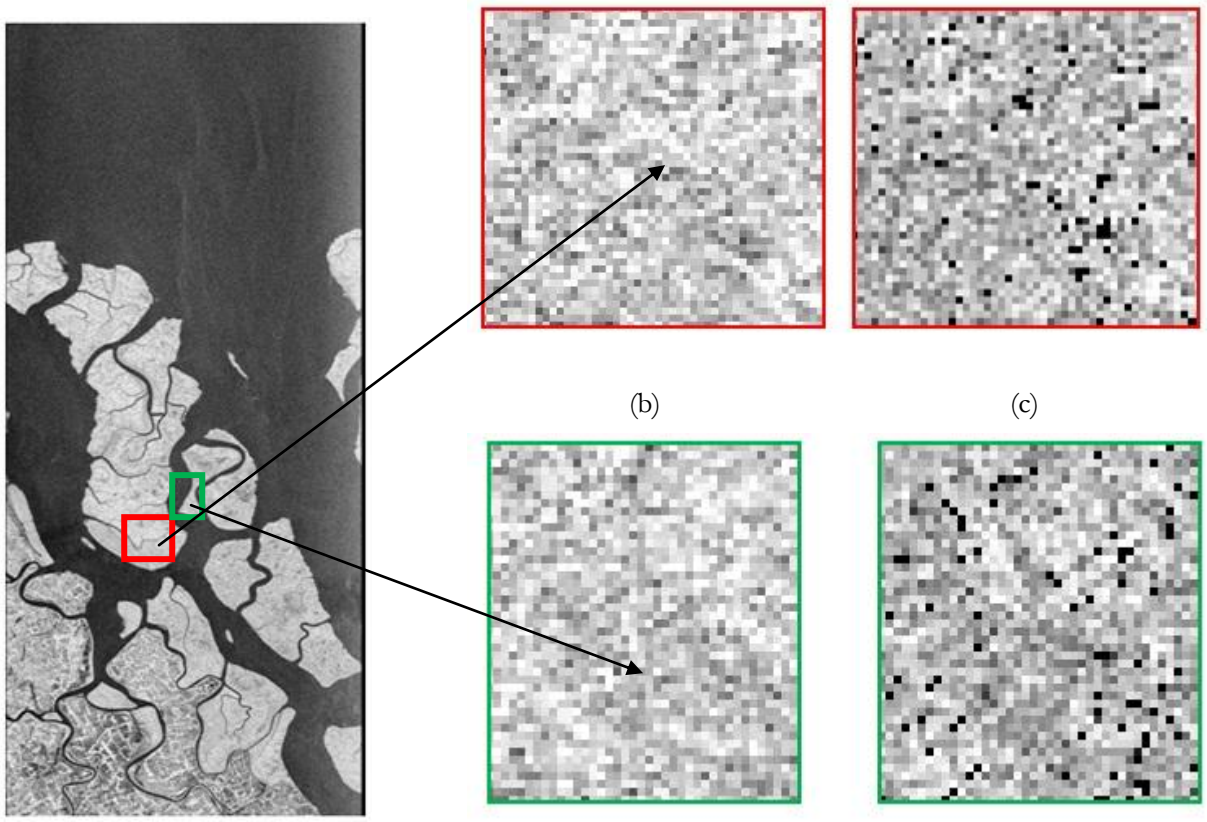

(a) (b) (c) (d) (e)

Figure 6-43: (a) Reference data $2S_{HV}$ - Sundarbans area (b) Forest area subset - reference data (c) Forest area subset - volume scattering decomposed image-CP mode (d) Sample subset - reference data (e) Validation subset - volume scattering decomposed image-CP mode

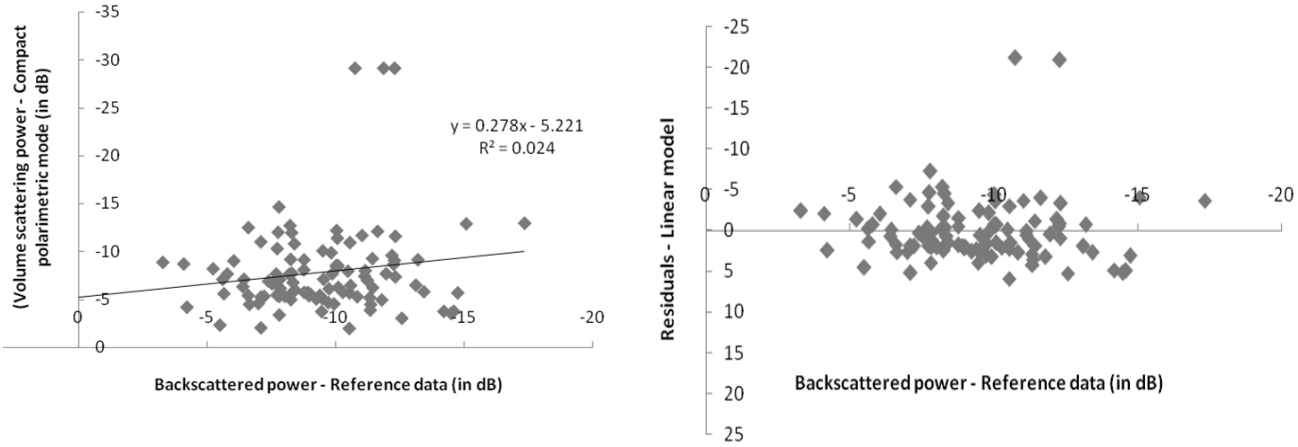

(a) (b)

Figure 6-44: Regression analysis - Validation - Study area II - (a) Linear model (b) Residual plot

Similar to the Barkot area, the same procedure was done on the Sundarbans. Linear model approach (figure: 6-44 (a)) was used between the volume scattering power from the Mangrove forests of Sundarbans, of 100 points taken from the sample subset (figure: 6-43 (c)) against the backscattered power values from the same pixels from the sample subset of the reference data $2S_{HV}$ (figure: 6-43 (b)). The residual graph (figure: 6-44 (b)) showing the relation between the backscattered power values from the reference data and the difference between the predicted value and the original pseudo-quadrature polarized data, shows random trend with negative and low correlation coefficient and mean absolute error, close to zero. Therefore it can be presumed that the linear model fits the data. This model was used in another sample consisting of 100 pixels from the same population of forested areas (figures: 6-43 (b) and (d)), to validate the volume scatterer contribution from the Mangrove forests of Sundarbans.

Table 5: Statistical summary for accuracy measures after validation-Study area II

Statistical Measure	**Regression from first sample**			**Regression from the validated sample**		
	Reference data	**$\pi/4$ mode**	**Predicted value ($\pi/4$ mode)**	**Reference data**	**$\pi/4$ mode**	**Predicted value ($\pi/4$ mode)**
Mean	-9.472 dB	-7.651 dB	-7.651 dB	-9.83 dB	-7.502 dB	-7.502 dB
Standard deviation	2.58 dB	4.124 dB	0.524 dB	2.364 dB	5.258 dB	1.436 dB
RMS error of regression	4.07 dB			5.03 dB		
Average Residual	9×10^{-11} dB			10^{-10}dB		
Mean absolute error (MAE)	2.64 dB			3.31 dB		
Correlation coefficient (Residuals)	2.28×10^{-11} dB			-2.24×10^{-11} dB		

Table 6 shows the summary of different statistical parameters used for validating the volume scatterer contribution from the compact polarimetric mode against the fully-polarimetric mode, from the Mangrove forests of Sundarbans. Alike the results from the Barkot forest area, the mean of the backscattered power from the sample of the reference data from both the samples are almost identical with suggests homogeneity in the selection of forest class sample from the population. The mean of the predicted value of the reconstructed mode after using the build model also remains identical. The RMS error of the residuals obtained, after modelling from the first sample was found to be 4.07 dB. While validating the test sample, which represents the population of forest class, the linear model produced the RMS error of 5.03 dB, almost identical to the RMS error from the first sample. The average value of residuals was calculated and found to be identical and close to zero. The mean absolute error was also found to be identical and close to the standard errors of 4.11 dB and 5.08 dB. The correlation coefficient between the reference data and the residuals obtained after modelling was also found to be negative with identical values close to zero

7. DISCUSSIONS

This chapter presents a discussion of the research carried out reviewing the methodology carried out to achieve the research objectives and questions, evaluating and interpreting the findings in the form of results from different data analysis and hypothesize on the possible reasons about the findings.

7.1. Importance of coherency matrix approach- (π/4) mode.

The concept of using the coherency matrix using the fully-polarimetric data has already proven to provide information on the different scattering mechanisms present in a particular area. The coherency matrix is considered to be important since the coherency matrix is closely associated to the physical and geometrical properties of the different scattering mechanisms and therefore facilitate direct physical interpretation of the features under investigation. Moreover the coherency matrix is susceptible to orientation angle shift, which may produce higher cross-polarization intensity especially from the forested areas, sensitive cross-polarization term S_{HV} and makes the coherency matrix reflection asymmetric. The coherency matrix also becomes a factor for the local variations in the scattering matrix and is suitable to study the different polarization parameters. The research has analyzed a few of these parameters like the total power and the entropy. When compared to the covariance matrix, which also gives similar kind of information, the coherency matrix due to its complexity of the matrix elements due to the combination of multiple polarizations, gives precise information on these scattering mechanisms. Especially the three diagonal elements T_{11} , T_{22} and T_{33} of the coherency matrix $[T_{FULL}]$, gives polarimetric information on the single-bounce, the double-bounce and the volume scattering mechanisms.

7.2. Discussion on the analysis of the diagonal elements

Thorough regression analysis and assessing the model fit using residual plots has showed decrease of power for the single-bounce and the double-bounce scattering mechanism, after reconstruction of the pseudo-quadrature polarized data. In case of the volume scattering power obtained from the T_{33} elements for both the areas, it was found that there is irregular variation in the cross-polarized power sensitive to the volume scattering mechanism. The positive values of the median of the relative error for all the three diagonal elements show that the reconstructed values are lower than the original fully-polarimetric data. The large standard deviations for the cross-polarized reconstruction using the $(\pi/4)$ technique mean that the cross-polarized returns were not well reproduced at an individual pixel level.

The linear model for fitting the values of the T_{11} elements for both study areas sensitive to the surface scattering was found to be effective, with the residual plots showing low correlation coefficient and average residual value close to zero. In case of T_{22} element, the linear model showed very high correlation between the original and the reconstructed values, the residual plot showed a non-random trend of the residuals, especially from the urban areas of Haridwar region of the first Study area Image. The trend showed a linear decreasing trend showing that the error variance was decreasing with the sum of the co-polarized power. The residual analysis showed very low negative correlation coefficient and the average of the residuals was close to zero. This contradiction was not analyzed in this research. In case of the man-made features from the Sundarbans, the similar effect was observed, although a linear non-random pattern was observed. Random pattern was observed when the double-bounce power of the fully-polarimetric mode increased to more than 1.5 dB. The man-made features from the Sundarbans in

the SAR image are not present as a township area; instead the area shows some buildings with agricultural areas in a definite pattern and trees in between. The agricultural features show fallow land exhibiting single-bounce scattering, while the areas in green exhibits multiple reflections similar to that of the volume scattering from the mangrove forested areas. The trees present in between also causes distraction for the man-made features to exhibit the double-bounce scattering. Moreover, the subset was taken as polygon rather than points. Therefore, the sample points might have had pixels which had not exhibited the double-bounce scattering. Consequently, the agricultural areas and the trees in between the man-made features must have caused the residual errors to show non-random trend with a pattern and the man-made features showing random trend.

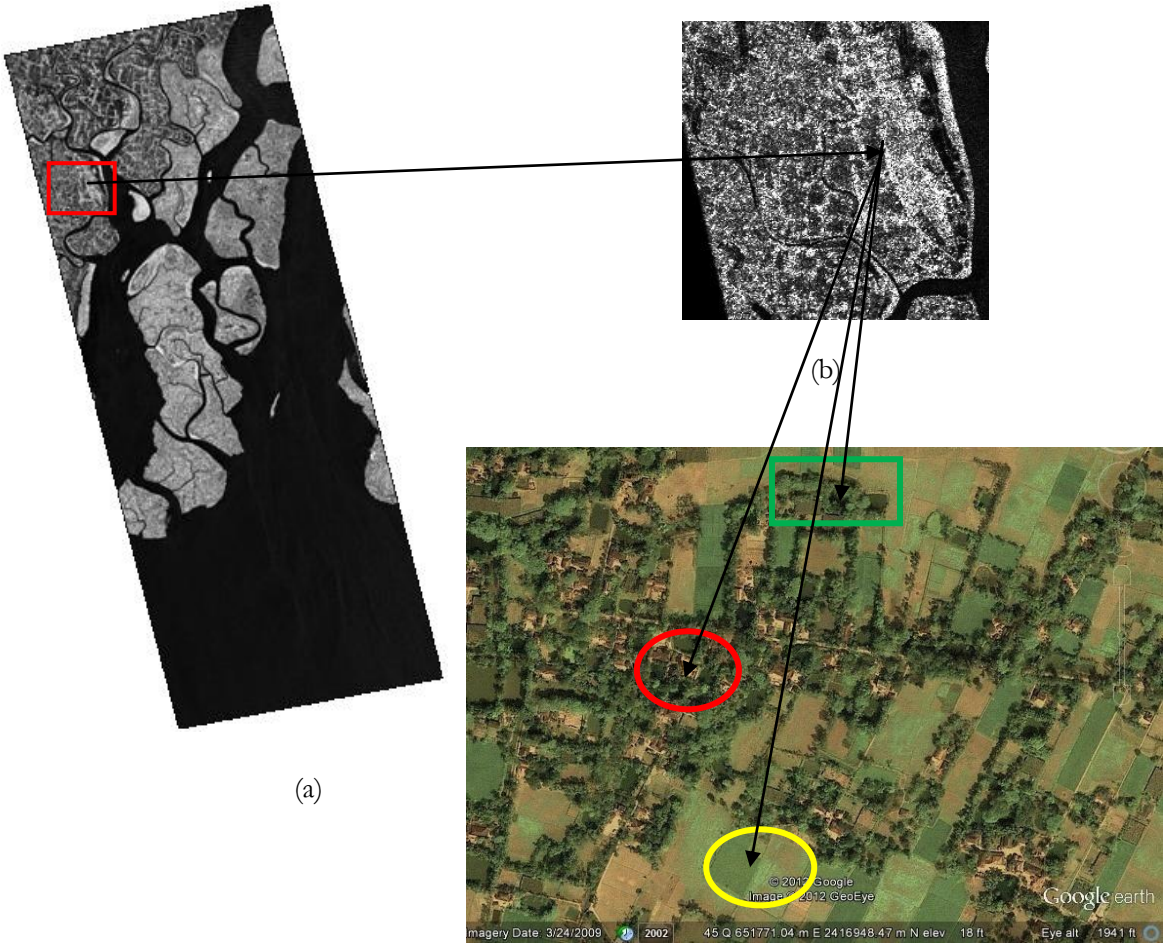

Figure 7-1: (a) Georeferenced T_{22} element-Sundarbans (b) zoomed image of the subset (c) Subset area from Geoeye-I sensor-Buildings (red), Agricultural areas (yellow), Trees (green) Source: Google Earth

7.3. Discussion on analysis of variation in volume scattering power

The research was focused on studying the effect of the volume scattering contribution from the tree leaves, trunk and from the ground from both the forested areas of Barkot and the Sundarbans. The analysis of T_{33} element and the decomposed volume scattering contribution showed very low correlation between the original and the reconstructed values. It was found that some of the pixels taken from the area sensitive to volume scattering mechanism had shown uneven and abrupt changes in the volume scattering power before and after decomposition. This had in turn caused the uneven variation in the volume scattering power

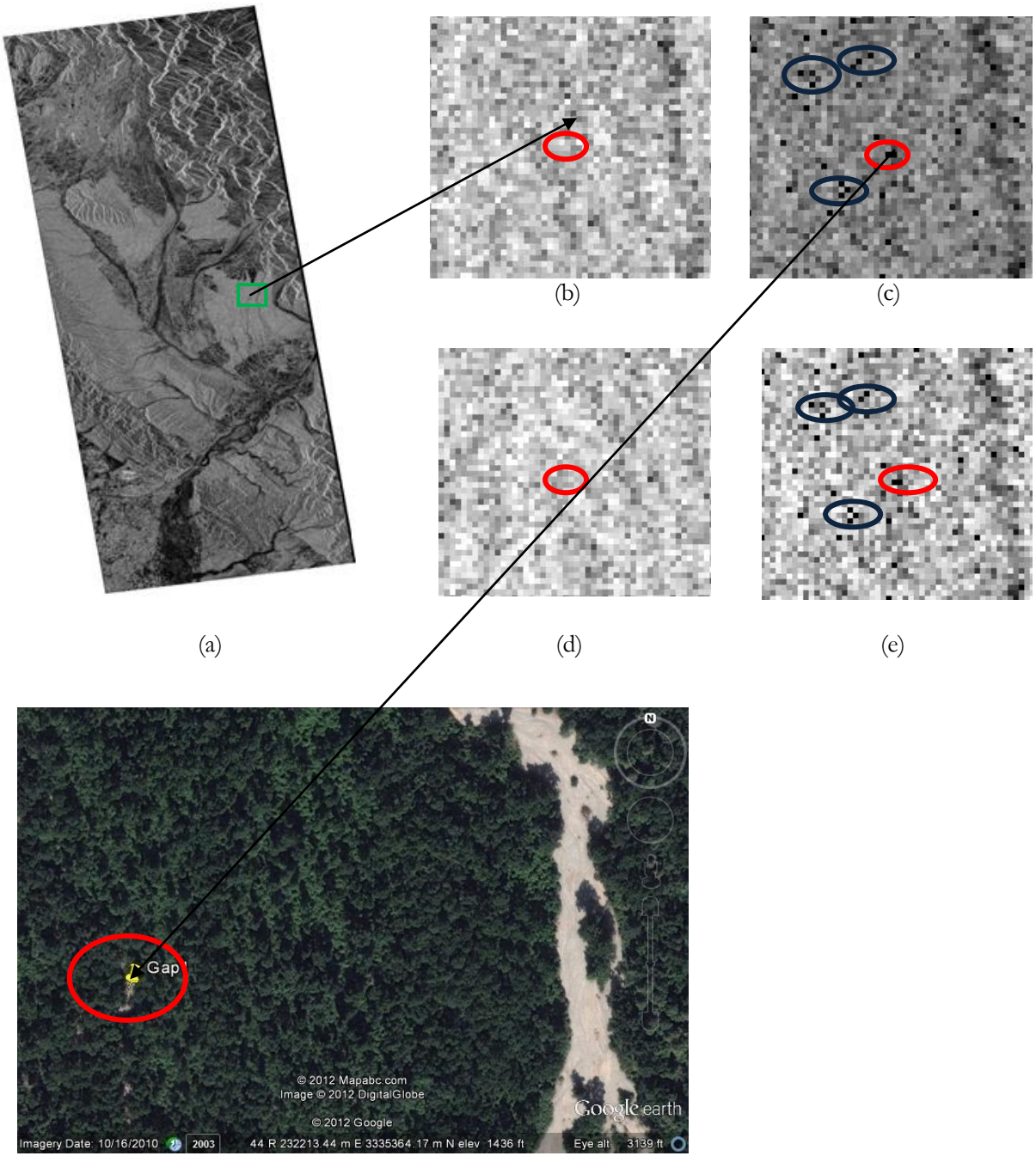

Figure 7-2: (a) Georeferenced T_{33} element - Barkot forest (b) zoomed image-FP mode(c) CP mode (d) Freeman-volume-FP mode(e) CP mode (f) Image - Geoeye-I sensor. Source: Google Earth

The sets of figures 7-2 (a) to (e) shows an example of one among many pixels from the areas sensitive to volume scattering with abrupt changes in the cross-polarized power after reconstruction of the pseudo-quadrature polarized followed by decomposition using the three-component model. The figure 7-2 (a) shows the georeferenced image of the original T_{33} element of the coherency matrix from the fully-polarimetric mode from the first study area. The image shown in (b) shows the subset sample taken from the original T_{33} element. The next image (c) shows the same subset taken from the T_{33} element after reproducing the coherency matrix for the compact polarimetric mode. Image (d) shows the decomposed volume scattering image subset from the same area for the fully-polarimetric (FP) mode and image (e) shows the same for the compact polarimetric (CP) mode. The last image (f) encircled in red shows the features responsible for the abrupt change of the power. The red circles on the images (b) to (e) show a pixel which shows change. Few other pixels similar to this are shown in blue circles.

Table 6: Cross-polarized power variation before and after reconstruction

Output image	Cross-polarized power (in dB)
T_{33} - FP mode	-7.74
T_{33} - CP mode	**-inf**
Decomposed volume scattering power - (FP mode)	-3.33
Decomposed volume scattering power - (CP mode)	-24.54

The values from table 7 show abrupt change in the cross-polarized power for the test pixel. Comparing the cross-polarized power of the pixel from the T_{33} element from both the modes after reconstruction using the polarization state extrapolation technique, the value was found to be showing "-inf", which means infinite data value with a negative sign. This was obtained after taking the logarithm of zero in linear scale. But while decomposing the coherency matrix elements using the three-component decomposition model, the volume scattering power increased from the cross-polarized power in the fully-polarimetric mode. While decomposing the volume scattering contribution from the reconstructed elements, the volume scattering power drastically changed to a much lower value.

From the comparison of the same area on the image obtained from the Geoeye-I sensor in Google Earth tool, it was found that the backscatter took place from a part of the Sal forest area with a large gap between the trees (shown as a place mark with "Gap1" title in figure 7-2 (f)) showing a continuous tributary flowing to a river depicted next to the gap. There is no proof that the tributary is moist or dry. There are few reasons to justify this abrupt change.

- The backscatter for that particular pixel must have occurred considering the forests and the dry tributary as a mixed pixel which must have hampered the polarization extrapolation algorithm to reconstruct that particular pixel. Assuming the tributary to be dry, which accounts for specular reflection from a smooth surface, the pixel may have contribution from the tree leaves, trunk, ground surface below the trees and also from this tributary surface.

- The polarization extrapolation algorithm assumes the relation linking to the degree of coherence and the cross-polarized power. The algorithm also assumes the reflection symmetry condition

also, which is usually observed from natural scatterers such as forests, water surface. In this case, considering the pixel to be mixed, the backscatter contribution can the volume scattering contribution from the tree trunks, leaves and from the ground, surface scattering from the dry tributary and even may be double-bounce scattering from the trees present alongside the tributary and the dry bed.

- The first assumption holds true for the features exhibiting the volume scattering mechanism. But the assumption fails while considering the super position of all the three scattering mechanisms in the same imaged pixel [7].

- In case of the reflection symmetry condition, for a high resolution SAR imagery, this condition holds true only while considering the averaging of more pixels [7]. This research has not considered this method of averaging pixels using different window size. Therefore, it might be possible that, for the pixel exhibiting all the three scattering mechanisms, the reflection symmetry may not hold true.

- Another reason may be due to the fact that the coherency matrix is sensitive to the polarimetric orientation angle shifts which cause the cross-polarization intensity from the forested areas to become high and make the coherency matrix reflection asymmetric.

- The pixel representing the features is located at an altitude of 1400 ft. Ambiguities may occur, if the region is having high azimuth slopes, especially regions exhibiting orientation angle effects (features not oriented parallel to the radar line of sight).

- The polarization extrapolation algorithm used here employs the assumptions already developed. The modifications on the degree of coherence relation assumption studied in [7], [37] hasn't been included in this algorithm. The modification was to use the ratio of the double-bounce scattering power and the volume scattering power to compensate the effect of dihedral scattering, which affects the degree of coherence assumption.

The same phenomenon was noticed for some other pixels also, before and after the three-component decomposition. The abrupt change in the volume scattering power lowered the correlation between the original and the reconstructed data. Even though the quality of the regression analysis was confirmed through the residual plots with the residuals showing random trend with very low value of correlation coefficient and mean absolute error, the outliers showing unexpected variations in the volume scattering power in the reconstructed data has caused the difficulty to predict precisely whether the volume scattering power has been increased or decreased. The same phenomenon has caused problems in the validation procedure also, which is discussed in the next sub-section.

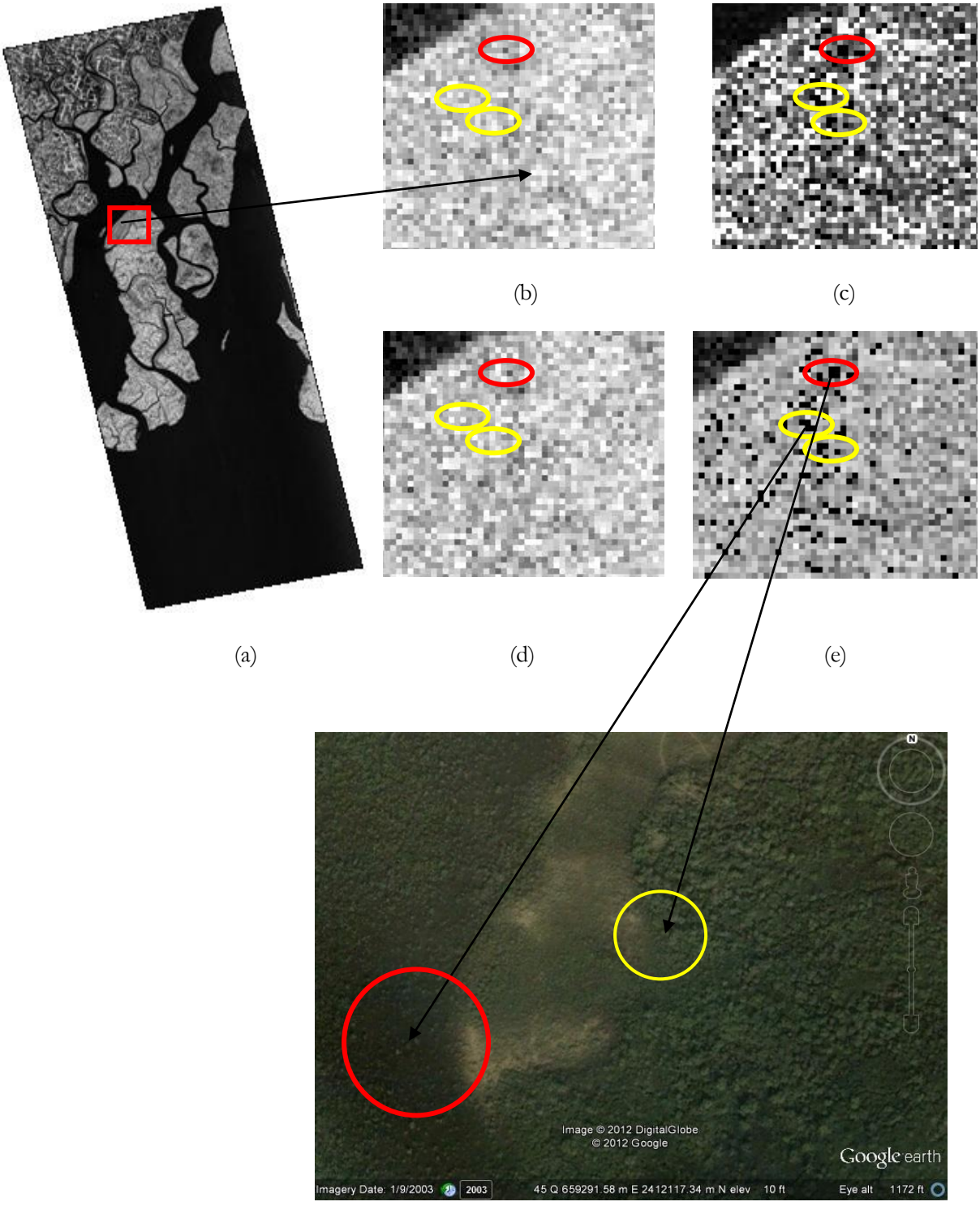

Figure 7-3: (a) Georeferenced T_{33} element-Mangrove forest area, The Sundarbans (b) zoomed image-FP mode(c) CP mode (d) Freeman-volume-FP mode(e) CP mode
(f) Image - Geoeye-I sensor. Source: Google Earth

The phenomenon of showing abrupt change in the pixel values after reconstruction and decomposition was also observed in the Mangrove forests. On closely observing the features represented in red circle in the figure 7-3 (f), the forest area is present in swampy areas where the moisture content is very high. The forest density was also found to be fluctuating with varying tree heights and low canopy area. Similar to the reason observed from the Barkot area, considering the pixel to be mixed, the volume scattering from the forested area is not uniform due to the varying tree heights and forest density, the low lying marshy areas, wetland with poorly drained land section lying near to the forests contribute to double-bounce scattering from the ground as well as from the tree trunks [50]. The whitish portion in the optical image represents depicts a marshy area with high soil moisture and tributaries leading to the Bay of Bengal. The contribution of the surface-scattering mechanism cannot be reasoned off since; the marshy areas can also leading to specular reflection from standing water.

Ambiguities due to azimuth slopes can be reasoned out since the region is low lying close to the sea with a low elevation of only 3 m (as shown in the Google Earth image).

The first assumption in the polarization extrapolation algorithm does not hold true, since the contribution of the double-bounce mechanism also plays an important part in the imaged pixel which violates the equivalence [7].

Another observation is that, even though there is no proof of standing water below the forests, the forested areas which are away from these marshy lands hold the two assumptions and the reconstruction mechanism works.

The assumption does not hold true for cross-polarized term, where there are complete marshy areas, which prominently exhibit double-bounce scattering. This again causes the degradation of the algorithm which causes the volume scattering power to decrease drastically when compared to the original values.

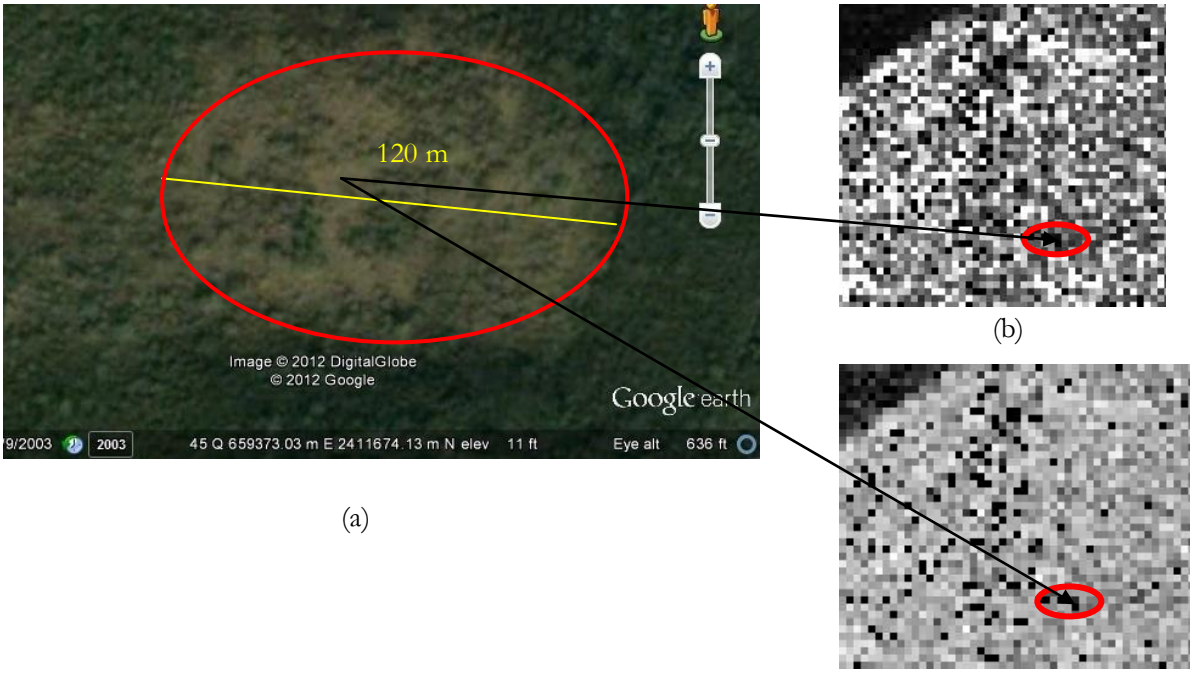

Figure 7-4: (a) Marshy areas of the Sundarbans. Source: Google Earth (b) T_{33} element-CP mode (c) Freeman- volume -CP mode

The figure 7-4 (a) depicts a marshy area with some trees in between from the Sundarbans area with 120 m (shown with an yellow line) length measured using the measurement tool in the Google Earth tool. The corresponding 5 to 7 pixels with approximate 20 m ground resolution on both the subset images shows abrupt power values after T_{33} reconstruction (figure: 7-4 (b)) and decomposition (figure: 7-4 (c)). All the pixels show power value of -29 dB in the reconstructed T_{33} element and -13 to -15 dB power range in the decomposed element. It has to be understood that the marshy land contributes to the double-bounce scattering mechanism which was proved also from the polarization signature analysis. This clearly proves that presence of dihedral scattering mechanism along with the volume scattering mechanism degrades the polarization state extrapolation algorithm used in this research. The abrupt change in the volume scattering power has caused the reconstruction of the forest class to perform with uneven variations in the original and the reconstructed values.

7.4. The "factor 2" factor

The research followed the reconstruction algorithm based on the original technique developed in [10], [11]. The studies implemented by them had omitted the constant ½ used as a multiplier outside the 2×2 covariance matrix in the $\pi/4$ mode, describing its impact on the computation of the SAR power budget, even though it does not affect the polarimetric performance [6]. While calculating the single-bounce power $\langle|S_{HH}+S_{VV}|^2\rangle$, the double-bounce power $\langle|S_{HH}-S_{VV}|^2\rangle$ and the volume scattering power $4\langle|S_{HV}|^2\rangle$ from the original coherency matrices, the T_{11} and T_{22} elements were divided by 2 and the T_{33} element was multiplied by 2, since the constant $1/2$ was present outside the coherency matrix in the fully-polarimetric mode however not present in the covariance matrix obtained from the fully-polarimetric mode. The coherency matrix reproduced for the $\pi/4$ mode also had the effect of the omission of the constant, since the reproduced coherency matrix was transformed from the covariance matrix using the unitary transformation matrix. Therefore, it is possible that omission of the constant might have caused decrease in the reconstructed values when compared to the fully-polarimetric values.

The algorithm developed in [10], [11] should have considered the possibility for using the same method using coherency matrix approach without considering the omission of the factor 2. Especially while converting the covariance matrix into coherency matrix, the factor 2 causes variation in the reconstructed results while comparing the two matrices. This aspect was not studied in this research. The algorithm used in the PolSAR pro tool used for this research also show this omission factor, which can be modified for future work.

7.5. Relevance of Polarization Signature analysis

In case of volume scattering from Sal forests of Barkot, the polarization signature of the cross-polarized channel HV from both the modes appeared to show very high pedestal value, almost unity, which meant that a significant portion of the backscattered power is not polarized and proved that the signature is from a heavy forested area. The value for cross-polarized channel signature for both the modes was found to be 0.734 which is high, which clearly suggests that there is increase in the relative amount of backscattered power from the randomly oriented vegetation which might have caused due to increase in tree height and density [59], which is true in case of Sal forests with tree height ranging up to 11 m. It was also understood from the high value of coefficient of variation that there is an appreciable amount of volume scattered power which is not polarized. Even, for a heavily forested area, the scattering from the branches dominate depending on the tree density and surface conditions which in turn causes a large amount of unpolarized backscattering component in the radar return.

The polarization signature from the mangrove forests of Sundarbans showed the effect in the pedestal factor, similar to the Sal forests. The value of pedestal was found to be very high, almost unity, which meant that there is significant portion of the backscattered power that is unpolarized and proved that the signature is from a forested area. The value of coefficient of variation for cross-polarized channel signature for both the modes was found to be 0.884 which is very high, more than from Sal forests which clearly suggests that there is a high degree of randomness in the scattering mechanism from the mangrove forest area. It might be attributed to the fact that, mangrove forests are very dense with high tree density. From high coefficient of variation, it can also be inferred that there is an appreciable amount of volume scattered power from the forested area which is not polarized. Due to the climatic and terrain conditions of mangrove forests, the mangrove forests were modelled as a forest with relatively thin canopy and with a surface having high dielectric constant, due to the presence of standing water [50].

The polarization signature of the swampy areas resemble to those predicted for dihedral corner reflector geometry [50], [60]. The main difference in the radar return from the swampy areas is the 180° (approx) phase difference between vertical and horizontal polarizations. Moreover, the coefficient of variation from the swampy areas was found to be larger than that from the dense forests of Barkot. Hence, for large coefficient of variation, VV polarization dominates over HV. For swampy areas, trunk-ground double-bounce scattering dominates even though there is no negligible branch scattering. Even though the coefficient of variation for the double-bounce scattering is almost unity, the presence of branch scattering which has caused volume scattering mechanism to take place has caused the coefficient of variation to reduce to 0.884. This theory has abided with the studies implemented in [50], [60]. Even though there is a decrease in volume scattering power in the reproduced pseudo-quadrature polarized data, the reduction in the power has not affected the polarization signature of both the modes.

The common conclusion from this analysis is that, even though there is a decrease in the volume scattering power from both the modes from both the forested areas, the signature and texture were preserved, after reproduction of pseudo-quadrature polarized data using dual-polarimetric techniques. This may provide the opportunity for using polarization signature as a reliable tool for analyzing the features responsible for single and double-bounce scattering mechanisms.

7.6. Entropy analysis

The study has analyzed the variation in the entropy values from the areas responsible for volume scattering mechanism, especially from the forested areas of both study areas. The entropy analysis proved that, there is only a slight increase in the randomness in the volume scattering mechanism forest pixels, after reconstruction of the pseudo-quadrature polarized data. The very high entropy values from the areas from both the modes from both the forested areas proved that the feature under study was responsible for volume scattering mechanism and therefore the randomness was found to be high. The window size selected for calculating entropy was 3×3 and therefore, the features in the neighbouring pixels around the central pixel value has great importance, since presence of different features in these pixels can affect the entropy of the central pixel.

The analysis from the Barkot area showed low correlation when compared to that of Mangrove forests, since it was found that there is an uneven variation in the reconstructed entropy values when compared to the entropy values from the fully-polarimetric mode. This occurs due to various reasons. In Barkot area, along with Sal forests, it might be possible that there can be other tree species of different canopy area, tree height and density whose presence along with a different species causes variation in the volume scattering power. Another reason being the fact that, the entropy values were calculated from the third

diagonal element T_{33} of the coherency matrices $[T_{FULL}]$ and$[T_{MOD}]$ but not from the volume scattering images decomposed from the coherency matrices using the three-component decomposition model. The diagonal T_{33} is sensitive to the areas responsible for volume scattering. If the entropy values were calculated from the decomposed volume scattering images, then the effect of the entropy variation may have been different.

The variation graph and the model fit results from the Mangrove forests showed increase in the entropy values after reconstruction, with an even variation. This may be due to the fact that, the forest area from which the sample points were chosen is dense and thick and is homogenous. Therefore, neighbouring pixels are expected to exhibit the same scattering mechanism and therefore do not substantially contribute to the entropy of that particular pixel. Another reason for increase in the entropy values may be due to the fact that, the single linearly polarized transmit of the compact polarimetric ($\pi/4$) mode will not be able to stimulate the target response from the linear features (tree trunks, trunks, urban features), which are slanting orthogonal to the incident electric field. It might be possible that circular polarization may be able to fully characterize the polarization state of these features.

From the residual analysis conducted for both model fit approaches, it was concluded that the models could not fit the entropy values due to the decreasing trend in the residuals in both the plots. Studies have shown that decreasing trend is equivalent to a non-random trend in the residual plot that causes error in calculating the slope and the intercept values while calculating the model equation for prediction.

The polarization signature from the mangrove forests was found to be similar to that of a dihedral corner reflector. Therefore, on correlating this concept with the variation in entropy values after reconstruction, the increase in the entropy value may be due to the rotated dihedral scattering. In theory, a dihedral with zero orientation angle gives a low entropy return and only the coherency matrix diagonal element responsible for double-bounce scattering is non zero. Rotating this dihedral still provides low entropy, since both cross-polarized power and the double-bounce power are highly correlated. But in the compact polarimetric mode, under the assumption of reflection symmetry, this correlation becomes zero which causes the entropy to increase. Even though, entropy analysis was not implemented for urban areas responsible for double-bounce scattering from coherency matrix approach, the theory holds true in case of over estimation of entropy in urban areas, based on covariance matrix approach [37].

This research has proved that, after reproduction of the pseudo-quadrature polarized data from the dual-polarized mode, the randomness from both the forested areas has increased when compared to the entropy from the fully-polarimetric mode.

7.7. Selection of study areas

The presence of prominent double-bounce scattering mechanism in the mangrove forests of the Sundarbans hampered the reconstruction of the cross-polarized term causing abrupt change in the volume scattering power for many forest class pixels. The reconstruction mechanism failed to follow the assumptions especially in pixels depicting swampy areas. Considering the climate of the area and the region being moist throughout the year, and being close to sea (sensitive to the specular reflection), the reconstruction algorithm used here was found vulnerable to these effects.

High elevated terrain of the Barkot area caused the reconstruction to be affected the reconstruction, since high azimuth slopes caused violation of the assumptions in the algorithm which caused high variations in the volume scattering power after the reproduction and consequently the decomposition. The analysis of

the double-bounce power from the urban areas of Haridwar showed intriguing residual plot with a non-random pattern but with high correlation between the original and the reconstructed values.

The analysis of different parameters from the mangrove forests was given special importance, since the forests are considered to be ecologically important and the monitoring of these forests are difficult manually due to the adverse climatic conditions and the density and area coverage of the forests. In case of the Barkot forests, the area comes under the monitoring of Rajaji National park and the areas are stable considering the climate and coverage area factors.

7.8. Validation

The volume scattering contribution from the tree leaves, trunk and from the ground of both the forested areas were validated against the reliable reference data which used $2S_{HV}$ single polarized element, taken from the fully-polarimetric data, sensitive to the volume scattering mechanism. Even though, the validation was done using modelling approach, the cross-polarized power with high variation caused the RMSE range to be close varied by approximately 1 dB for both the forested areas. The modelling approach used two samples from different parts of the forest areas to represent the population consisting of forest class. The regression line fitted for the first sample was used for predicting the reconstructed values from the original values and compared with the expected reconstruction values. The difference between the mean absolute error from both the samples from both study areas was found to be close varied by less than 0.7 dB. The research was not focused on studying the effect of the single-bounce and the double-bounce scattering contribution from the earth features sensitive to these mechanisms. Therefore, these components were not validated.

8. CONCLUSIONS AND RECOMMENDATIONS

The aim of this study was to explore the potential of the compact polarimetry ($\pi/4$) mode to reproduce the pseudo-quadrature polarized data from the dual-polarized scattering vectors, based on coherency matrix approach. The coherency matrix so reproduced was then separated into the three basic scattering mechanisms using the three-component decomposition model, to study the backscatter contribution from tree leaves, trunk and ground from the forested areas of Barkot and the ecologically important mangrove forests of the Sundarbans.

This chapter gives the conclusions of the results obtained from the method outlined in section 4.2. It also outlines the answers to the research questions posed in section 1.7.3.

8.1. How, pseudo-quadrature polarimetric 3×3 coherency matrix can be derived and reproduced from dual polarimetric mode using compact polarimetric technique?

The answer to the first research question became the backbone of this research, since the reproduction of the pseudo-quadrature polarized data became mandatory to study and assess the backscatter contribution of the volume scatterers from the forested areas. The polarization state extrapolation algorithm developed in [10] was used here, where reflection symmetry condition and the relation linking the degree of coherence and the cross-polarized power were taken as the two assumptions. The pseudo-quadrature polarized data generated as 3×3 covariance matrix was then used to derive the reconstructed data in the form of 3×3 coherency matrix. The 3×3 unitary transformation matrix was multiplied with the 3×3 covariance matrix and the transpose of the transformation matrix to transform the 3×3 covariance matrix into 3×3 coherency matrix derived in equation: (A-II-9). This matrix was then used to decompose the single-bounce, the double-bounce and the volume scattering mechanisms, out of which the effect of the volume scattering contribution from the tree leaves, trunk and the ground was studied and assessed. The diagonal elements T_{11}, T_{22} and T_{33} of the reconstructed matrix $[T_{MOD}]$ were used to compare and analyze the variations in the backscattered power, from both the fully-polarimetric and the compact polarimetric ($\pi/4$) modes.

8.2. What is the relation between the entropy obtained from the fully polarimetric data and the entropy obtained from compact polarimetry mode?

The third diagonal element T_{33} of both the matrices $[T_{FULL}]$ and $[T_{MOD}]$, sensitive to the cross-polarized power from the areas responsible for the volume scattering mechanism was used to calculate the entropy values and then to study the variations in both the modes. It was found that, from the forested areas, the randomness was found to be increasing in the compact polarimetric ($\pi/4$) mode. The randomness on the scattering mechanism from these forests was found to be very high in the fully-polarimetric mode (> 0.92). It was also understood that the entropy value ranges from 0 to 1 and therefore, the maximum increase in the entropy values in the compact polarimetric ($\pi/4$) mode was found to be approximately to 0.999. That meant that the range of the entropy values was very low. The relationship between the entropy values from both the modes was conducted using regression analysis. The residual analysis showed decreasing trend in the errors, which is a non-random phenomenon; showing that the linear model used could not fit the entropy values. A non-linear model may be a possible solution for this problem.

8.3. How to validate the volume scattering contribution from the compact polarimetric data against the fully-polarimetric data?

The research concentrated in studying and assessing the backscatter contribution from the tree leaves, trunk and the ground of the forested areas, in the compact polarimetric ($\pi/4$) mode. Therefore, it was compulsory to validate the pseudo-quadrature polarized data against the fully-polarimetric data. The single polarized cross-polarized image$2S_{HV}$ was used as the reliable reference data against which the reproduced data was validated. Two samples taken from different areas, sensitive to the volume scattering mechanism were used to validate the contribution. The two samples had represented the population of forest pixels. Regression analysis using linear model was used to model the cross-polarized power from both the modes. The residual plot assessed the quality of the linear model used. The model equation was then used in the second sample to predict the values from the reference values. The predicted values and the reconstructed values were then compared and assessed for accuracy in terms of RMSE and mean absolute error. This process was carried out for both study areas.

Since the research was focused more on retrieving the volume scatterer information, the single-bounce and the double-bounce scattering mechanisms were not validated.

8.4. What is the accuracy of the estimated volume scatterer contribution obtained from compact polarimetry mode against to that obtained from fully polarimetric data, using Freeman-III model?

It was vital to assess the quality of the reconstruction mechanism which was adopted in this research. The volume scattering contribution from both study areas were validated and assessed. It was found that, the linear model used for predicting the volume scattering power had an RMSE range of $2.28\ \text{dB} \leq \text{RMSE} \leq 3.19\ \text{dB}$ and mean absolute error (MAE) range of$1.86\ \text{dB} \leq \text{MAE} \leq 2.19\ \text{dB}$ for Barkot forest area. In case of the mangrove forests of the Sundarbans, the range of RMSE was in the range $4.07\ \text{dB} \leq \text{RMSE} \leq 5.03\ \text{dB}$ and MAE range of$2.64\ \text{dB} \leq \text{MAE} \leq 3.31\ \text{dB}$. Even though the values are similar for both the estimated and the predicted values, the presence of mixed pixels and the features exhibiting all the three scattering mechanisms caused the algorithm to degrade which caused so many pixel values to show abrupt change in the volume scattering power. This caused the accuracy range to vary. The reasons were discussed and shown on images figures: 7-2 (a) to (e) and 7-3 (a) to (e).

By answering the research questions, understanding the research objective and the sub-objectives proposed in this research were fulfilled. The research reviewed various literature and selected Freeman and Durden decomposition model because of its main characteristic to detect and decompose volume scattering information from the forested areas along with the two other mechanisms. The previous studies on compact polarimetry have not worked on the coherency matrix approach. Therefore this research had the freedom to opt for this model. Speckle filtering was not carried out in the pre-processing stage, because we did not want to degrade spatial information. Different data analysis was conducted on the results for both the areas, as the research had to explore the different interesting outcomes, which were reported and analyzed.

As a concluding remark to this research work, the reconstructed pseudo-quadrature polarized data reproduced using the compact polarimetry ($\pi/4$) mode technique, based on coherency matrix and thereby studying the contribution of volume scatterers from the forests shall help the forest management authorities and researchers in monitoring the forested areas, in event of flooding, forest fire and deforestation scenario, where manual methods and the fully-polarimetric data availability become a constraint.

8.5. Recommendations

The following recommendations may be considered, taking into account the implementation and the results obtained from this research.

- First and the most important has to be to modify the polarization state extrapolation algorithm, already implemented in [10] and [37], and but not modified in the algorithm incorporated in the latest 4.2 version of the PolSAR pro tool. The revision to be executed shall be to modify the second assumption relating the degree of coherence and the cross-polarized power, in which studies carried out in [10] and [37] had replaced the denominator term (the constant 4) of equation: (A-II-5) with $\frac{|S_{HH}-S_{VV}|^2}{|S_{HV}|^2}$. This term gives a correct estimate of the ratio of the double-bounce power to the cross-polarized power, thereby giving a consistent estimate for the pseudo-quadrature polarized data [10].

- Comparison studies may be carried out between different hybrid polarimetry modes such as ($\pi/4$) mode, DCP (Dual circular polarization) mode and CLTR (Circular transmit, linear receive) mode, based on coherency matrix approach and thereby studying and assessing the variation in the different scattering mechanisms.

- The effect of speckle filtering while during the pre-processing stage may show interesting results, even though loss of spatial information due to averaging a possible risk!

- The "factor 2" factor in the coherency matrix element to be modified in the polarization state extrapolation algorithm.

- Field data was not available for this research, due to restricted rights in the study area. If stem volume and tree height is available, the above ground biomass can be calculated and the pattern of biomass can be studied for both the modes.

LIST OF REFERENCES

[1] D. Massonnet and J-C. Souyris, "Imaging with Synthetic Aperture Radar," 1st edition, CRC Press: Florida, 2008.

[2] Y. S. Zhou, W. Hong and F. Cao, "An Improvement of Vegetation Height Estimation Using Multi-baseline Polarimetric Interferometric SAR Data," *PIERS ONLINE*, vol. 5, no. 1, pp. 6-10, 2009.

[3] Canada Centre for Remote Sensing, Tutorial: Radar Polarimetry, *Advanced Radar Polarimetry Tutorial.* [Online], Available: http://www.ccrs.nrcan.gc.ca/resource/tutor/polarim/pdf/polarim_e.pdf Last accessed on 12th March 2012.

[4] S. Cloude, *Polarisation applications in remote sensing,* Oxford: New York, 2010.

[5] Canada Centre for Remote Sensing, Tutorial: Radar Polarimetry, *Educational Resources for Radar Remote Sensing.* [Online], Available: http://www.ccrs.nrcan.gc.ca/resource/tutor/gsarcd/pdf/gsarcd_e.pdf Last accessed on 12th March 2012.

[6] A. Freeman and S. L. Durden, "A three-component scattering model for polarimetric SAR data," *IEEE Trans. Geosci. Remote Sens.*, vol. 36, no. 3, pp. 963-973, 1998.

[7] T. L. Ainsworth, J. P. Kelly and J. S. Lee, "Classification comparisons between dual-pol, compact polarimetric and quad-pol SAR imagery," *ISPRS. J. Photo. Remote Sens.,* vol. 64, pp. 464-471, 2009.

[8] J. C. Souyris, N. Stacy, T. L. Ainsworth, J. S. Lee and P. D. Fernandez, "SAR Compact Polarimetry (CP) or Earth Observation and Planetology: Concept and Challenges - A study case at P band", 2007. [Online], Available: http://earth.esa.int/workshops/polinsar2007/papers/231_souyris.pdf Last accessed on 12th March 2012.

[9] M. Lavalle, "*Full and Compact Polarimetric Radar Interferometry for Vegetation Remote Sensing*," Ph.D.Dissertation, Univer. De. Rennes. France, 2009.

[10] J. C. Souyris, P. Imbo, R. Fjortoft, S. Mingot and J. S. Lee, "Compact polarimetry based on symmetry properties of geophysical media: the /spl pi/4 mode," *IEEE Trans. Geosci. Remote Sens.,* vol. 43, no. 3, pp. 634-646, 2005.

[11] J. C. Souyris and S. Mingot, "Polarimetry based on one transmitting and two receiving polarizations:the π/4 mode," *IEEE Intl. Geosci. Remote Sens. Symp*, vol. 1, pp. 629-631, 2002.

[12] H. Skiriver, "Signatures of Polarimetric Parameters and their Implications on Land Cover Classification", *IEEE Intl. Geosci. Remote Sens. Symp.*, pp. 4195-4198, 2007. [Online]. Available: http://orbit.dtu.dk/Publications,$Form.sdirect, Last accessed on 12th March 2012.

[13] E. Pottier, J. S. Lee and L. F. Famil, "Advanced Concepts in Polarimetry-Part 1," presented at *RTO SET Lecture Series on Radar Polarimetry and Interferometry*, Brussels, Belgium, 2004 [Online].Available: http://ftp.rta.nato.int/public//PubFullText/RTO/EN/RTO-EN-SET-81///EN-SET-081-04.pdf, Last accessed on 12th March 2012.

[14] J-S. Lee and T. L. Ainsworth, "The Effect of Orientation Angle Compensation on Coherency Matrix and Polarimetric Target Decompositions," *IEEE Trans. Geosci. Remote Sens.,* vol. 49, no. 1, pp. 53-64, 2010.

[15] ISRO, "Miniature Synthetic Aperture Radar (Mini-SAR)", 2008. [Online]. Available: http://www.isro.org/chandrayaan/htmls/minisar_nasa.htm, Last accessed on 12th March 2012.

[16] T. M. Lillesand, R. W. Kiefer and J. W. Chipman, "*Remote Sensing and Image Interpretation,*" 6th Edition, New York: Wiley & Sons, 1998.

[17] F. M. Henderson and A. J. Lewis, "*Principles and Applications of Imaging Radar,*" 3rd Edition, New York: Wiley & Sons, 1998.

[18] D. P. Lusch, *Introduction to Microwave Remote Sensing,* Michigan: TRFIC 1999. [E-book] Available: www.trfic.msu.edu/products/profcorner_products/Intro_Microwave.pdf, Last accessed on 12th March 2012.

[19] E. Luneburg, "Aspects of Radar Polarimetry," *Turk. Jour. Elec. Engg*, vol.10, no. 2, pp. 219-243, 2002.

[20] G. Sinclair, "Modification of the Radar Target Equation for Arbitrary Targets and Arbitrary Polarization," *Report 302-19*, Antenna Laboratory, The Ohio State University Research Foundation, 1948.

[21] G.Sinclair, "The Transmission and Reception of Elliptically Polarized Waves," *Proceedings of the IRE*, vol. 38, no. 2, pp. 148-151, 1950.

[22] E. M. Kennaugh, "*Polarization Properties of Radar Reflections,*" Master's Thesis, Ohio State University, Columbus, 1952.

[23] E. M.Kennaugh, "Effects of the Type of Polarization on Echo Characteristics,"*Reports 381-1 to 394-24*, Antenna Laboratory, The Ohio State University Research Foundation, 1949-1954.

[24] J. R. Huynen., "*Phenomenological Theory of Radar Targets,*" Ph.D. thesis, University of Technology, Delft, The Netherlands, 1970.

[25] W. M Boerner and M.B. El-Arini, "Polarization Dependence in Electromagnetic Inverse Problem," *IEEE Trans. Ante. Propag.*, vol.29, no. 2, pp. 262-271, 1981.

[26] W. M Boerner C. L. Liu, and Zhang, "Comparison of Optimization Processing for 2x2 Sinclair, 2x2 Graves, 3x3 Covariance, and 4x4 Mueller (Symmetric) Matrices in Coherent Radar Polarimetry and its Application to Target Versus Background Discrimination in Microwave Remote Sensing," *EARSeL Advances in Remote Sensing*, vol. 2(1), pp. 55-82, 1993.

[27] G.G Stokes, "On the composition and resolution of streams of polarized light from different Sources,"*Trans. Cambridge Philos. Soc.*, vol. 9, pp. 399-416, 1852. (Full literature not available)

[28] J. S. Lee and E. Pottier, "*Polarimetric Radar Imaging: from basics to Applications,"* 1st edition, Boca Raton: CRC Press, 2009

[29] C. Putignano, "*PolSOM and TexSOM in Polarimetric SAR Classification*," Ph.D Thesis, Tor Vergata University, Rome, Italy, 2009.

[30] R. Touzi, W. Boerner, J. Lee, and E. Lueneburg, "A review of polarimetry in the context of synthetic aperture radar: concepts and information extraction," *Canadian Journal of Remote Sensing*, vol. 30, no. 3, pp. 380-407, 2004.

[31] S. Anfinsen, A. Doulgeris, and T. Eltoft, "Estimation of the Equivalent Number of Looks in Polarimetric SAR Imagery," *IEEE International, Geoscience and Remote Sensing Symposium,* pp. IV - 487-IV – 490, 2008.

[32] T. Zou, W. Yang, D. Dai, and H. Sun, "Polarimetric SAR Image Classification Using Multifeatures Combination and Extremely Randomized Clustering Forests," *EURASIP Journal on Advances in Signal Processing*, vol. 2010, pp. 1-10, 2010.

[33] S. Cloude and E. Pottier, "A review of target decomposition theorems in radar polarimetry," *IEEE Transactions on Geoscience and Remote Sensing,* vol. 34, no. 2, pp. 498-518, 1996.

[34] W. Holm and R. Barnes, "On radar polarization mixed target state decomposition techniques," *In Proceedings of the 1988 IEEE National Radar Conference,* pp. 249-254, 1988.

[35] R. K. Raney, "Hybrid-polarity SAR architecture," in *Proc. IEEE IGARSS*, pp. 3846–3848, 2006.

[36] R. K. Raney, "Hybrid-polarity SAR architecture," *IEEE Trans. Geosci. Remote Sens.,* vol. 45, no. 11, pp. 3397-3404, 2007.

[37] M. E. Nord, T. L. Ainsworth, J. S. Lee, and N. J. S. Stacy, "Comparison of Compact polarimetric Synthetic Aperture Radar Modes," *IEEE Trans. Geosci. Remote Sens.*, vol. 47, no. 1, pp. 174-188, 2009.

[38] F.J. Charbonneau, B. Brisco, R. K. Raney, H. McNairn, C. Liu, P. W. Vachon, J. Shang, R. DeAbreu, C. Champagne, A. Merzouki, and T. Geldsetzer., "Compact polarimetry overview and applications Assessment," *Can. J. Remote Sensing*, vol. 36, suppl. 2, pp. S298–S315, 2010.

[39] R. K. Raney, "Synthetic Aperture Radar Hybrid-Quadrature-Polarity Method and architecture for obtaining the Stokes parameters of Radar backscatter", U.S. Patent 7 746 267, July 21, 2011.

[40] E. Pottier, J. Lee, and L. Ferro-Famil, "PolSARpro_v4.2.0-Tutorial-Part1 RadarPolarimetry-4 Polarimetric Decompositions," 2007.

[41] M. Karam and A. Fung, "Radiative Transfer Theory For Active Remote Sensing Of A Forested Canopy," *International Geoscience and Remote Sensing Symposium, IGARSS'89*, pp. 2493-2496, 1989.

[42] E. Krogager, "New decomposition of the radar target scattering matrix," *Electronics Letters*, vol. 26, no. 18, pp. 1525-1527, 1990.

[43] S. Cloude and E. Pottier, "An entropy based classification scheme for land applications of polarimetric SAR," *IEEE Trans. Geoscie. Remote Sens.,* vol. 35, no. 1, pp. 68-78, 1997.

[44] S. Durden, J. van Zyl, and H. Zebker, "Modelling and observation of the radar polarization signature of forested areas," *IEEE Trans. Geosci. Remote Sens.*, vol. 27, no. 3, pp. 290-301, 1989.

[45] A. Freeman and S. Durden, "A three-component scattering model to describe polarimetric SAR Data,"*SPIE Radar Polarimetry*, vol. 1748, pp. 213-224, 1992.

[46] A. Freeman and S. L. Durden, "A three-component scattering model for polarimetric SAR data," *IEEE Trans. Geosci. Remote Sens.*, vol. 36, no. 3 pp. 963-973, 1998.

[47] Y. Yamaguchi, T. Moriyama, M. Ishido, and H. Yamada, "Four-component scattering model for polarimetric SAR image decomposition," *IEEE Trans. Geosci. Remote Sens.*, vol. 43, no. 8, pp. 1699-1706, 2005.

[48] L. Zhang, B. Zou, H. Cai and Y. Zhang, "Multiple-Component Scattering Model for Polarimetric SAR Image Decomposition," *IEEE Geoscience and Remote Sensing Letters,* vol. 5, no. 4, pp. 603-607, 2008

[49] D. L. Evans, T. G. Farr, J. J. V. Zyl, and H. A. Zebker, "Radar Polarimetry: Analysis Tools and Applications," *IEEE Trans. Geosci. Remote Sens.,* vol. 26, no. 6, pp. 774-789, 1988.

[50] J. J. Van Zyl, and H. A. Zebker, "Imaging Radar Polarimetry: A Review," *in Proc. of the IEEE,* vol. 79, no. 11, pp. 1583-1606, 1991.

[51] Y. S. Rao and V. Turkar, "Classification of Polarimetric SAR Data over Wet and Arid regions of India," *in Geoscience and Remote Sensing Symposium, 2009 IEEE International, IGARSS 2009,* vol. 3, pp. III-892-III-895, 2009.

[52] United Nations Environmental Programme, World Conservation Monitoring Centre, World Heritage Sites, Protected Areas and World Heritage, *The Sundarbans, Bangladesh,* [Online], Available: http://www.unep-wcmc.org/medialibrary/2011/06/24/ac3e5a3a/Sundarbans%20Bangladesh.pdf, Last accessed on 12th March 2012.

[53] A. Matsumoto, T. Hamazaki, Y. Osawa and Ichitsubo, "A Development Status of ALOS's Sensors," in *Proc. ISPRS, Commission VII WG6*, Kyoto, Japan, 2003.

[54] M. Shimada,"Calibration and Validation of PALSAR (Version 4),"2*nd ALOS Cal/Val and Sci. Meet.*, Tokyo, Japan, Nov. 2004.

[55] A. Rosenqvist, M. Shimada and M. Watanabe, "ALOS PALSAR: Technical outline and mission concepts," *4th Intl. Symp. Retrie. Bio. Geophysi. Parameters SAR Land Appli.,* Nov. 2004.

[56] S. R. Cloude and K. P. Papathanassiou, "Polarimetric SAR interferometry," *IEEE Trans. Geosci. Remote Sens.,* vol. 36, no. 5, pp. 1551-1565, 1998.

[57] European Space Agency., *POLSARPRO VERSION 4.2 (January 2011).* [Online]. Available: http://earth.eo.esa.int/polsarpro/default.html, Last accessed on 12th March 2012.

[58] R. K. Panigrahi and A. K. Mishra, "Comparison of Hybrid-polarization with Quad-polarization schemes based on airborne SAR images," *Workshop on Advanced antenna technology, IEEE,* pp. 1-4, 2010.

[59] J. J. van Zyl., N. Engheta, C. H. Papas, C. Elachi, and H. Zebker, "Modelling of backscatter from vegetation layers," *in IGARSS Dig.,* pp. 389-391, 1985.

[60] J. J. V. Zyl, H. A. Zebker and C. Elachi, "Imaging radar polarization signatures: Theory and observation," *Radio Science*, vol. 22, no. 4, pp. 529-543, 1987.

APPENDIX - I

Table 7: Radar bands and designations

Band Designation	Wavelength (in cm)
Ka	0.75 - 1.10
K	1.10 -1.67
Ku	1.67 - 2.40
X	2.40 - 3.75
C	3.75 - 7.5
S	7.5 - 15.0
L	15.0 - 30.0
P	30.0 - 130

Table 8: Dataset description

Description	**Study area I**	**Study area II**
Mission/Sensor	ALOS/PALSAR	ALOS/PALSAR
Date	22nd November 2009	29th May 2010
Polarization	HH+HV+VV+VH (Fully - polarimetric)	HH+HV+VV+VH (Fully - polarimetric)
Orbit Number	20402	23144
Mode	Ascending	Ascending
Center Latitude	30.1365400	21.7001860
Center Longitude	78.1433180	88.5911910
Incidence Angle	25.8°	25.8°

Table 9: Dataset Characteristics

Description	**Value**
Pixel Spacing (Range) in SLC format	9.368 m
Pixel Spacing (Azimuth) in SLC format	3.792 m
Ground Resolution	20 m
Ground Pixel resolution (Range)	18.737 m
Ground Pixel resolution (Azimuth)	3.792 m
Swath Width	30 km
Wavelength	23.5 cm

APPENDIX - II

Polarization state extrapolation algorithm - Technical details

The first step in the reconstruction derivation process involves the polarization synthesis resulting as 2×2 scattering matrix from quadrature polarized data. The scattering matrix representation of quad-polarized data in linear (H, V) basis is given by:

$$[S] = \begin{bmatrix} S_{HH} & S_{HV} \\ S_{VH} & S_{VV} \end{bmatrix} \tag{A-II-1}$$

The next step involves the extraction of scattering vectors for compact polarimetric mode ($\pi/4$ mode) from the scattering matrix, which is given by

$$K_{\pi/4} = \frac{1}{\sqrt{2}}[S_{HH} + S_{HV} \quad S_{VV} + S_{VH}]^T \tag{A-II-2}$$

Here the combination of scattering vectors $(S_{HH} + S_{HV})$ and $(S_{VV} + S_{VH})$ are obtained from the standard dual-polarimetric scattering vectors $[S_{HH}, S_{HV}]$ and$[S_{VV}, S_{VH}]$.

The factor $\sqrt{2}$ in equation (A-II-2) accounts for 3*dB* loss (half-power beam width) in the radar output with respect to classical dual or fully polarimetric modes which in turn is a direct consequence of the mismatch between transmitting and receiving polarization basis [9], [58].

The 2×2 covariance matrix for $\pi/4$ mode is calculated in the next stage by multiplying the scattering vector $K_{\pi/4}$ extracted in the previous step, with its complex conjugate transpose ${K_{\pi/4}}^{*T}$ to form $[C_{\pi/4}]$ given as:

$$[C_{\pi/4}] = K_{\frac{\pi}{4}} \times K_{\frac{\pi}{4}}^{*T}$$

Therefore, the covariance matrix $[C_{\pi/4}] = \begin{bmatrix} C_{11} & C_{12} \\ C_{21} & C_{22} \end{bmatrix}$ becomes

$$\frac{1}{2}\begin{bmatrix} |S_{HH}|^2 & S_{HH}\, S_{VV}^* \\ S_{VV}\, S_{HH}^* & |S_{VV}|^2 \end{bmatrix} \times \begin{bmatrix} |S_{HV}|^2 & |S_{HV}|^2 \\ |S_{HV}|^2 & |S_{HV}|^2 \end{bmatrix}$$

$$+\frac{1}{2}\begin{bmatrix} 2\mathrm{Re}\,(S_{HH}\ S_{HV}^*) & S_{HH}\ S_{HV}^* + S_{VV}^*\, S_{HV} \\ S_{HH}^*\, S_{HV} + S_{VV}\, S_{HV}^* & 2\mathrm{Re}(S_{VV}\quad S_{HV}^*) \end{bmatrix} \tag{A-II-3}$$

The first term in equation (A-II-3) represents the polarimetric behavior of co-polarized channels [10]. The second term is proportional to cross-polarization magnitude [10] while the third term consists of co-polarized/cross-polarized correlations [37]. Here the constant $1/2$ before the covariance matrix are discarded, since they may affect the computation of SAR power budget [10], even though they don't have any impact on the polarimetric performance of the compact polarimetric ($\pi/4$) modes [37].

Souyris et al. [10] developed a scattering model which assumed reflection symmetry and established a relationship between the degree of coherence and the cross-polarization ratio in order to reproduce pseudo-quadrature polarized data in the form of 3×3 covariance matrix from the 2×2 covariance matrix in the ($\pi/4$) mode.

Reflection symmetry condition is assumed when the observed media is symmetric with respect to the plane of incidence especially in case of water surfaces and in all natural scatterers like forest, snow, sea ice and also in case of volume scatterers containing spherical particles. Therefore, under reflection symmetry condition, there is a complete decorrelation of co-polarized and cross polarized backscatter coefficients. Thus co-polarized and cross-polarized correlations are set to zero. Therefore,

$$\langle S_{HH}\ S_{HV}^{*}\rangle = \langle S_{VV}\ S_{HV}^{*}\rangle = 0 \tag{A-II-4}$$

With the reciprocity [37] and the reflection symmetry [37] assumption, the quadrature polarized covariance matrix becomes a function of $|S_{HH}|^2, |S_{VH}|^2, |S_{VV}|^2$ and the real and imaginary components of co-polarized term$S_{VV}\ S_{HH}^{*}$. However, in case of 2×2 dual-polarimetry, the covariance matrices contain only information on four independent variables and therefore an extra condition or assumption is required to derive the pseudo-quadrature polarized data from the dual-polarimetric mode represented by the 3×3 covariance matrix.

To solve this problem, the second assumption developed by Souyris et al. [10] was used. They proposed a mathematical relationship between the degree of coherence $|\rho|$ and the cross-polarization ratio $(\langle|S_{HV}|^2\rangle/(\langle|S_{HH}|^2\rangle + \langle|S_{VV}|^2\rangle))$.

$$\frac{\langle|S_{HV}|^2\rangle}{\langle|S_{HH}|^2\rangle+\langle|S_{VV}|^2\rangle} = \frac{(1-|\rho|)}{4} \tag{A-II-5}$$

where ρ is the degree of coherence given by

$$\rho \equiv \frac{\langle S_{HV}\ S_{VV}^{*}\rangle}{\sqrt{\langle|S_{HH}|^2\rangle+\langle|S_{VV}|^2\rangle}} \tag{A-II-6}$$

The relationship established above in equation: (A-II-5) are either for a fully polarized or a fully depolarized backscattered wave and was subsequently extrapolated for any polarization state. For a fully-polarized wave reflected from a natural environment, the degree of coherence $|\rho|$ is equal to 1 and the cross-polarized term is equal to 0. For a fully-depolarized wave, the degree of coherence $|\rho|$ becomes 0

and

$$\langle|S_{HH}|^2\rangle = \langle|S_{VV}|^2\rangle = 2\langle|S_{HV}|^2\rangle$$

Therefore merging the equations (A-II-3) and (A-II-5), the non-linear system consisting of four equations and four unknowns were solved through an iterative process to obtain estimates of$|S_{HV}|^2$. Therefore considering reflection symmetry condition shown in equation: (5.4), the degree of coherence $|\rho|$ shown in equation (A-II-6) and the cross-polarization term $\hat{X}^{(0)}$, where $\hat{X}^{(0)}$=$\langle|S_{HV}|^2\rangle$ becomes

$$\left|\rho^{(0)}\right| = \frac{C_{12}}{\sqrt{C_{11}\times C_{22}}} \text{ and}$$

$$\hat{X}^{(0)} = \langle|S_{HV}|^2\rangle = \frac{(C_{11}+C_{22})}{2} \times \frac{\left(1-\left|\rho^{(0)}\right|\right)}{(3-|\rho^{(0)}|)}$$

The iterative process is carried out using $\hat{X}^{(0)}$ to refine the estimates of $|\rho|$ and thereby

$$|\rho^{(1)}| = \frac{C_{12} - \hat{X}^{(0)}}{\sqrt{[(C_{11} - \hat{X}^{(0)}) \times (C_{22} - \hat{X}^{(0)})]}} \quad \text{(A-II-7)}$$

It has to be noted that, since this is an iterative process, which is based on approximation, the degree of coherence $|\rho^{(n)}|$, may become greater than one or the denominator term of equation (A-II-7) can become a square root of a negative number. Therefore the iterative process was halted when the degree of coherence $|\rho^{(n)}| = 1$and the cross-polarized term $|\hat{X}^{(0)}| = 0$.

Therefore the n[th] order estimate of the pseudo-quadrature polarized data in the form of 3×3 covariance matrix is given by

$$[\bar{\bar{C}}_{MOD}] = \begin{bmatrix} C_{11} - \hat{X}^{(n)} & 0 & C_{12} - \hat{X}^{(n)} \\ 0 & 2\hat{X}^{(n)} & 0 \\ C_{12}^{*} - \hat{X}^{(n)} & 0 & C_{22} - \hat{X}^{(n)} \end{bmatrix} \quad \text{(A-II-8)}$$

In the next step, a 3×3 similarity transformation matrix $[A]$, was used to convert the derived pseudo-quadrature polarized data, in the form of 3×3 covariance matrix to 3×3 coherency matrix using the relation

$$[T_{MOD}] = [A] \times [\bar{\bar{C}}_{MOD}] \times [A^{T}]$$

$$\text{Where } [A] = \begin{bmatrix} \frac{1}{\sqrt{2}} & \frac{1}{\sqrt{2}} & 0 \\ 0 & 0 & 1 \\ \frac{1}{\sqrt{2}} & -\frac{1}{\sqrt{2}} & 0 \end{bmatrix}$$

Therefore, after calculation of the above relation, the final estimates of pseudo-quadrature polarized data in the form of 3×3 coherency matrix$[T_{MOD}]$ becomes

$$[T_{MOD}] = \begin{bmatrix} \frac{1}{2}(C_{11} - \hat{X}^{(n)}) + \frac{1}{\hat{X}^{(n)}} & \frac{1}{\sqrt{2}}(C_{12} - \hat{X}^{(n)}) & \frac{1}{2}(C_{11} - \hat{X}^{(n)}) - \frac{1}{\hat{X}^{(n)}} \\ \frac{1}{\sqrt{2}}(C_{12} - \hat{X}^{(n)}) & C_{22} - \hat{X}^{(n)} & \frac{1}{\sqrt{2}}(C_{12} - \hat{X}^{(n)}) \\ \frac{1}{2}(C_{11} - \hat{X}^{(n)}) - \frac{1}{\hat{X}^{(n)}} & \frac{1}{\sqrt{2}}(C_{12} - \hat{X}^{(n)}) & \frac{1}{2}(C_{11} - \hat{X}^{(n)}) + \frac{1}{\hat{X}^{(n)}} \end{bmatrix} \quad \text{(A-II-9)}$$

The pseudo-quadrature polarized data reproduced as 3×3 coherency matrix $[T_{MOD}]$, from dual-polarized mode, based on polarization state extrapolation algorithm and the 3×3 coherency matrix, calculated from fully-polarimetric data, were used to decompose the volume scattering contribution, using three-component incoherent decomposition model.

APPENDIX - III

Table 10: Statistical summary (a) Regression analysis - Study area I (b) Study area II (c) Residual analysis - Study area I (d) Study area II

T elements	r	Linear Model	
		R^2	RMSE
T_{11}	0.985	0.979	0.128
T_{22}	0.999	0.998	0.001
T_{33}	0.231	0.053	0.048

(a)

T elements	r	Linear Model	
		R^2	RMSE
T_{11}	0.996	0.992	0.027
T_{22}	0.999	0.999	0.002
T_{33}	0.006	0.00005	0.026

(b)

T elements	r	Linear Model	
		R^2	RMSE
T_{11}	0.996	0.992	0.027
T_{22}	0.999	0.999	0.002
T_{33}	0.006	0.00005	0.026

(c)

T elements	Residual plot Trend	Linear Model	
		r	Mean absolute error
T_{11}	Random	-1.9×10^{-9}	0.01
T_{22}	Non-random	-6.089×10^{-10}	0.017
T_{33}	Random	-0.027	0.021

(d)